THESIS

INVESTIGATING THE SOURCES OF SOUTHERN OCEAN AND COASTAL ANTARCTIC ICE NUCLEATING PARTICLES: THE CLOUD AND AEROSOL IMPACTS OVER THE SOUTHERN OCEAN (CAISO) PROJECT

Submitted by

Chelsea A. Bekemeier

Department of Atmospheric Science

In partial fulfillment of the requirements

for the Degree of Master of Science

Colorado State University

Fort Collins, Colorado

Fall 2025

Master's Committee:

Advisor: Sonia Kreidenweis
Co-Advisor: Jessie Creamean

Kristen Rasmussen
Megan Willis

ABSTRACT

INVESTIGATING THE SOURCES OF SOUTHERN OCEAN AND COASTAL ANTARCTIC ICE NUCLEATING PARTICLES: THE CLOUD AND AEROSOL IMPACTS OVER THE SOUTHERN OCEAN (CAISO) PROJECT

The Southern Ocean is the cloudiest region on Earth, where low-level mixed-phase clouds are a critical control on climate feedbacks. The liquid or ice content within these clouds controls their reflectivity, thus modulating shortwave radiation reaching the surface. Climate models struggle to accurately simulate absorbed shortwave radiation over the Southern Ocean due to limitations in representing these unique mixed-phase clouds. Increased observations of ice nucleating particles (INPs) provide necessary insights to resolve cloud microphysical schemes. Here we present data from Southern Ocean INP observations across six voyages, from 2016 to 2023. The last three voyages are featured as part of the Cloud and Aerosol Impacts over the Southern Ocean (CAISO) project.

These new datasets provide insights into Southern Ocean INP concentrations and sources, as well as a latitudinal framework to evaluate them in. Southern Ocean INP concentrations remained low and consistent with previous voyages, ranging from 2×10^{-4} to 2.64 INP/L at –30 °C. The Southern Ocean exhibits clear latitudinal gradients, with higher INP concentrations near low-latitude terrestrial sources and the lowest INP concentrations below 60 °S. We also identify the Antarctic continent as a weak but non-negligible INP source for the high-latitude Southern Ocean. Additionally, we discuss the need to treat various latitudinal regions of the Southern Ocean as independent sectors to better isolate sources and define representative INP spectra. Our

findings provide new insights to improve cloud microphysical schemes and resolution of these low-level mixed-phase clouds in climate model.

ACKNOWLEDGEMENTS

The research in this thesis was made possible by grant number AGS-2246489 from the National Science Foundation (NSF). Additionally, field research was supported by a grant of sea time on the RV Investigator from the Commonwealth Scientific and Industrial Research Organisation (CSIRO) Marine National Facility.

I would like to extend my gratitude to Dr. Sonia Kreidenweis and Dr. Jessie Creamean for their patience and support throughout this process. Additionally, I would like to acknowledge Dr. Kevin Barry and Dr. Tom Hill for their help in discussions, preparation, and emergency help while in the field. I would also like to extend my gratitude to everyone involved with previous work, including Dr. Christina McCluskey, Dr. Kathryn Moore, and Dr. Paul DeMott.

A very special thanks to all my colleagues from other universities that have contributed to sample collection throughout the Cloud and Aerosol Impacts over the Southern Ocean (CAISO) project. SOTS and MISO samples were collected by Dr. Jay Mace and Kelsey Barber. SWOT samples were collected by Jason Zhengchang Pei and Dr. Luis Ackerman. Denman Marine Voyage samples were collected by myself with support from the rest of the atmospheric team: Dr. Jacob Pernov, Salvatore Soldano, Kelsey Barber, and Thomas Paynter. COAST-K samples were collected by my colleague Samantha Greeney. Davis Station samples were, and currently are being collected by Thomas Paynter and James Newland, respectively.

Additional gratitude to our colleagues Dr. Marc Mallet, Dr. Ruhi Humphries, Dr. Simon Alexander, and Dr. Alain Protat for their help and collaboration throughout these voyages. Thank you to Dr. Alan Griffiths of the Australia Nuclear Science and Technology Organization

(ANSTO) for voyage radon data and to Sally Benson of Dr. Mace's group for the MERRA-2 parcel trajectory plots.

I would like to acknowledge CSIRO, the Institute for Marine and Antarctic Studies (IMAS) as part of the University of Tasmania (UTAS), and Australian Antarctic Division (AAD) colleagues for the orchestration, funding, training, and support during these expeditions.

Thank you to my husband, Michael, for his patience, support, and moving across the country for me – I could not have done this without you. Special thanks to my dog, Korra, for her emotional support and for allowing me to be away for 3 months on expedition. Finally, I'd like to extend my gratitude to my family and friends for their unwavering support and love. This paper is dedicated to everyone who has helped me get to where I am today; may we all leave this world a little better than we found it.

TABLE OF CONTENTS

LIST OF TABLES

LIST OF FIGURES

1. INTRODUCTION

1.1 The Southern Ocean: A Dynamic System

The Southern Ocean is a critical component of the coupled Earth system, shaping global heat transport, atmospheric and oceanic circulation, and climate feedbacks (Rintoul 2007; Hwang and Frierson 2013). Its remote location makes it one of the few regions where natural cloud-aerosol interactions can be studied with minimal anthropogenic influence (Hamilton et al. 2014; McCluskey et al. 2018a; Mace et al. 2021; Humphries et al. 2021; Moore et al. 2024). Within the Southern Ocean, the unique mixed-phase clouds (MPCs) play a pivotal role in regulating incoming shortwave radiation (Kay et al. 2016; Mace and Protat 2018a; Kremser et al. 2021; Vignon et al. 2021; Zhao et al. 2021; Fiddes et al. 2022; Järvinen et al. 2022; Mace et al. 2023; Pei et al. 2025; McCluskey et al. 2023; Burrows et al. 2022). MPCs are composed of both supercooled liquid and ice, and have a net shortwave cooling effect (Kay et al. 2016; Bodas-Salcedo et al. 2014). MPCs are typically low-level (< 3km) clouds and their reflectivity, coupled by their ubiquity over the Southern Ocean are critical drivers in radiative budget for this region (Mace et al. 2009, 2021b). Radiative biases in Earth System Models such as those participating in the Coupled Model Intercomparison Projects (CMIP5, CMIP6) are partly due to difficulties in representing cloud extent and microphysics (McCluskey et al. 2023; Xi et al. 2022). While progress has been made between CMIP5 and CMIP6, improvements to cloud phase feedbacks and parameterizations are necessary, as models still underestimate ice in Southern Ocean MPCs (Bjordal et al. 2020; Desai et al. 2023). The key is that the Southern Ocean is a dynamic system, composed of multiple sectors with varying aerosol sources and influence. The persistence of a

shortwave radiative bias associated with low clouds, especially over the high-latitude Southern Ocean, indicates a failure of the models to resolve sector-specific aerosol – cloud interactions (Kay et al. 2016; Fiddes et al. 2022; Burrows et al. 2022; McCluskey et al. 2023).

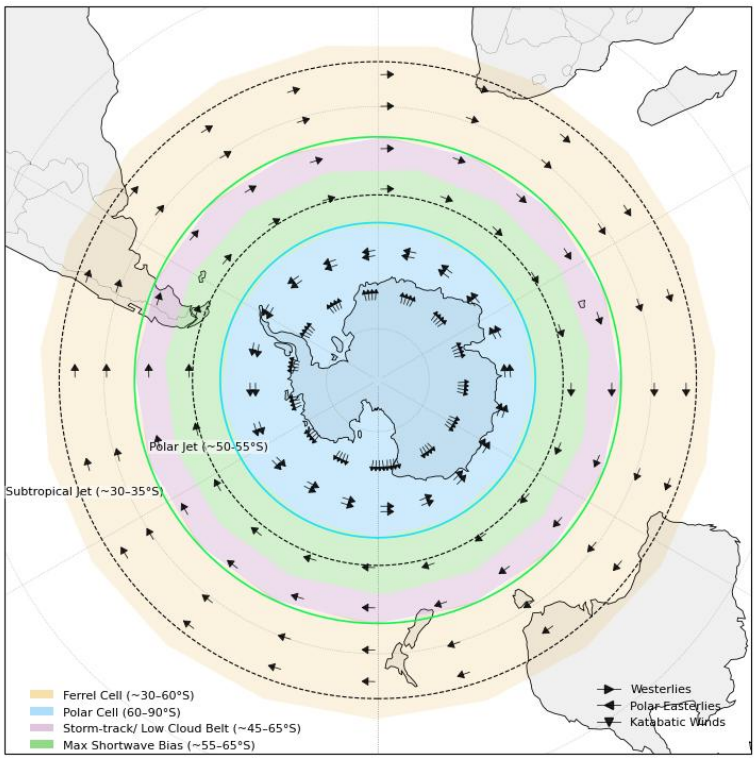

Figure 1. Schematic representing the various atmospheric regions of the Southern Ocean. Wind barbs indicate the prevailing boundary layer wind directions (not scaled by magnitude). Shaded regions represent Ferrel (30-60 °S orange) and Polar (60-90 °S, blue) circulation cells as well as the storm-track and low-cloud belt (45-60 °S, purple), and the global climate model radiative bias region (55-65 °S, green). Dashed lines indicate the presence of the subtropical and polar jet streams. The green solid line indicates the 45 °S latitude, and the teal blue line indicates the 60 °S latitude. *note that shaded regions overlap*

Figure 1 shows the various atmospheric regimes across the Southern Ocean region. In the Ferrel cell, westerlies and large-scale transport dominate (Martin 2007; Neff and Bertler 2015; Moran 2022). Within this cell, the belt between 45-60 °S is the cloudiest and stormiest region on Earth (Hoskins and Hodges 2005; Huang et al. 2015; Mace and Protat 2018a, b; Xi et al. 2022). The absence of land in this cell allows the strong prevailing westerlies and polar jet stream (~50-55 °S) to effectively isolate the high latitude Southern Ocean and Antarctic continent (Martin 2007; Moran 2022). The Southern Ocean is also home to the largest and most powerful ocean

current in the world, known as the Antarctic Circumpolar Current (ACC), helping separate the warm subantarctic and frigid Antarctic water masses (Bennetts et al. 2024). The ACC is coupled to the westerlies and polar jet (Allison et al. 2010; Bracegirdle et al. 2018; Lamy et al. 2024). These intricate ocean-atmosphere dynamics help create the polar front, which marks the boundary between the warmer, northern air masses and the colder Antarctic air (Moran 2022; Martin 2007). The position of this front fluctuates seasonally in conjunction with the location of the polar jet (Figure 2) (Scientific Committee on Antarctic Research (SCAR)).

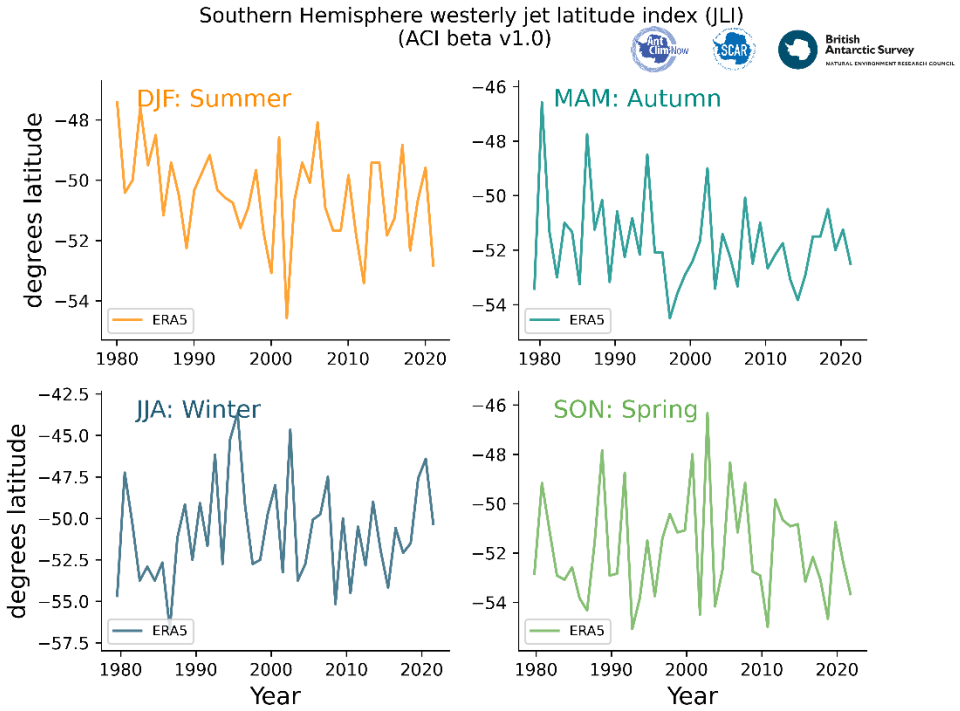

Figure 2. Southern Hemisphere Westerly Jet Latitude Index (JLI, °S) by austral season from 1980–2021, derived from the Bracegirdle et al. 2018 dataset (Scientific Committee on Antarctic Research (SCAR)).

Below the jet, the polar cell is particularly unique. Here, winds shift to easterlies due to the cold, katabatic winds from Antarctica and the Coriolis force deflecting this air to the left (Parish and Bromwich 2007; Caton Harrison et al. 2022). Katabatic winds develop when cold, dense air descends the sloping Antarctic ice sheet, accelerating downslope toward the coast. As this air mass is compressed and warmed slightly during descent, it transports cold, dry, and dense

conditions to coastal regions (Vignon et al. 2021; Pei et al. 2025). This air can influence offshore meteorological phenomena, such as suppression of clouds and the sublimation of snow. Katabatic winds can also transport aerosols from sources along the ice sheet and coastline into the Southern Ocean marine boundary layer (Chambers et al. 2018; Truong et al. 2020). Both the polar easterlies and katabatic winds that are unique to this region can also help further isolate the continent and the high latitude Southern Ocean (Parish and Bromwich 2007). Apart from the regions described above, a shortwave radiative bias peaks within 55-65 °S (Kay et al. 2016). This particular region is also home to the marginal ice zone (MIZ), where pack ice meets the open ocean, which fluctuates by season and can impact marine biological productivity and weather patterns (Yu et al. 2017; Willis et al. 2023; Turner et al. 2024; Zhong et al. 2025). Global climate models struggle with simulating Southern Ocean cloud microphysics, with a persistent shortwave bias peaking between 55-65 °S (Figure 3) (Kay et al. 2016; Burrows et al. 2022; McCluskey et al. 2023; Tan et al. 2024). These biases can, in turn, lead to errors in modeling climate sensitivity and related parameters (Tan et al. 2016).

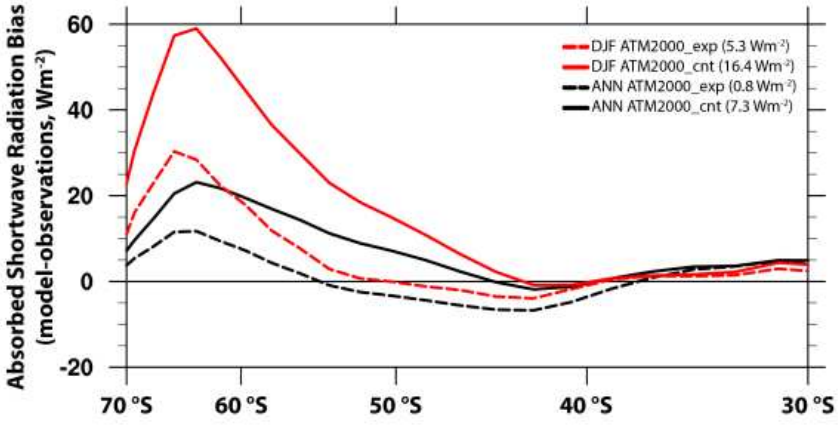

Figure 3. Zonal mean absorbed shortwave radiation bias over the Southern Ocean in atmosphere-only runs. Values in parentheses in the legend indicate Southern Ocean (30-70 °S) bias. Observations are from CERES-EBAF v2.8 for the years 2000-2013 (Loeb et al. 2009). Both annual (ANN) and Southern Hemisphere summer (DJF) means are plotted. Figure reproduced from (Kay et al. 2016).

While it is generally accepted that the Southern Ocean is a critical part of our Earth system, the very definition of the Southern Ocean remains elusive. Current atmospheric science literature ranges from defining it as any ocean region between 30-70 °S (McCluskey et al. 2018a; Welti et al. 2020; McFarquhar et al. 2021; Tatzelt et al. 2022; Moore et al. 2024). Some studies define the Southern Ocean as the region between 40-65 °S but divide the basin into separate latitude bins (Zhao et al. 2021; Humphries et al. 2021; McCluskey et al. 2023; Humphries et al. 2023). Others define the Southern Ocean as 50-70 °S (Neff and Bertler 2015; Uetake et al. 2020; Sanchez et al. 2021; Niu et al. 2024). Despite the variation in definition, it remains evident that the 30-70 °S region (hereby referred to as the Southern Ocean in this paper to avoid confusion) is comprised of latitudinal sectors, separated by atmospheric and ocean currents, wind patterns, and varying aerosol patterns (Uetake et al. 2020; Humphries et al. 2021; Sanchez et al. 2021; Humphries et al. 2023; Niu et al. 2024; Mallet et al. 2025). Consistent definitions of the of the Southern Ocean are critical for comparing sector specific aerosol – cloud observations across latitudes. Resolving differences in aerosol sources and concentrations across latitudes can help provide insights into the representation of these particles in climate models.

1.2 The Role of Ice Nucleating Particles in Southern Ocean MPCs

MPCs typically form at temperatures between –5 and –25 °C, where both liquid and ice can coexist (DeMott et al. 2010; Kanji et al. 2017). In the Southern Ocean, observations show that liquid-containing clouds are especially frequent in summer, while winter conditions favor colder clouds with more ice particles (Mace et al. 2021; Xi et al. 2022; Sauerland et al. 2024). Higher ice particle concentrations within these low-level MPCs can alter their reflectivity by decreasing the liquid water path (Tan et al. 2016; Sauerland et al. 2024). The balance between ice and liquid in MPCs depends in part on a subset of aerosols called ice nucleating particles (INPs),

which provide a favorable surface to initiate the formation of ice from the vapor or liquid phase (Vali 1966; DeMott et al. 2010). Because of the relatively warm temperatures in these low-level MPCs, homogeneous freezing (i.e., ≤ –38 °C) of water is not possible and instead, ice formation is initially driven by INPs (Vali 1994; Pruppacher and Klett 2010; Kanji et al. 2017).

Primary mechanisms of heterogeneous nucleation can occur via deposition nucleation, condensation freezing, collisional contact nucleation, and immersion freezing (Kanji et al. 2017; Hoose and Möhler 2012). Deposition nucleation is when ice forms directly from vapor on insoluble or porous particles. Condensation freezing occurs when supercooled water condenses on an INP, triggering freezing. Some droplets freeze when colliding with an INP, known as collisional contact nucleation. Immersion freezing is when an INP inside a supercooled droplet triggers freezing. Deposition and condensation freezing require supersaturations (>100% relative humidity) and collision contact nucleation requires rare particle-droplet collision events. However, immersion freezing only requires that supercooled liquid contain an INP that is active at an appropriate temperature. Of the primary ice production mechanisms, immersion freezing is considered the most important pathway in the Southern Ocean because supercooled liquid droplets are ubiquitous in MPCs, making immersion freezing more efficient (Hoose et al. 2010; Hande and Hoose 2017; Burrows et al. 2022; Raman et al. 2023). It is important to note that secondary ice production can also contribute to ice particle concentrations. Mechanisms such as rime splintering (Hallet-Mossop), ice-ice collisions, and droplet shattering can help increase ice concentrations in MPCs beyond what can be explained by INPs (Korolev and Leisner 2020; Korolev et al. 2020). However, INPs are responsible for the initiation of ice in these mixed-phase clouds.

A wide variety of aerosol types can serve as INPs, including mineral dust, soils, sea spray aerosol (SSA), and select bacteria, fungi, and other biogenic or inorganic materials (Schnell and Vali 1976; Vali et al. 1976; DeMott et al. 2010; Hoose and Möhler 2012; Niemand et al. 2012; DeMott et al. 2015, 2016; Hill et al. 2016; Kanji et al. 2017). INPs nucleate ice at various temperatures within the range that most MPCs exist, depending on particle type, structure, and composition (DeMott et al. 2010). Biological INPs tend to nucleate at warmer temperatures (typically ≥ -12 °C) and inorganic (e.g., dust) INPs tend to dominate the colder end of the heterogenous range (≤ -12 °C), due to the crystal organization provided by the substrate (Schnell and Vali 1976; Vali et al. 1976; Hill et al. 2016; Lukas et al. 2022). SSA are produced as primary marine aerosol via bubble-bursting and sea spray. Aerosols over ocean regions can also contain secondary marine biogenic particles formed from gas-phase precursors such as dimethyl sulfide, the latter of which do not serve as INPs (McCluskey et al. 2018b,c; Moore et al. 2022; DeMott et al. 2023). Primary SSA includes inorganic sea salt and organic materials that include phytoplankton exudates, fragments of bacteria/viruses, and other biogenic materials (Sanchez et al. 2021). Previous studies have demonstrated that marine SSA tend to comprise a large fraction of the aerosol over most of the Southern Ocean and are a source of INPs (McCluskey et al. 2018a; Twohy et al. 2021; Moore et al. 2024). While diverse aerosol types contribute to ice nucleation, SSA dominates in the marine boundary layer over the open Southern Ocean. While only a small fraction of SSA particles are active as INPs, they play a critical role in cloud phase partitioning and can influence cloud ice fraction, even at low concentrations (DeMott et al. 2010; McCluskey et al. 2018a; Moore et al. 2024).

While inorganic INPs are less dominant over this region within the marine boundary layer, mineral dust aerosols have more ice nucleation site densities by nearly three orders of

magnitude than marine aerosols (DeMott et al. 2016). Thus, even trace amounts of mineral dust can greatly influence ice nucleation. Several Southern Ocean and Antarctic observations reported an inorganic signature present in their INP measurements (McCluskey et al. 2018a; Schmale et al. 2019; Tatzelt et al. 2022; Moore et al. 2024). Inorganic INP composition varies depending on source region, but typically includes feldspar, quartz, clays, and iron oxides (DeMott et al. 2015; Hill et al. 2016). McCluskey (2023) demonstrated that while SSA largely dominates within the lower boundary layer, mineral dust was relatively more abundant aloft from Earth System Model simulations in the Southern Ocean domain. Proximity to land where air masses can include more terrestrial dust and other anthropogenic sources can lead to higher INP concentrations within the low-latitude Southern Ocean (DeMott et al. 2010; Kanji et al. 2017; McCluskey et al. 2018b; Welti et al. 2020; Tatzelt et al. 2022). Part of this inorganic signature has been hypothesized to be from long-range transported dust from South America, South Africa, Australia, and New Zealand. Neff and Bertler (2015) illustrated that air masses originating from dust point sources from these continents can reach Antarctica, although deposition in East Antarctica is sparse and shows signatures of more aged, mixed transport (Figure 4). New Zealand and Patagonia provide the most efficient pathways due to their southerly location but their dust emissions are relatively low, whereas Australia has more extensive dust sources and thus has historically been an important contributor to Southern Ocean dust (Albani et al. 2012).

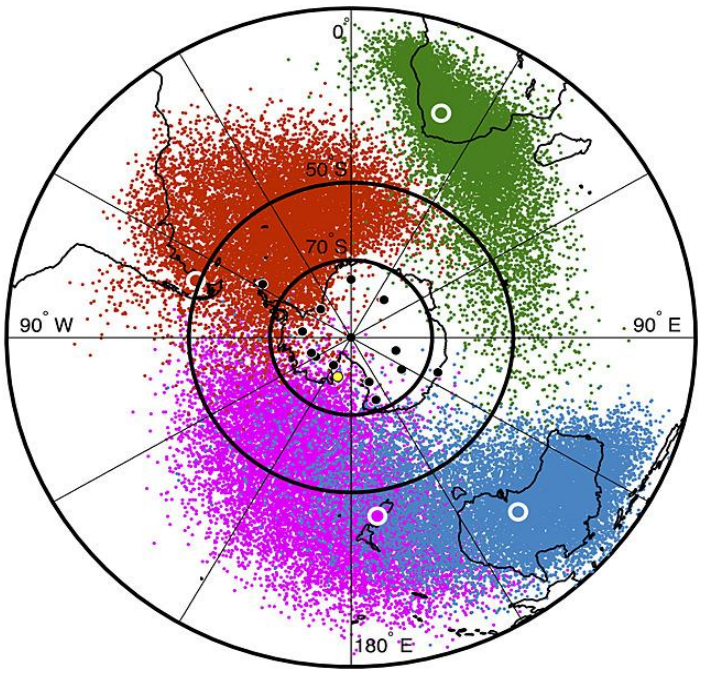

Figure 4. From Neff and Bertler (2015), showing 5-day HYSPLIT forward trajectory endpoints, calculated daily from 1979 to 2013 for each dust source region: New Zealand (magenta), Patagonia (Argentina, red), southern Africa (green), and Australia (blue). Larger, white-outlined circles indicate trajectory starting points; black circles mark Antarctic ice core sites, with the yellow circle highlighting the RICE ice core. Bold parallels indicate the northern boundaries of the Southern Ocean (50°S) and Antarctica (70°S) as defined by Neff and Bertler.

Understanding the sources of INPs within the Southern Ocean is critical to improving climate models, as cloud phase feedbacks are the main source of uncertainty. Determining the relative contribution of regional sources versus long-range transport can help elucidate cloud ice formation processes in this region.

1.3 Previous INP Measurements in the Southern Ocean Region

While past voyages have allowed us to gain critical insights, observations within the Southern Ocean remain scarce, particularly at high latitudes. First campaigns by Commonwealth Science and Industrial Research Organisation (CSIRO) occurred in 1969-1972 and most observations of INPs in this region did not resume until the last decade. Previous voyages can be found in Table 1. Comparisons across voyages are highlighted in Figure 5.

Table 1. Previous Southern Ocean voyages and campaigns with INP measurements.

Voyage	Full Name	Dates	Latitudinal extent	Longitudinal extent	INP instruments
Bigg	Bigg	1969 – 72	20-65 °S	60-140 °E	Filters, 12-hours
ACE-SPACE	Antarctic Circumnavigation Expedition – Study of Pre-industrial Aerosols and their Climate Effects	20 Dec 2016 – 19 Mar 2017	35-70 °S	Full circum-navigation	Filters, 8 to 24-hours
MARCUS	Measurements of Aerosols, Radiation, and Clouds Over the Southern Ocean	29 Oct 2017 – 1 Apr 2018	43-70 °S	90-150 °E	CFDC, Filters 24 to 28 hours
CAPRICORN I	Clouds, Aerosols, Precipitation, Radiation, and Atmospheric Composition Over the Southern Ocean I	1 Mar – 5 Apr 2016	43-53 °S	140-145 °E	CFDC, Filters, 21 to 63 hours
CAPRICORN II	See above (II)	11 Jan – 21 Feb 2018	43-66 °S	130-150 °E	CFDC, Filters, 24 to 48
SOCRATES	Southern Ocean Clouds, Radiation, and Aerosol Transport Experimental Study	15 Jan – 26 Feb 2018	43-63 °S	134-163 °E	CFDC, Filters over multiple legs (on board the NCAR/NSF GV aircraft)

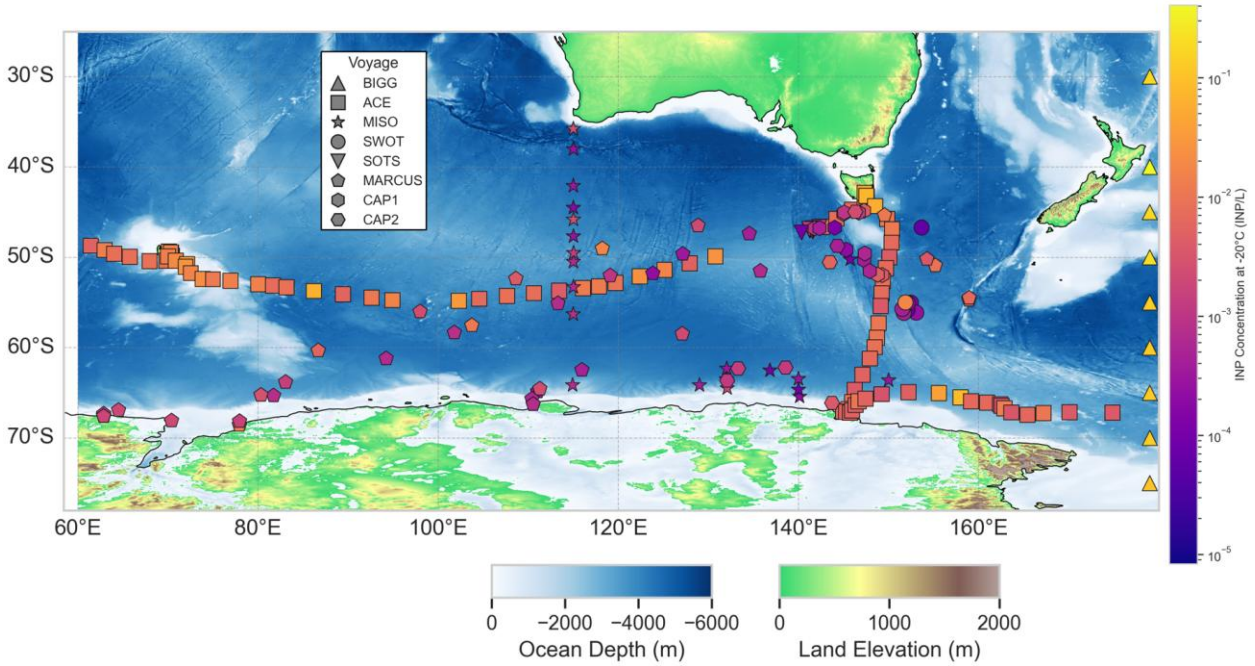

Figure 5. Adapted from McFarquhar et al. (2021). Concentrations of ice nucleating particles (INPs) active at –20 °C observed during voyages listed in Table 1. Voyages are indicated by shape and colored by INP concentration (INP concentration color bar, INP L^{-1}). Bathymetry and topography imagery are reproduced using the General Bathymetric Chart of the Oceans (GEBCO Bathymetric Compilation Group 2024). Land elevation and ocean depth data are from 2024 (last accessed June 2025). Land elevation is colored from 0 to 2000 m (Land Elevation color bar, m) and ocean depth is colored from 0 to -6000 m depth (Ocean Depth color bar, m).

1.3.1 Bigg 1969-1972

Membrane filters were collected over 12-hour periods across Australia and 20-80 °S over the course of multiple voyages and years aboard the United States Naval Ship *Eltanin* (Bigg 1973). INP concentrations reported from these voyages were anomalously high compared to more recent voyages (McCluskey et al. 2018a; Welti et al. 2020; Tatzelt et al. 2022; Moore et al. 2024). The stark contrast makes these observations difficult to compare with other Southern Ocean voyages. Additionally, due to sample averaging and averaging of blanks, it is difficult to compare to our data. Due to these discrepancies, Bigg's data will not be included in our analysis.

1.3.2 ACE-SPACE

ACE-SPACE took place in austral summer to early autumn on board the Research Vessel (RV) *Akademik Tryoshnikov*. The circumnavigating voyage included 3 legs across 35-70 °S surrounding the Antarctic continent (Schmale et al. 2019; Tatzelt et al. 2022). INP filter collection was the primary method of investigation; filters were collected for 8 to 24 hours each. While INP concentrations collected during this campaign were insightful due to the larger longitudinal nature of the samples within the Southern Ocean, the concentrations were not background corrected and thus are not comparable to INP data from the other voyages.

1.3.3 MARCUS

MARCUS took place on board the Research and Supply Vessel (RSV) *Aurora Australis* in austral spring to autumn across 43-70 °S (Humphries et al. 2021; Moore et al. 2024; Sanchez et al. 2021; McCluskey et al. 2023; McFarquhar et al. 2021). Since the *Aurora Australis* is an Antarctic base resupply ship, most of the ship tracks followed a route to Casey, Davis, Mawson, and Macquarie Island Stations. INP filter samples using the same methodology described in Section 2.2 were collected in conjunction with measurements using a Continuous Flow Diffusion Chamber (CFDC) (DeMott et al. 2016). Ship stack contamination was an issue during this voyage for most aerosol measurements as noted by McCluskey (2023) and Humphries (2023) but was not suspected to impact INP concentrations.

1.3.4 CAPRICORN (I & II)

The CAPRICORN project occurred over two voyages on board the RV *Investigator* (Mace and Protat 2018a; Moore et al. 2024; McCluskey et al. 2018a; Mallet et al. 2025; McFarquhar et al. 2021). INP filters were collected and processed using the same methodology described in Section 2.2 and CFDC measurements were taken for both installments.

CAPRICORN I occurred in austral autumn and remained between 43-53 °S due to its main purpose of servicing Southern Ocean buoys, while CAPRICORN II took place during austral summer (Mace and Protat 2018b). This latter voyage traveled to the Antarctic coast briefly, providing samples as far south as 66 °S.

1.3.5 SOCRATES

SOCRATES was an aircraft campaign run in conjunction with CAPRICORN II over 43-63 °S (Mace and Protat 2018a; Moore et al. 2024; McCluskey et al. 2018a; Mallet et al. 2025; McFarquhar et al. 2021, Järvinen et al. 2022). The NCAR Gulfstream-V (GV) conducted 15 research flights over the course of this period, taking observations below, in, above clouds over the Southern Ocean (Mace et al. 2021; Moore et al. 2024). CFDC and filter samples were collected on board the GV. While some samples were obtained in the marine boundary layer, SOCRATES filters will not be included in this analysis as they are not ship-based, sea-level observations consistent with the other voyages.

1.4 Research Questions

Despite a growing body of data, there still exists a paucity of Southern Ocean observations compared to other locations globally. Additional INP observations are needed to improve cloud microphysical schemes in this unique and critical region of the world. The Cloud and Aerosol Impacts over the Southern Ocean (CAISO) project discussed in this thesis seeks to at least double Southern Ocean INP observations and provide new insights into these critical particles and their impacts on MPCs. While there are many questions to be answered, this thesis will address the following three research questions:

1. How do INP observations from the first three CAISO voyages compare with previous observations and known ice nucleation parameterizations?
2. Are there latitudinal differences in the sources and abundance of INPs over the Southern Ocean?
3. What are the main sources of INPs observed in the atmospheric boundary layer over the high-latitude Southern Ocean and coastal Antarctica?

2. DATA AND METHODS

2.1 The Cloud and Aerosol Impacts Over the Southern Ocean (CAISO) Project

The Cloud and Aerosol Impacts over the Southern Ocean (CAISO) project is a collaborative effort between Colorado State University (CSU), National Center for Atmospheric Research (NCAR), Common Scientific and Industrial Research Organization (CSIRO), University of Tasmania Institute for Marine and Antarctic Studies (IMAS), and Australian Antarctic Program (AAP). CAISO consisted of five Southern Ocean research voyages (SOTS, SWOT, MISO, Denman, and COAST-K; see Figure 6) conducted from May 2023 to May 2025 in tandem with approximately 2 years of ground observations at Davis Station, Antarctica (68.5762° S, 77.9696° E). The main objective of CAISO is to double the quantity of in-situ aerosol-cloud observations in the Southern Ocean, including expanding the spatial and temporal resolution of samples. This paper will report data from the first three CAISO voyages (SOTS, SWOT, and MISO) and compare them to findings from relevant previous studies. Additionally, we present an in-depth analysis of the MISO observations since these represent a unique data set from across all latitudes of the Southern Ocean, with a focus on the Antarctic coast.

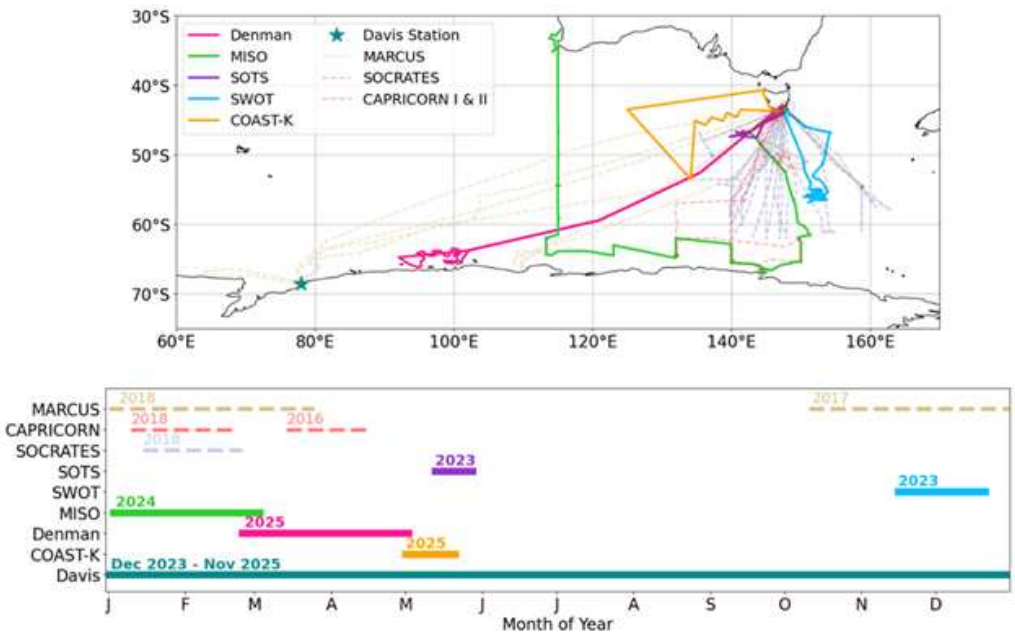

Figure 6. CAISO (solid lines) and previous research voyage study locations. Note that SOCRATES (grey dashed) was an aircraft mission and Davis Station (teal star) is a stationary 2-year period of observations. The remainder are research voyages on vessels.

Table 2. CAISO Voyages and Davis Station observations

Voyage	Full Name	Dates	Latitudinal extent	Longitudinal extent	INP instruments
SOTS	Southern Ocean Time Series	12 May – 25 May 2023	43-47.5 °S	139-147.5 °E	Filters, 24 hours
SWOT	Surface Water Open Topography	15 Nov – 20 Dec 2023	43- 57 °S	147-154.5 °E	Filters, 24 to 48 hours
MISO	Multidisciplinary Investigations of the Southern Ocean	5 Jan – 5 Mar 2024	43-67 °S	112-147.5 °E	Filters, 24 to 72 hours
Davis	Davis Station, Antarctica	30 Jan 2024 ~ Apr 2026 (tbd)	68.5775 °S	77.983917°E	Filters, 24 to 72 hours
Denman	Denman Marine Voyage	1 Mar – 2 May 2025	43-67 °S	98.5-147 °E	Filters, 24 hours
COAST-K	Clean Ocean Air Sampling upwind of Tasmania - Kennaook	28 Apr- 17 May 2025	41.5-43 °S	143-147 °E	Filters, 48 hours

2.1.1 The Southern Ocean Time Series (SOTS) Voyage

The SOTS voyage took place from 12 – 25 May 2023 (austral autumn) on the Research Vessel (*RV*) *Investigator* (operated by CSIRO). The voyage departed from Hobart, Tasmania and traveled only to 47.5 °S to deploy a new set of moorings and recover two others. 10 samples were collected between 46 to 47.5 °S before returning to Hobart (Figure 7).

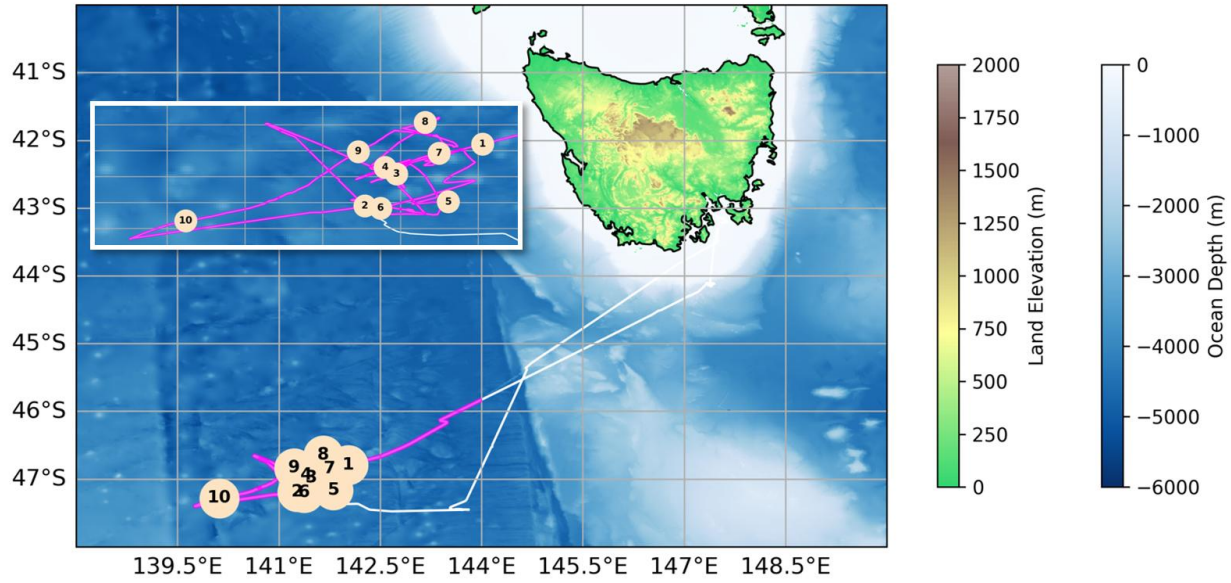

Figure 7. SOTS ship track with sample midpoints of 24-hour filters for offline INP analyses. Pink lines indicate active sampling, and white lines indicate transit periods. The numbers indicate the filter number. Inlay to help expand the samples is shown in the white box at the top left. Land elevation and ocean depth data are from 2024 (last accessed June 2025), see Figure 5 for details.

2.1.2 The Surface Water Ocean Topography (SWOT) Voyage

The SWOT voyage took place from 15 Nov – 20 Dec 2024 (austral spring-summer) on the *Investigator*. The voyage was part of the on-going SWOT program at CSIRO which aims to combine in situ ocean measurements with the SWOT satellite to better understand how currents in the Southern Ocean and the Antarctic Circumpolar Current (ACC) impact sea ice melt. The voyage departed from Hobart and traveled slightly east and down to 56.5 °S. Most samples (30 total) were taken between 54 to 56.5 °S before returning to Hobart (Figure 8).

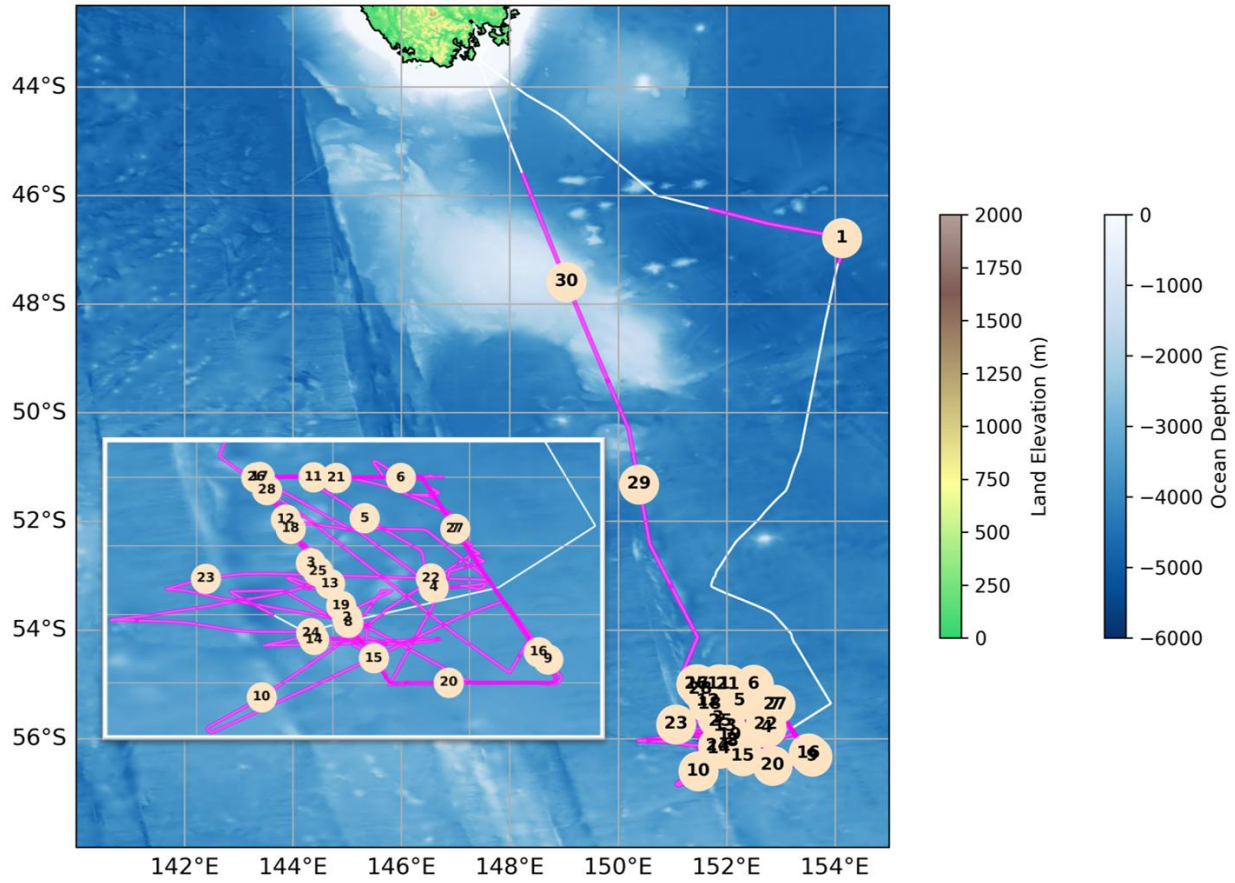

Figure 8. Same as Figure 7, but for the SWOT ship track. Inlay at the bottom left to help expand samples 2-28 is shown in the white box at the bottom left.

2.1.3 The Multidisciplinary Investigations of the Southern Ocean (MISO) Voyage

This paper will mainly focus on the MISO voyage, due to the duration of the voyage (63 days on the *Investigator*) and its coverage of the entire latitudinal Southern Ocean (Figure 9). This voyage took place from 2 Jan – 5 Mar 2024 (austral summer-autumn). The MISO voyage was interdisciplinary, aiming to connect the atmosphere, biosphere, and ocean in critical Antarctic climate phenomena. The voyage departed from Hobart, Tasmania, traveled to the Antarctic coast (~ 70 °S) and then back up the I09S ocean transect extending from Antarctica back up to Fremantle (leg 3), Western Australia (Figure 9). The I09S transect is a Global Ocean Ship-based Hydrographic Investigation Program (GO-SHIP) globally recognized hydrographic section, which cuts through multiple critical oceanic zones, with data taken along this transect

providing key insights over the last 30 years. More than half of the MISO voyage was spent along this transect (leg 3), due to its oceanographic importance and its connection to Antarctic phenomena, such as sea ice and glacier melt.

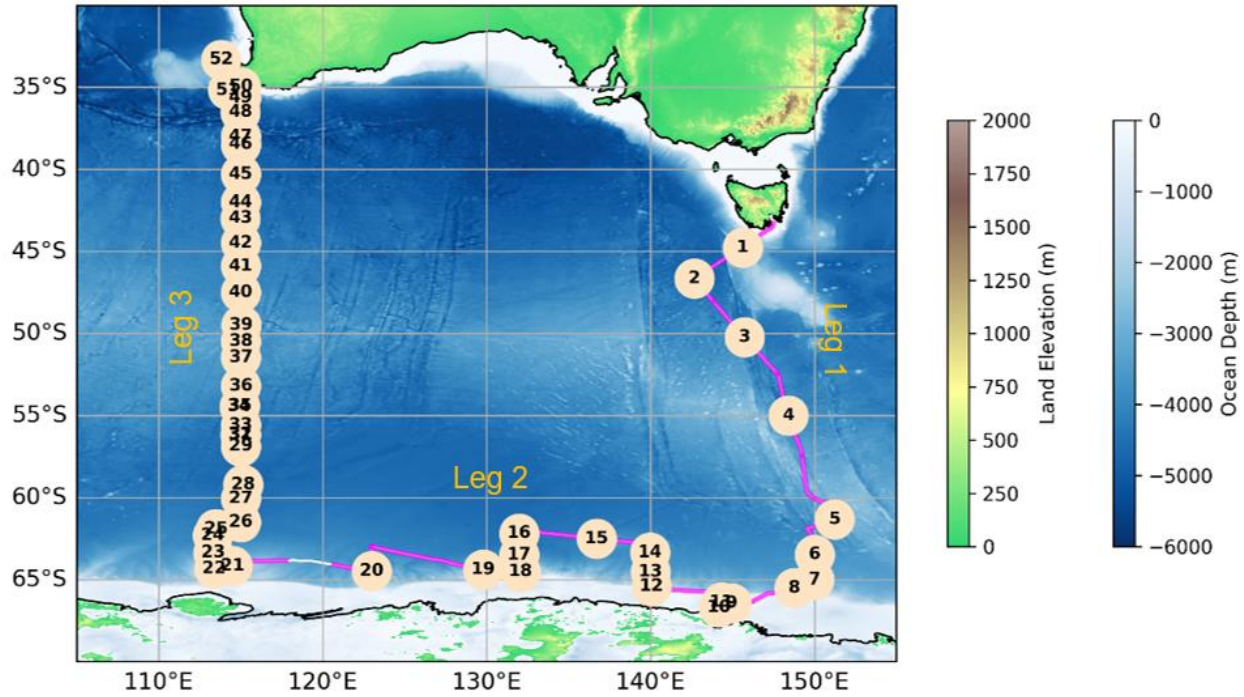

Figure 9. Same as Figure 7, but for the MISO ship track with voyage legs 1-3 overlaid.

2.1.4 Forthcoming Datasets

While this paper only provides results from the first three voyages of the CAISO mission, Denman, COAST-K, and the first year of Davis station samples have recently been completed. These samples will likely be analyzed within the next year and added to the current CAISO database for further analysis. Abbreviated details on each are provided below.

Denman Marine Voyage

The Denman Marine Voyage took place 1 March – 2 May 2025 on board the RSV *Nuyina* from Hobart, Tasmania to the Denman glacier region on the Antarctic coast. The 2-month voyage spent nearly 7 weeks off the Antarctic coast, providing a unique data set for high-latitude

Southern Ocean and coastal INPs. The Denman voyage spanned 98.5-147 °E and just past 67 °S. A total of 62 INP filter samples were taken over the course of the voyage, at approximately 24-hour intervals (Figure 10). Blank filters were collected every week. The same INP sampling tower methods used on the *Investigator* (Section 2.2) were used for Denman, with the exception being that the tower was placed on Deck 9 of the *Nuyina*, at nearly 30 m. The placement of the tower was much lower than the ship stack and shielded by the ship itself, mitigating ship contamination as much as possible. Days of stagnant winds and heavy snow were likely contributing the most to wet deposition and contamination of samples, which will be accounted for in the upcoming filter analysis.

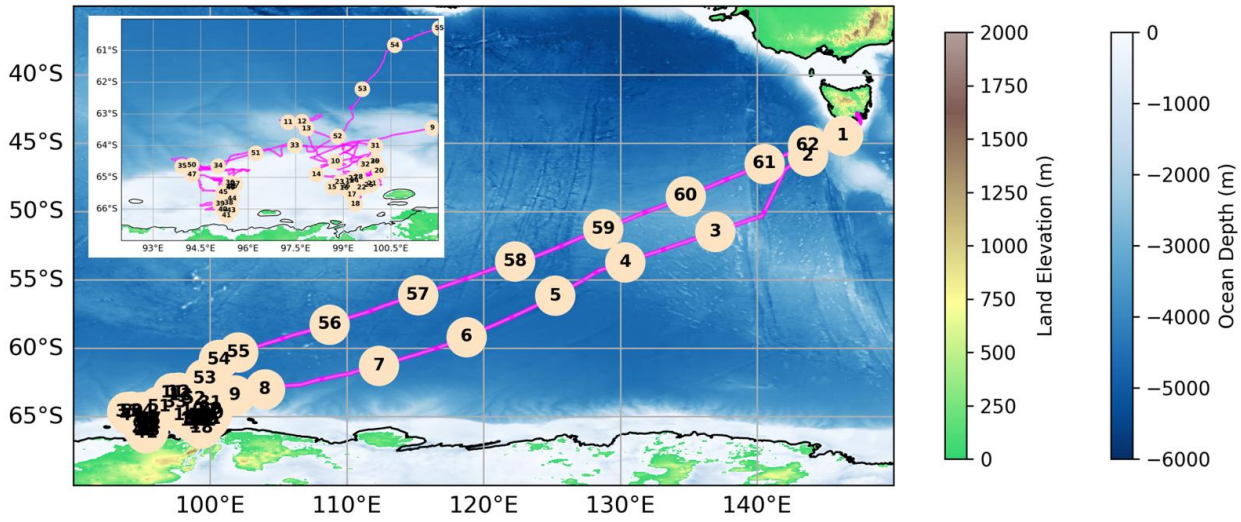

Figure 10. Same as Figure 7, but for the Denman Marine Voyage.

COAST-K

The Clean Ocean Air Sampling upwind of Tasmania – Kennaook occurred 28 April to 17 May 2025 on board the *Investigator* (Figure 11). INP sampling towers were consistent with previous *Investigator* set-ups (Section 2.2), except pump switches were not used for this voyage and the INP tower was set up on Deck 5. 10 INP filter samples were collected over a period of roughly 48 hours each. 2 blank filters were collected on the first and second week of the voyage.

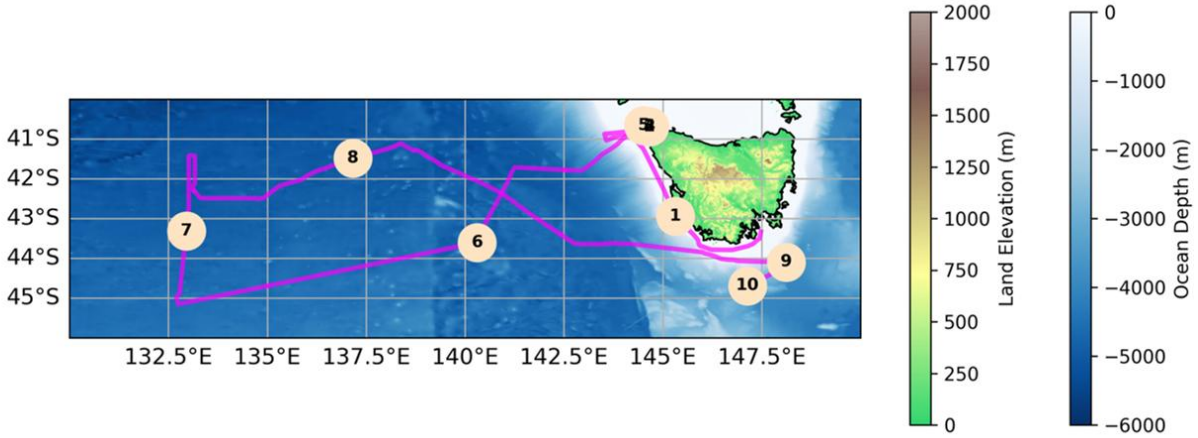

Figure 11.Same as Figure 7, but for COAST-K. Samples 2-5 are nearly at the same location outside of Cape Grim, Tasmania.

Davis Station

INP filters towers were set up at 68.5775 °S, 77.983917 °E, just outside of the main Davis Station base. Filter towers were set up consistent with voyage methods and samples were taken at various intervals (24 and 72 hours, or as dictated by meteorological conditions). Sample towers were placed atop scaffolding connected to a shipping container at approximately 4.5 m above ground level (Figure 12). Due to high winds and blowing snow, mesh nets were used to avoid sample contamination. Samples have been collected from 30 January 2024 and will continue through to approximately April 2026. The first year of samples are on their way back to CSU where they will be processed along with the Denman and COAST-K samples.

Figure 12. Davis Station INP tower set-up

2.2 Instrumentation, Sample Collection, and Analysis Methods

2.2.1 Ship-board Instrumentation

INP filter preparation and collection

Aerosol samples analyzed for INP concentrations were collected on pre-sterilized 0.2 µm pore size, 47 mm track-etched polycarbonate membrane filters, following McCluskey et al. (2018a); Creamean et al. (2022); Moore et al. (2024); Barry et al. (2025). Given the extremely clean nature of the air in this region of the Earth, to avoid contamination as much as possible, filters were pre-treated (sterilized) and handled carefully. INP filter sterilization included pre-soaking in a 10% hydrogen peroxide solution for 10 minutes, followed by 3 rinses with deionized (DI) water. The process was completed with a fourth rinse with 0.1-µm-filtered DI and then filters were dried on aluminum foil in a UV-sterilized laminar flow hood. 10-µm pore size, 47 mm track-etched polycarbonate membrane filters were prepped in the same manner to serve as a backing for the INP filters. Individual INP filters were then loaded into Nalgene sterile

analytical filter units on top of the 10-µm backing filter. Units were placed in sterile Ziploc bags until use. Filter units were placed on collection towers on the Level 3 deck of the *Investigator* at approximately 15m ASL, overlooking the bow for SOTS and SWOT (Figure 13). For MISO, filter units were placed on Level 2 at approximately 7.5m ASL.

Figure 13. INP tower set-ups onboard the RV Investigator for SOTS, SWOT, and MISO voyages. Note that the aerosol lab inlet is also pictured at the front of the bow in the SWOT image.

Filter set-ups included a shield to keep out precipitation and sea spray and were anchored to withstand Southern Ocean conditions. The INP filter units were connected to a flow meter (TSI 5000 series; TSI Inc.) to monitor flow rate and total collected sample volume, followed by a 230 V vacuum pump (Thomas) via antistatic tubing, pulling air through the unit continuously for approximately 24 to 48 hours. Flow was maintained at approximately 15-20 L min^{-1} to improve collection efficiencies of both super and submicron size aerosols. Air was sampled for roughly 24-hour periods, except for periods of inclement weather. Filters were collected after the allocated period and placed with sterile forceps in individual petri dishes, sealed with parafilm, wrapped in aluminum foil and placed in Ziploc bags for transport. To minimize contamination, sterile protocols were followed as outlined in Barry et al. (2021).

All samples were kept at -20 °C on board the *Investigator* until shipment to CSU. Samples were shipped back to CSU while held below -80 °C using Cryport dry nitrogen containers. Detailed field logs accompanied each sample and listed details of collection period, weather, and other pertinent information.

Radon

Atmospheric Radon-222 (^{222}Rn) was measured to detect continental air masses (McCluskey et al. 2018a; Mallet et al. 2025). Measurements were taken continuously throughout the duration of the voyage using a dual flow loop two-filter detector (700-L) following the methodology described in (Griffiths et al. 2016; Chambers et al. 2018). Atmospheric Radon-222 was sampled through the *Investigator* aerosol inlet, located 18.4 m above MSL on the bow of the ship. Ambient air was sampled through a conical inlet (16 cm inner diameter, tapered to 4 cm) at approximately 440 L/min. Air flows through roughly 9 m of tubing to the aerosol laboratory to be sampled by various instrumentation. The inlet was oriented horizontally to avoid precipitation and point into the wind. Further information on the inlet and sizing instruments can be found in Mallet et al. (2025).

Ship meteorological data

The *Investigator* has an on-ship suite of meteorological data including wind speed (knots) and direction (°), ambient air temperature (°C), barometric pressure (mbar), relative humidity (%), solar radiation (Wm^{-2}), precipitation (mm), and sea surface temperature (°C). Navigational data were also included in this underway data. The data were quality controlled and provided by CSIRO.

Ship Exhaust Contamination

Ship-based voyages are not without their challenges. For both the bow aerosol inlet and the filter towers, the largest sources of particle contamination were from ship engine exhaust and waste incineration. While ship exhaust typically does not affect INP concentrations (McCluskey et al. 2018a; Creamean et al. 2022), due to the extremely clean nature of the atmosphere in this region, we used sector based sampling to further mitigate possible INP artifacts. Specifically, a pump switch was used which only supplied power to the pump when the ship's relative wind speed was between 10 and 80 knots and wind direction was from the forward 90°. Further information on contamination and data quality assurance can be found in reports from previous studies onboard the *Investigator* (Moore et al. 2024).

2.2.2 Ice Nucleating Particle (INP) Analysis

INP filters were analyzed offline using the CSU Ice Spectrometer (IS). Roughly 70% of the total filters for each voyage were analyzed. The IS simulates immersion freezing, in which INPs immersed in supercooled water droplets trigger freezing at specific temperatures above homogenous freezing (≤ -38 °C). Details on sample preparation, analysis, and the mechanics of the IS can be found in Hill et al. (2016); Suski et al. (2018); Creamean et al. (2024); Testa et al. (2021), but are briefly reiterated here.

Total INPs

Total or "non treated" INP concentrations are measured by resuspending INPs from the filters by placing them in 50 ml Corning tubes with 8-10 mL of 0.1-um-filtered DI water. The tube is then placed on a Roto-Torque for 20 minutes to resuspend the particles off the filter and into the liquid solution. The resuspension is serially diluted and pipetted into 28 to 32 aliquots of 50 µL sterile 96-well PCR trays. The trays are placed in temperature-controlled aluminum blocks

inside the IS and sealed with a glass cover. A chiller reduces the temperature of the blocks at a rate of approximately 0.33 °C/minute and freezing of the wells is monitored optically by pixel monitors down to -30 °C. INP concentrations are calculated using the following equation (Vali 1971).

$$n_{INP,\ air} = \frac{\ln(1-f)}{V_{drop}} \times \frac{V_{suspension}}{V_{air}} \quad (1)$$

Equation 1 is the Vali (1971)-derived atmospheric INP concentration, where $n_{INP,\ air}$ is the atmospheric concentration of INPs, f is the fraction of unfrozen wells and V_{drop} is the volume per well, $V_{suspension}$ is the volume of the of the filter suspension and V_{air} is the volume of the air sampled as determined by the TSI flowmeters during the sample period. It is prudent to note that V_{air} is calculated in L at standard temperature and pressure (0 °C and 101.32 kPa). Sampled air volumes are normalized to the standard temperature and pressure by scaling the volume using the ambient temperature and pressure within the TSI flowmeter software. Concentration uncertainties are reported as binomial sampling 95% confidence intervals, as detailed in Agresti and Coull 1998.

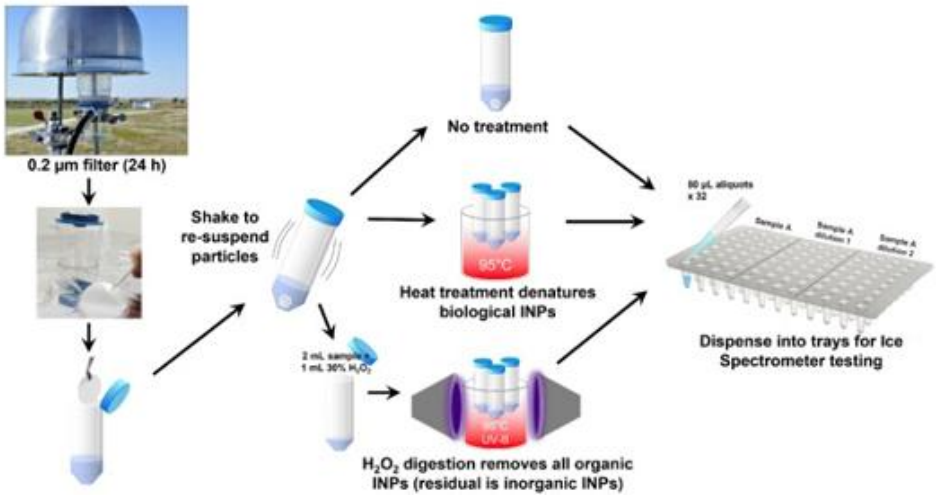

Figure 14. Ice Spectrometer workflow schematic and treatments (Adapted with permission from Dr. Christina McCluskey)

Heat-treated INPs

Data for total INPs can provide helpful insights into overall concentrations, but further information is needed to infer INP composition, which can range from biological to inorganic (Kanji et al. 2017). Treatments of the total suspensions are a helpful tool to investigate these compositions. Heat treatments yield information on heat-labile (likely proteins) contributions to the INPs measured, as heating denatures proteins associated with biological (typically bacteria and fungi) INPs (Hill et al. 2016; Suski et al. 2018). Heat treatments involved placing 2 mL of the resuspended sample in a Corning tube and immersing the tube in a boiling water bath (approximately 95 °C) for 20 minutes. The sample was then cooled to room temperature in an ice water bath, and normal IS processing procedures were followed as outlined above. The difference between the total and the heat-treated temperature spectra can be inferred as the heat-labile (proteinaceous) concentration (Figure 15).

Peroxide-treated INPs

After heat treatments, the remaining re-suspended sample is theoretically composed of heat-stable organics (carbonaceous) and inorganic (mineral) INPs. Oxidation via hydrogen peroxide and UV effectively destroys the remaining heat-stable organic components, leaving behind refractory, typically inorganic, INPs (Hill et al. 2016; McCluskey et al. 2018b. 1-2 mL of the resuspended sample were placed in a Corning tube and digested with 10% H_2O_2 in a boiling water bath and under UV light for 20 minutes. The sample was then cooled to room temperature, and catalase was added to remove the residual H_2O_2. Once the digestion had completed, normal IS procedures were followed. The resulting temperature spectra were then used to infer the inorganic INP concentrations (Figure 15).

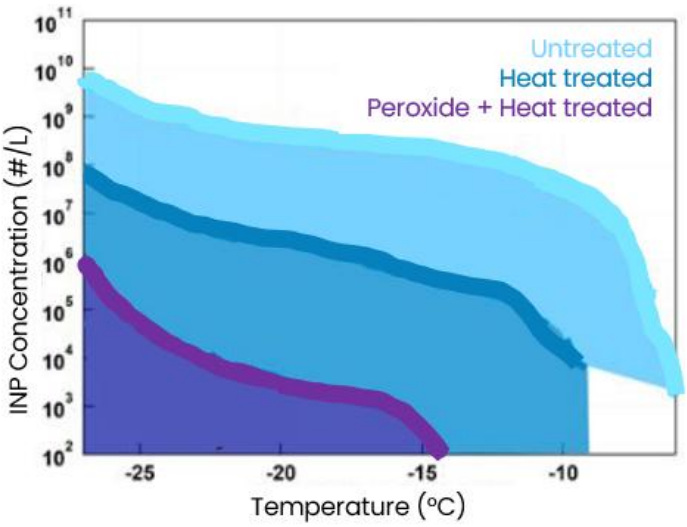

Figure 15. Example of cumulative INP spectra for untreated, heat-treated, and peroxide-treated samples from Creamean et al. (2020). Spectra are the blue dashed lines, and shaded regions indicate the heat-labile organic (light blue), bio-organic (darker blue), and inorganic (purple) concentrations.

Blank Corrections

Various blanks were collected during the voyages, with roughly 1 blank filter per week. Blanks were collected by briefly exposing INP filter units to ambient air. Blanks were processed on the IS following the same procedures listed above. Blank spectra were used to account for background INPs and possible contamination. As such, the blank spectra for each voyage were averaged and then subtracted from the total INPs. For treatments, blanks were treated in the same manner described above and the same process of subtracting blanks from the original treated spectra. All INP concentrations reported in this thesis have been blank corrected.

Due to the pristine nature of the Southern Ocean, blank corrections often substantially reduced the number of observations above detection limit. After blank correction, concentrations falling below zero at individual temperatures were discarded. MISO sample 8 was excluded from further analysis because the entire spectrum fell below zero after correction. Additionally, MISO samples 18 and 42 were discarded due to errors in handling which led to suspicious concentrations and respective spectra.

Parameterizations

McCluskey et al. (2023) demonstrated that the best approach for predicting Southern Ocean INP concentrations was to sum the contributions from sea spray (McCluskey 2018 parameterization, hereby referred to as M18) and mineral dust (DeMott 2015 parameterization, hereby referred to as D15). While we will not directly test their applicability, due to lack of needed input variables, nor sum the contributions, we will overlay the data with estimates from both parameterizations as reference lines to help guide the eye. We also use the Vignon et al. (2021) (hereby referred to as V21) piecewise parameterization to characterize coastal Antarctic INPs. The D15 parameterization is calculated using an assumed number concentration of dust particles with a diameter larger than 0.5 μm ($n_{a>0.5\mu m}$); this variable was set to 0.45 cm $^{-3}$, which is demonstrated to work as an upper limit for the Southern Ocean, following McCluskey et al. (2023). The M18 parameterization predicts the surface site density, from which INP number concentrations are calculated using an assumed surface area concentration of 40 μm^{2}cm $^{-3}$, also an upper range value for pristine marine conditions, such as in the Southern Ocean (Geerts et al. 2022; Moore et al. 2022; McCluskey et al. 2023). The D15 and M18 inputs are not accurately scaled to our data and thus predictions cannot be interpreted against our observations but are meant to provide context. Only the V21 parameterization is not dependent on aerosol measurements for normalization and can thus be interpreted against our observations.

$$N_{INP}(T_k) = (cf)\left(n_{a>0.5\mu m}\right)^{(\alpha(273.16-T)+\beta)} \exp(\gamma\,(273.16 - T_k) + \delta) \quad (2)$$

Equation 2 represents the D15 parameterization, which characterizes mineral dust INPs and is valid over the temperature range -36 °C ≤ T ≤ -17 °C. N_{INP} is the concentration of INPs in INP L^{-1}. Here, T_k is the temperature in Kelvin. In this equation, cf is the calibration factor, used

to account for instrumental biases. Fit parameters α, β , γ , and δ are 0, 1.25, 0.46, and -11.6, respectively based on the fit derived in Figure 5 of DeMott et al. (2015), which shows CFDC laboratory and field measurements from Asian and Saharan dust campaigns. Following the same fit derived from this figure, the cf is set to 1.

$$n_s(T_k) = \exp(a(T_k - 273.15) + b) \quad (3)$$

Equation 3 is the M18 parameterization which represents INPs in marine sea spray, (McCluskey et al. 2018b). T_k is the temperature in Kelvin. Fit parameters a and b are -0.545(±0.01) and 1.0125(±0.29), respectively. These fit parameters were based on measurements at Mace Head Research Station (MHD) as discussed in McCluskey et al. (2018b), indicative of pristine North Atlantic conditions. Here, n_s is the active site density. We multiply n_s by the assumed surface area site density (40 $\mu m^2 cm^{-3}$) to get N_{INP}. This parameterization is valid for the temperature range -28 °C ≤ T ≤ -16 °C.

$$\log_{10}(N_{INP}) = \begin{Bmatrix} -0.14(T - T_1) - 2.88, & if\ T > T_1 \\ -0.31(T - T_1) - 2.88 & if\ T_2 \leq T \leq T_1 \\ 0.0 & if\ T < T_2 \end{Bmatrix} \quad (4)$$

Equation 4 represents the V21 parameterization. V21 was generated using six MARCUS observations near Mawson station (67.6033 °S, 62.8742 °E) and represents Antarctic coastal concentrations. Here, T is the nucleation temperature in °C, T_1 is -21.06 °C, and T_2 is -30.35 °C. The parameterization tapers the exponential increase between temperatures, with a steeper slope between -21.06 and -30 °C and a plateau at temperatures colder than -30.35 °C. It builds on the M18 parameterization and CAPRICORN observations which noted that INP concentrations plateau at temperatures colder than -28 °C. This parameterization can be directly compared to CAISO voyage data near the Antarctic coast, since it is only temperature dependent.

2.2.3 Air Mass Trajectory Analysis

The NOAA Hybrid Single-Particle Lagrangian Integrated Trajectory (HYSPLIT) transport and dispersion model was used to calculate forward and backward air mass trajectories for the MISO voyage (Stein et al. 2015). Both backward and forward trajectories were run using the Global Data Assimilation System (GDAS) reanalysis data at 0.5° gridded resolution (Rolph et al. 2017).

Backward Trajectories

Backward trajectories were used to investigate and classify air mass origins and thereby to infer INP source regions (Creamean et al. 2013; McCluskey et al. 2018a; Creamean et al. 2022; Moore et al. 2024). These trajectories were initiated for each latitude and longitude of the ship location every 3-hours. Trajectories were run at starting altitudes of 50,100, 500, and 1000 m and were run for the duration of the voyage, with an additional 10 days before and after to accommodate a run time of 240 hours back.

Forward Trajectories

Forward trajectories were used to identify transport from source regions of interest, especially mainland continental dust sources following Neff and Bertler 2015; Li et al. 2008, and Antarctic dust sources following (Albani et al. 2012; Schüpbach et al. 2013; Gillies et al. 2013; Duprat et al. 2019). Mainland continental trajectory starting points followed those selected by Neff and Bertler (2015) and included locations within dust source regions in Argentina (49 °S, 69 °W), South Africa (28 °S, 21), Australia (29 °S, 137.5 °E), and New Zealand (43.5 °S, 172 °E). Antarctic trajectory starting points followed the dry valley dust sources in Schüpbach et al. (2013) and included Victoria Land Highlands (starting at Talos Dome 72.8 °S, 159 °E), McMurdo Dry Valleys (77.6 °S,162.9 °E), Taylor Dome (77.8 °S, 158.7°E), and Vestfold Hills

(68.55 °S, 78.25 °E). While Talos Dome and Taylor Dome are ice-covered coring sites, they were selected as starting points for our trajectories due to their proximity to major ice-free dust source regions. Ice core records from both Talos and Taylor demonstrate that dust from Antarctic ice-free regions has been advected over these sites, indicating that the domes are situated downwind of local dust-producing terrain (Albani et al. 2012; Schüpbach et al. 2013; Aarons et al. 2019). Although these records reflect past interglacial climates, the same transport mechanisms remain relevant in today's interglacial environment, making Talos and Taylor appropriate trajectory starting points to capture the influence of multiple nearby dust sources (Aarons et al. 2016; Bullard et al. 2016). Forward trajectories were used to evaluate whether transport from dust regions reached the *Investigator* during various sample periods. Trajectories were run at starting altitudes of 50,100, 500, and 1000 m and were initiated every 3 hours for 240 hours, with additional time to accommodate the 10-days forward to ship locations during each voyage. Trajectories were plotted starting 10 days back from the start of each sample period up until the end of the sample period.

Air Mass Classifications

Dominant air mass classification flags were used following Mallet et al. (2025). Air masses were classified using HYSPLIT backward trajectories, in conjunction with radon data. Antarctic air masses were identified by trajectories with mean terrain elevations above 300 m and a mean latitude of ≥ 65 °S over the preceding 120 hours (5 days back). Trajectories with a mean latitude of ≤ 45 °S and mean radon levels ≥ 100 mBq/m^3 were classified as Australian. The rest were considered Oceanic. We modified this approach by adding Boolean flags for times when air masses switched during a sampling period. Periods where air masses switched multiple times during the sample period were labelled as Mixed. Depending on the types of air masses

involved during these switch periods, there are two Mixed types: Australian & Oceanic as well as Antarctic & Oceanic.

2.2.4 Meteorological Reanalysis

ECMWF ERA5 data

The European Center for Medium-Range Weather Forecasts (ECMWF) Reanalysis version 5 (ERA5) data were used to reconstruct meteorological conditions. While the ship meteorological data can provide us with a snapshot of local meteorological conditions, reanalysis data were used to investigate the larger scale meteorology surrounding the ship and air mass transport region. Hourly data on pressure levels 100, 250, 300, 500, 700, 850, 925, 1000 hPa were selected for the duration of the voyage for the following variables: vertical velocity (Pas^{-1}), divergence (s^{-1}), U and V wind components (ms^{-1}), relative humidity (%), potential vorticity ($m^2s^{-1}Kkg^{-1}$), and relative vorticity (s^{-1}). Hourly data on single levels were used to extract mean sea level pressure (Pa), surface pressure (Pa), wave height (m) and swell (m), and total precipitation (m) for the duration of the voyage. Grids were created using the latitude and longitude midpoints of each sample period and adding ± 5° bounds to either side of the midpoint. Reanalysis data were extracted for each sampling period within the designated grid.

NASA MERRA-2 data

Parcel forward and backward trajectory panel plots with parcel temperature (°C), pressure (hPa), relative humidity (%), wind speed (ms^{-1}), at 10m AGL) vertical velocity (cms^{-1}),), parcel height (km), precipitation rates (total and snow in mm/hr) along parcel track, were made by Sally Benson (Dr. Jay Mace, University of Utah) using NASA Modern-Era Retrospective analysis for Research and Applications, version 2 (MERRA-2) data, following Mace et al. 2024. Plots have been used with permission and adapted to represent filter sample periods.

3. RESULTS AND DISCUSSION

3.1 Ice Nucleating Particle Observations from CAISO Compared to Past Voyages and Existing Ice Nucleation Parameterizations

We will address the first research question by analyzing observations from the SOTS, SWOT, and MISO voyages and comparing the resulting INP cumulative temperature spectra with those from previous voyages. Following a standard approach, we will examine the full spectra across all sampled latitudes. As discussed in Chapter 2, M18 and D15 parameterization predictions shown on plots of CAISO data are meant to guide the eye, not to be representative of CAISO voyage conditions. The V21 parameterization provides the number concentration of INPs (N_{INP}) directly, allowing for more direct comparison for CAISO voyages.

INP concentrations from CAISO are comparable to other studies in the Southern Ocean as illustrated in Figure 16 (McCluskey et al. 2018a; Schmale et al. 2019; Welti et al. 2020; McFarquhar et al. 2021; Tatzelt et al. 2022; Moore et al. 2024). While many marine regions have comparable INP concentrations, high-latitude Southern Ocean concentrations were low by nearly 2 orders of magnitude compared to other marine locations (Welti et al. 2020). MARCUS had slightly higher concentrations at temperatures above –24 °C than the CAISO voyages, but these still fell within the ranges previously reported by Welti et al. (2020).

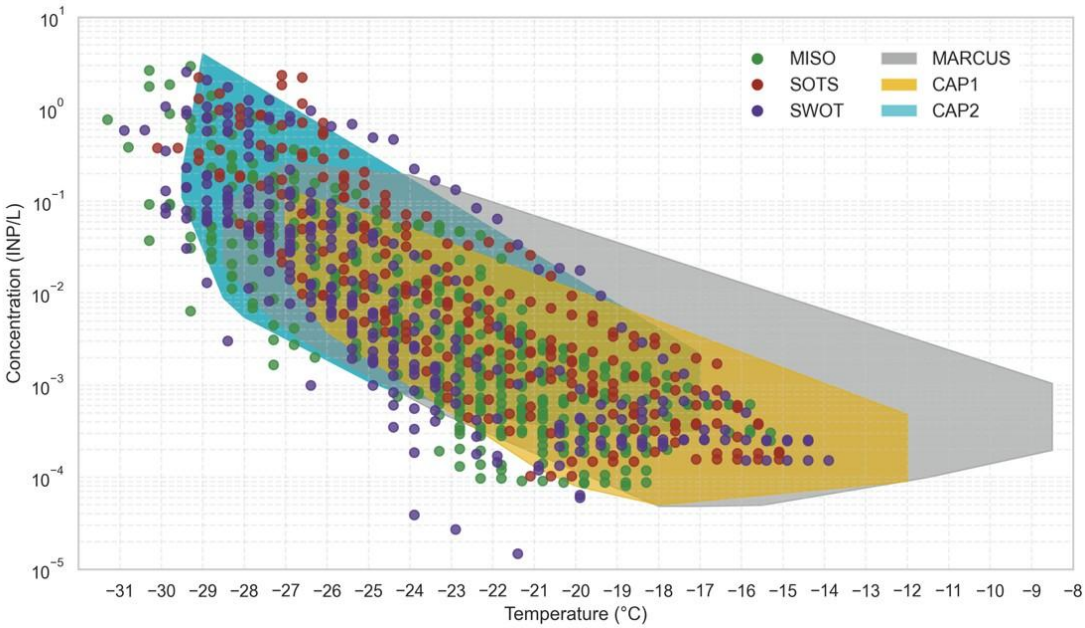

Figure 16. Cumulative INP spectra (in units of INP L^{-1}) from CAISO voyages (SOTS, SWOT, MISO), overlaid on polygons indicating concentration ranges reported in previous voyages, including MARCUS and CAPRICORN I and II (CAP1 and CAP2, respectively).

As shown in Figure 17, a closer examination of the CAISO cruises reveals distinct differences among voyages. SOTS consistently exhibited the highest INP concentrations, SWOT generally displayed lower concentrations except for one outlier, and MISO displayed a large spread in concentrations similar to both SOTS and SWOT combined. Comparisons with existing parameterizations highlight important discrepancies. Neither D15 nor M18 adequately capture the shape of the CAISO spectra, which displays an increased slope near – 21 to – 30 °C.

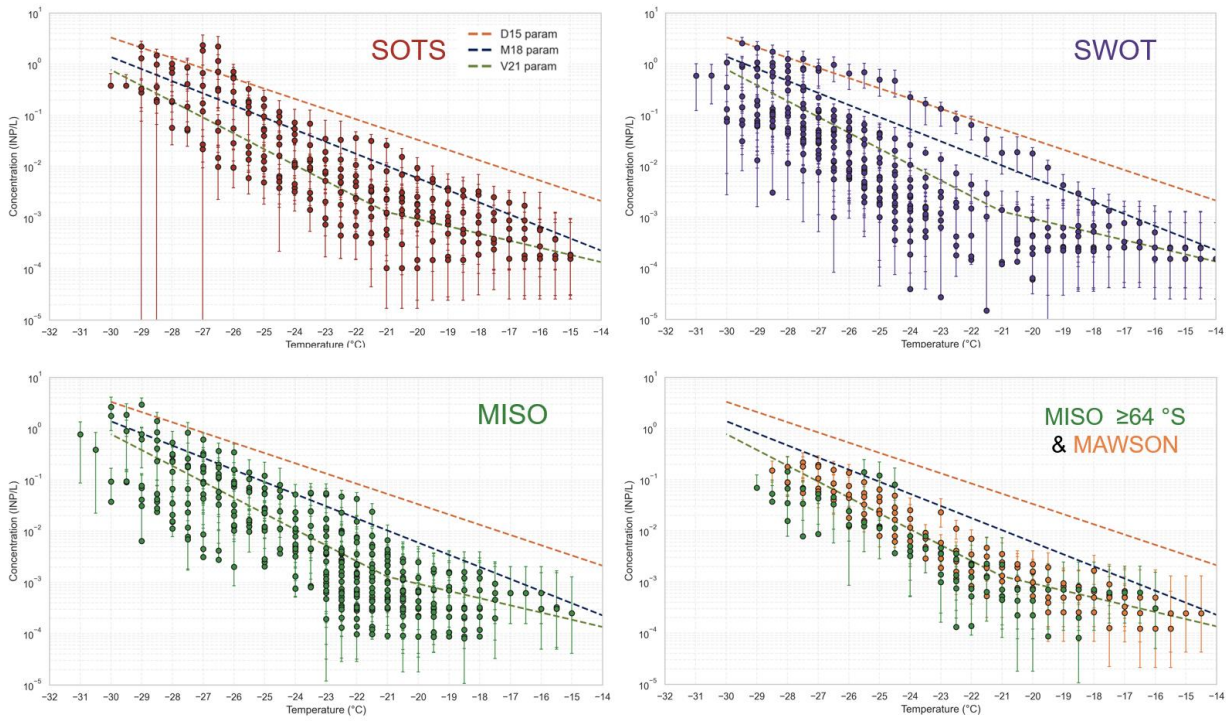

Figure 17. Cumulative INP spectra from SOTS (top left), SWOT (bottom left), MISO (top right), and MISO samples collected south of 64 °S near the Antarctic coastline (bottom right), plotted alongside ice nucleation parameterizations from DeMott et al. 2015 (D15; dust from laboratory and field observations), McCluskey et al. 2018b (M18; marine sea spray from the remote North Atlantic), and Vignon et al. 2021 (V21; Mawson Station, coastal Antarctica). The bottom right panel additionally includes MARCUS data from Mawson Station, Antarctica used to develop the V21 parameterization. Vertical bars indicate 95% confidence intervals.

When focusing on MISO samples collected along the Antarctic coast (south of 64 °S; Figure 17, bottom right), the only CAISO voyage with sufficient coastal coverage, a more direct comparison with V21 is possible. The V21 parameterization aligns closely with the coastal MISO and Mawson data, successfully capturing both the concentration and the shape of the spectra. Overall, the V21 parameterization captures the shape of the INP spectra well across all voyages, and most accurately captures the concentrations in coastal regimes like SOTS and high-latitude MISO, MARCUS (Vignon et al. 2021). However, it is apparent that lower concentrations within some of these voyages, as seen in SWOT and MISO, fall below V21 and may require a different approach to parameterize.

3.2 Southern Ocean Latitudinal Sectors that Define INP Concentrations

In this section, we address the second research question: Are there latitudinal differences in the sources and abundance of INPs over the Southern Ocean? As discussed in Figure 17, there is a distinct difference in costal concentrations and lower-latitude voyages like SOTS display the highest INP concentrations. Meanwhile, mid-latitude voyages such as SWOT display some of the lowest concentrations, even compared to the high-latitude voyages like MISO. To investigate whether latitudinal gradients in INP exist, we separated the Southern Ocean into three sectors: the Extra-Antarctic Southern Ocean (ESO; latitudes from 30 to 45 °S, herein denoted as ≤ 45 °S), the Sub-Antarctic Southern Ocean (SSO; latitudes between 45–60 °S), and the Antarctic Southern Ocean (ASO; latitudes from 60 °S extending to the Antarctic coastline, herein denoted as ≥ 60 °S). We base these latitude distinctions on the varying dynamics discussed previously (Figure 1), and following the Humpries et al. (2021, 2023) discussion of the Atmospheric Compositional Front of Antarctica (ACFA) that was observed at about 60 °S. Humphries et al. (2021, 2023) and Niu et al. (2024) also discuss other latitudinal boundaries such as the transition of boundary layer marine aerosol at 60-65 and 62°S, respectively, further indicating the need to separate the high-latitude Southern Ocean in our analysis.

3.2.1 Latitudinal and Seasonal Comparison Between All Voyages

Seasonal and latitudinal INP concentrations at four freezing temperatures are compiled for SWOT, SOTS, MISO, MARCUS, and CAPRICORN I and II in Figure 18 (see

Table 3 for further details). Only austral spring, summer, and autumn are shown, as no winter data currently exist. Most observations were made during summer, with more limited coverage in spring and autumn; thus, we focus here on comparisons during austral summer. The

central feature is the pronounced divergence in INP concentrations for MISO and slight divergence for MARCUS and CAP2 at colder freezing temperatures within the ASO (i.e., concentrations at –27, and –28.5 °C in the ≥ 60 °S sector). Concentrations across other latitude bands and warmer temperatures remain broadly comparable between all CAISO voyages and the prior studies shown. To statistically confirm the observed differences in concentration across latitude bins, Welch's t-tests were performed on average log-scale INP concentrations for each latitude bin at each of the identified temperatures. Significant differences ($p < 0.05$) were identified between all three sectors ESO (≤ 45 °S), SSO (45-60 °S) and ASO (≥ 60 °S) at –27 °C (ESO and SSO $p = 1.06 \times 10^{-5}$, ESO and ASO $p = 7.97 \times 10^{-13}$, SSO and ASO $p = 6.64 \times 10^{-6}$) and –28.5 °C (ESO and SSO $p = 3.01 \times 10^{-3}$, ESO and ASO $p = 4.69 \times 10^{-6}$, SSO and ASO $p = 1.45 \times 10^{-7}$). The greatest observed difference was between the ASO (≥ 60 °S) and ESO (≤ 45 °S) sector INP concentrations at both temperatures.

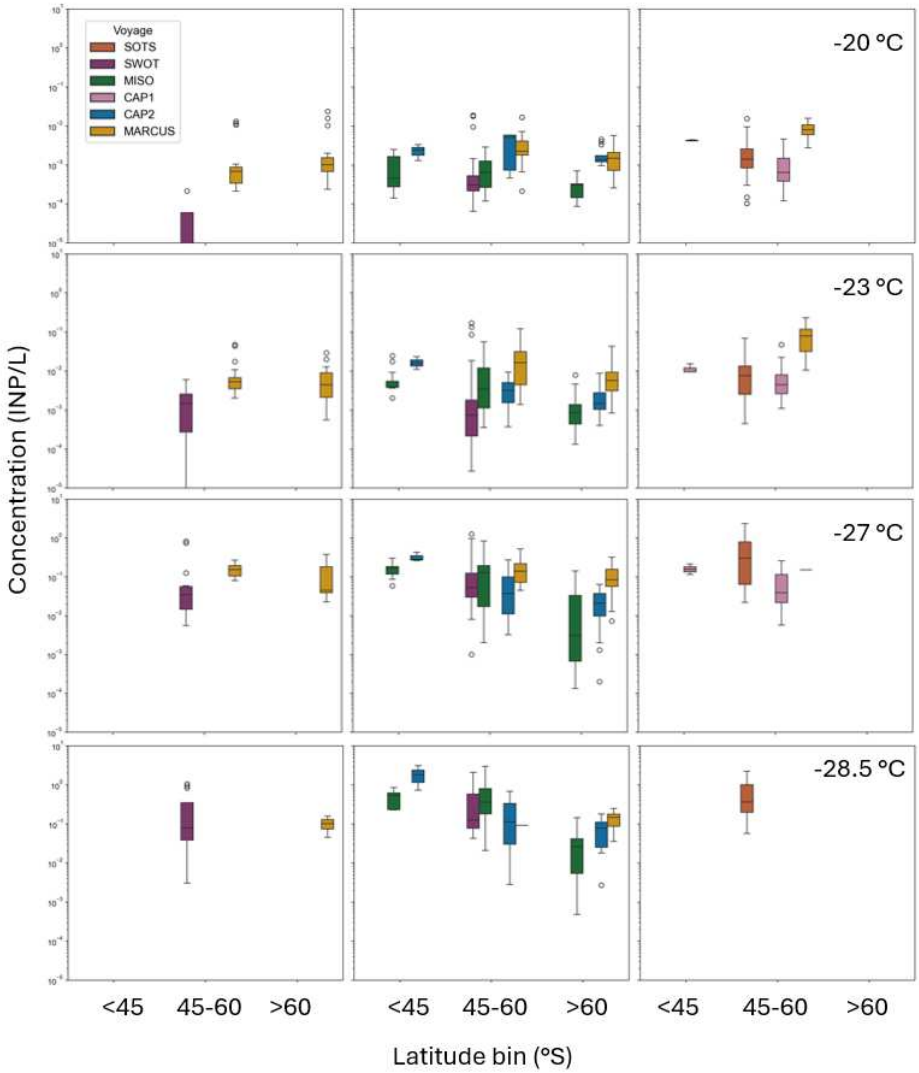

Figure 18. CAISO and past voyage INP concentrations shown as box-and-whisker plots by season (austral spring: September–November; summer: December–February; autumn: March–May) across three latitude sectors (≤ 45 °S, 45–60 °S, ≥ 60 °S) for freezing temperatures of –20, –23, –27, and –28.5 °C. Each box incorporates concentrations at the target temperature as well as the two nearest half-degree measurements. The middle line represents the median, box edges indicate the 25th and 75th percentiles, and whiskers extend ±1.5× the interquartile range. Outliers are shown as individual points. Boxes are colored by voyage, as indicated in the legend.

Table 3. Summary of the temporal and spatial coverage of selected voyages relevant to Figure 18.

Voyage	Dates	Latitudinal extent (°S)	Longitudinal extent (°E)
MARCUS	29 Oct 2017- 1 April 2018	43-70	90-150
CAP1	1 Mar – 5 Apr 2016	43-53	140-145
CAP2	11 Jan – 21 Feb 2018	43-66	130-150
SOTS	12 May – 25 May 2023	43-47.5	139-147.5
SWOT	15 Nov – 20 Dec 2023	43-57	147-154.5
MISO	5 Jan – 5 Mar 2024	43-67	112-147.5

CAISO voyage data reveal a clear latitudinal gradient at colder temperature INP concentrations across the Southern Ocean (Figure 19). Overall, concentrations were lower at colder temperatures in the ASO compared to the SSO and ESO. Within the ASO, values generally remained low but showed a slight increase closer to the Antarctic coast. Another notable feature is a decrease in concentrations near ~50–55 °S region, potentially linked to the polar jet and its associated frontal boundary, though this warrants further investigation (see Future Work Section). Current parameterizations based on spectra aggregated across all latitudes fail to capture important sector-specific variability, highlighting the need for more sector-specific analysis.

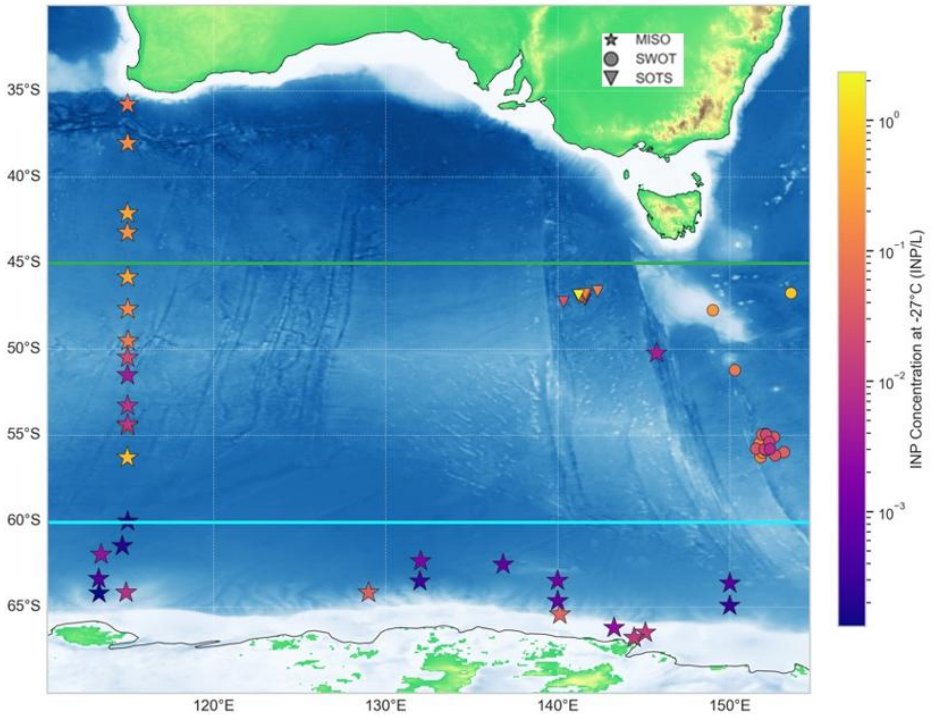

Figure 19. CAISO (SOTS, SWOT, MISO) INP concentration gradients at a freezing temperature of –27 °C. Bathymetry and topography are same as in Figure 5. Solid green and teal lines indicate the 45 °S and 60 °S latitude boundaries, respectively.

The remainder of this thesis will focus on MISO, since it was the only voyage to span all latitude sectors. Along the MISO ship track (Figure 20), the highest INP concentrations were

observed in the SSO (up to 2.6 INP L^{-1} at –30 °C), followed by the ESO (up to 1.77 INP L^{-1} at –30 °C), particularly at the coldest freezing temperatures where concentrations were greatest and most distinct. The lowest concentrations were observed in the ASO (up to 6.9×10^{-2} INP L^{-1} at –30 °C). It is important to note that fewer samples were collected during leg 1 along the transit to Antarctica, as the primary focus of the voyage was on legs 2 and 3.

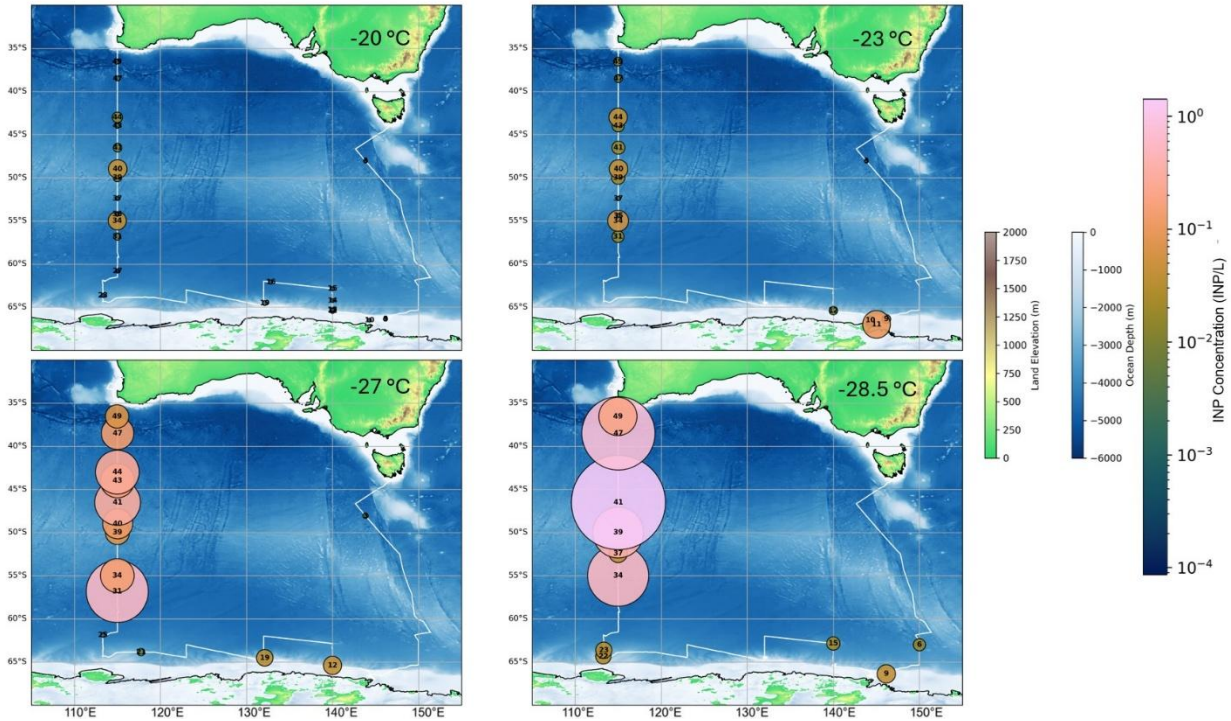

Figure 20. MISO total INP samples along the ship track (white), colored by concentration (INP L^{-1}, see color bar) and circles scaled by circle size, at freezing temperatures of –20, –23, –27, and –28.5 °C. Numbers inside circles indicate sample IDs. Bathymetry and topography are shown in Figure 5.

3.2.2 INP Concentrations by Air Mass Type

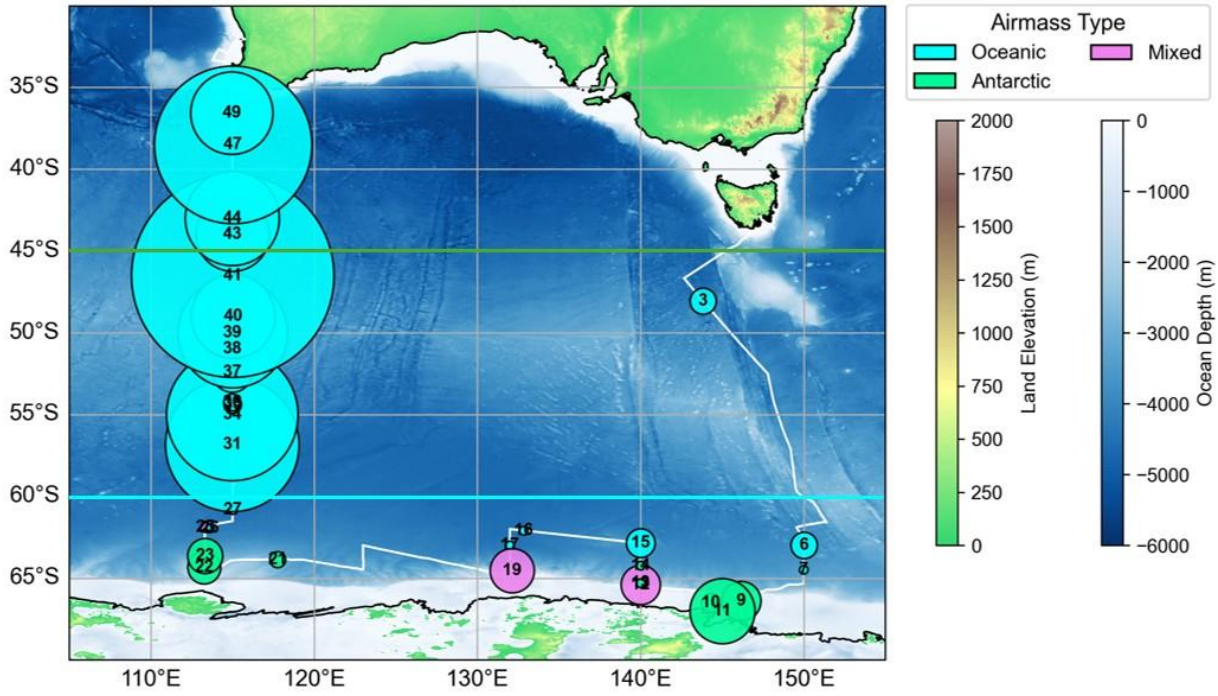

Figure 21. MISO total INP concentrations at a freezing temperature of –28.5 °C along the ship track (white), categorized by air mass type. Solid green and teal lines indicate the 45 °S and 60 °S latitude boundaries, respectively. Circle sizes correspond to the same concentrations as in the –28 °C panel of Figure 20 with colors matching the Figure 20 concentration color bar. Numbers inside circles indicate sample IDs. Bathymetry and topography are shown in Figure 5.

Air mass classifications were used to help diagnose potential aerosol and INP sources (Mallet et al. 2025). Figure 21 shows the results from the combined air mass trajectory and radon analysis. Five dominant air mass types were identified: Australian, Oceanic, Antarctic, and two Mixed categories (Antarctic–Oceanic and Australian–Oceanic). Australian air masses were only detected for samples 50–52, which were not analyzed on the IS and are therefore not presented here. Most samples were classified as Oceanic, including nearly all leg 3 transect samples north of 60 °S, which also coincided with the highest INP concentrations. Within the ASO, most air masses were classified as Antarctic, although several Oceanic and Mixed cases were observed. Mixed Antarctic and Oceanic airmasses typically occurred when samples were collected over extended periods (48–72 hours). These longer periods coincided with transitions between

Oceanic and Antarctic air masses throughout these periods. Notably, relatively higher INP concentrations within the ASO tended to correspond to Antarctic or Mixed (Antarctic–Oceanic) air masses.

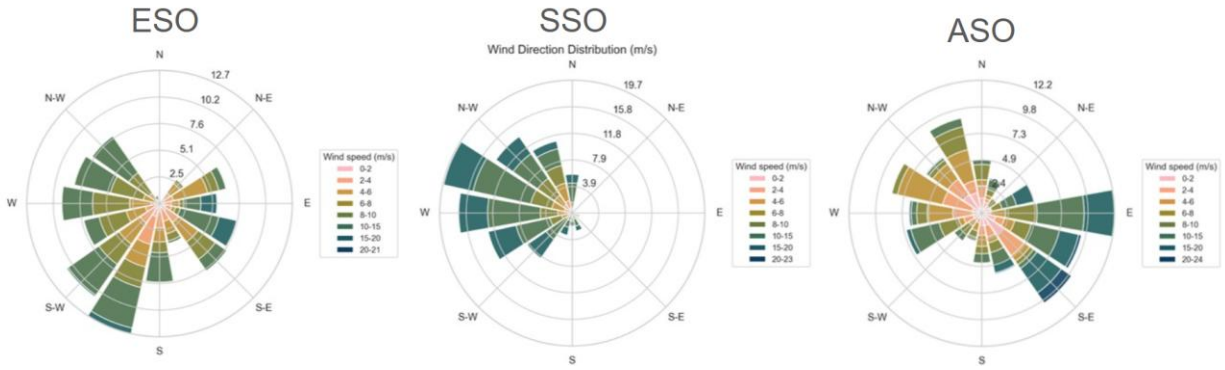

Figure 22. Wind rose showing wind direction distribution (radial spokes) and speed (color, m s⁻¹), taken from Investigator data during the entire duration of MISO and separated by latitude sector. Letter labels indicate cardinal directions, and the length of each sector to the concentric circles represents the normalized frequency of observations (percentage).

Wind patterns varied markedly across the Southern Ocean sectors, influencing the types of air masses and potential aerosol sources encountered (Figure 22). In the ESO, winds were predominantly from the south to southwest during MISO, steering air masses largely from midlatitude continental or marine regions. Moving poleward into the SSO, the circulation was dominated by strong westerlies, with mean wind speeds increasing relative to the ESO. In the ASO, the circulation shifted to predominantly easterly winds, which were more variable in both direction and magnitude, with the strongest winds experienced in this sector. These distinct wind regimes are critical, as they shape the origin, composition, and transport of air masses, thereby exerting strong controls on the availability and characteristics of INPs across each sector.

3.2.3 INP Treatments by Latitude Sector

To elucidate INP composition, heat and peroxide treatments were performed on approximately one-third of the samples. Inorganic contributions to INPs, likely indicative of

mineral dust, were the focus of these analyses. Samples were selected based on notable INP spectral features, prevailing meteorological conditions, or proximity to the Antarctic coastline within the ASO. The low concentrations of total INPs complicated the treatment process and often made it difficult to clearly distinguish between treatment and base spectra. Treatment results were considered significant if they differed from the unamended concentration by more than 1.64 times the propagated uncertainty, corresponding to 95% confidence under a one-tailed test, following McCluskey et al. (2018a). The one-tailed approach assumes that treatment concentrations should decrease relative to the unamended sample, although ASO spectra showed increases in concentration after treatment in some cases. These anomalies were treated as insignificant under this criterion. Future work may investigate these anomalies further. Here we present a subset of spectra selected based on data quality and interpretability; unusable spectra were excluded.

Figure 23 presents representative results from the treatment data within the ASO. Samples 9 and 10 displayed predominantly inorganic signatures as indicated by the lack of significant difference between the treatments and unamended spectra. These samples were associated with Antarctic airmasses as indicated in Figure 21. Sample 12 was classified as a mixed (Antarctic and Oceanic) air mass sample and exhibited an inorganic signature up to –23 °C, transitioning to a more heat-stable organic signature at colder temperatures. Sample 19 was also classified as a mixed air mass sample and showed a primarily heat-labile organic signature, with some heat-stable organic contribution at the cold end. Each sample was classified based on the majority of statistically significant INPs; for example, sample 12 was classified as inorganic because most freezing temperatures showed no statistically significant change in

concentration after treatment. Full treatment spectra for additional select days are provided in the appendix.

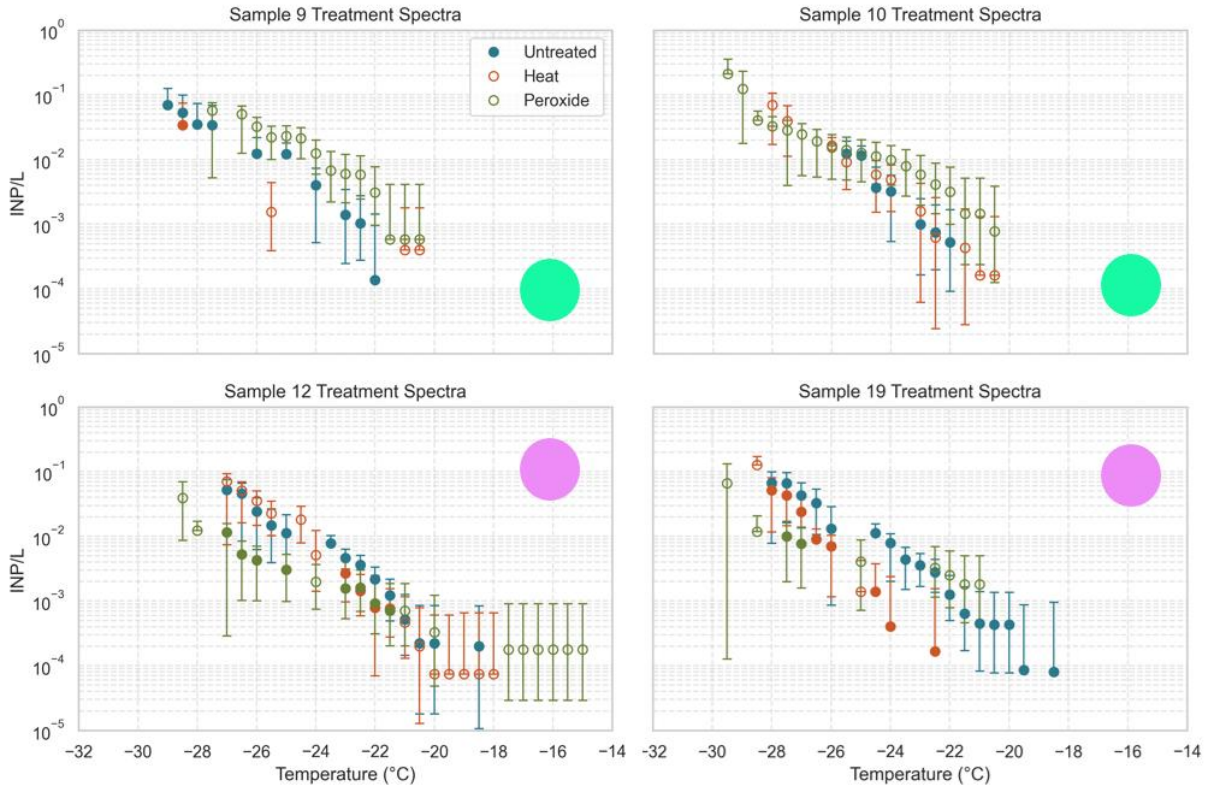

Figure 23. Selected representative INP spectra within the ASO showing total (blue), heat-treated (red), and heat + peroxide-treated (green) values. Heat and heat + peroxide values are filled only if the treatment differed significantly from the unamended value (Z >1.64, corresponding to a 95% confidence under a one-tailed test). Vertical bars represent 95% confidence intervals. Inlaid circles indicate air mass classifications corresponding to Figure 21. MISO total INP concentrations at a freezing temperature of –28.5 °C along the ship track (white), categorized by air mass type. Solid green and teal lines indicate the 45 °S and 60 °S latitude boundaries, respectively. Circle sizes correspond to the same concentrations as in the –28 °C panel of Figure 20 with colors matching the Figure 20 concentration color bar. Numbers inside circles indicate sample IDs. Bathymetry and topography are shown in Figure 5.: light green = Antarctic, purple = Mixed (Antarctic–Oceanic).

Selected treatment samples from the SSO (samples 31, 40, 41) and ESO (sample 44) are shown in Figure 24. These samples were largely influenced by oceanic air masses and treatment impacts are notably different than for the spectra from the ASO. These spectra exhibited heat-labile signatures as seen in samples 40, 41, and 44, where the INP concentrations in the heat-treated spectra significantly decreased from the total. Often, peroxide treatments had little to no effect on these samples at the coldest temperatures, but the lack of data at the warmest

temperature indicates this treatment eliminated all INPs at those temperatures, meaning they were heat-stabile organics (sample 40). An exception was sample 31, which displayed an inorganic signature up to –26 °C before transitioning to a heat-labile signature at colder temperatures. However, this is an unusual signature for an oceanic airmass sample, and it is not clear what might have caused this. We characterized this sample as primarily inorganic.

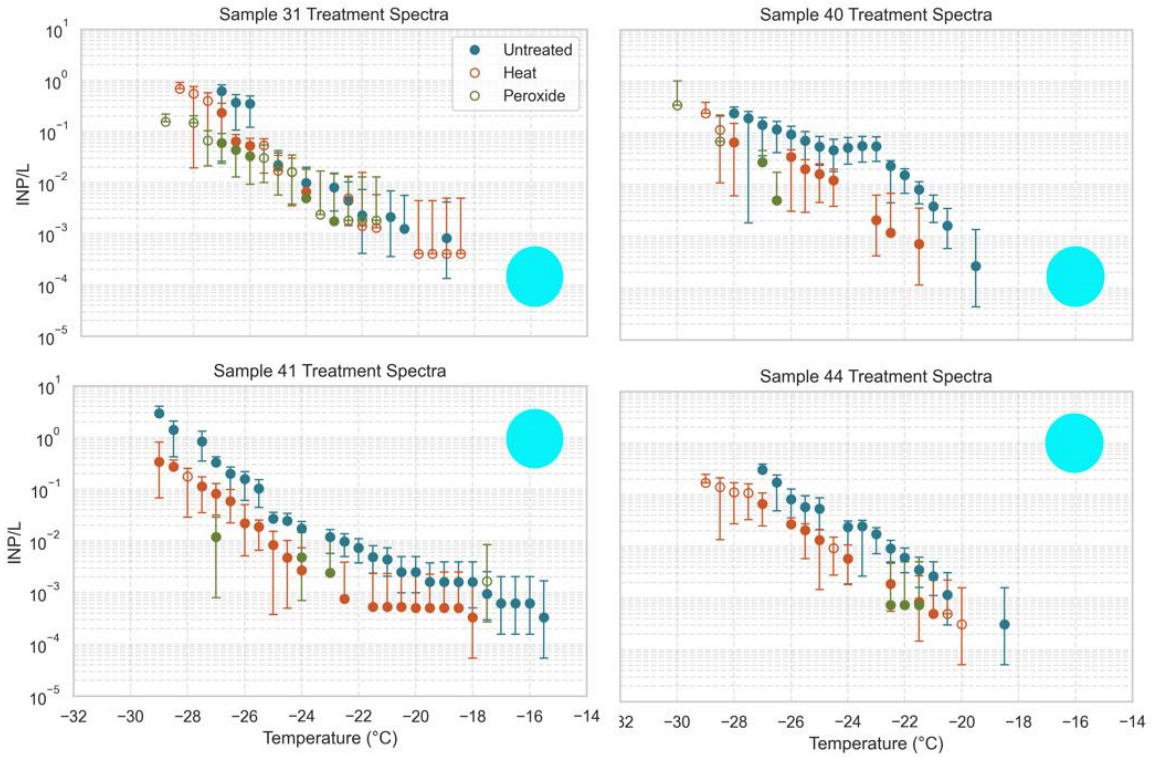

Figure 24. Same as Figure 23 but for selected representative spectra within the SSO and ESO. Inlaid circles indicate air mass classifications corresponding to Figure 21: light blue = Oceanic air mass classification.

A clear spatial pattern emerged between organic (heat-labile and heat-stable) and inorganic (likely mineral dust) INPs across the Southern Ocean, as shown in Figure 25. Within the ASO, samples associated with Antarctic or mixed (Antarctic–Oceanic) air masses generally displayed inorganic signatures, particularly near the Antarctic coastline. In contrast, oceanic air masses in the ESO and SSO were predominantly associated with organic signatures. Sample 31 was unique in that it was just north of the boundary for the ASO but was classified as inorganic.

The cause of this is described in more detail in the following section (3.3). However, these treatment results are generally consistent with the air mass analyses.

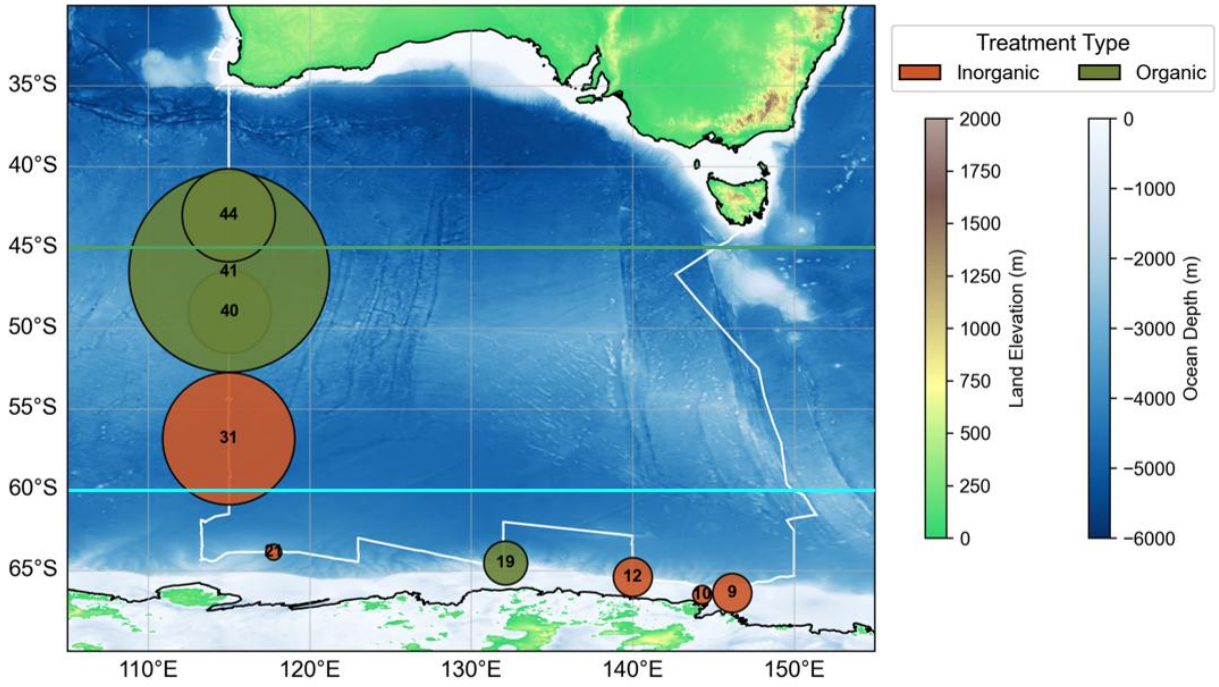

Figure 25. Same as Figure 21, but instead the circles are colored by dominant treatment INP identification type. Only samples that were subject to INP treatments are shown.

To answer research question 2, MISO data indicate that there are gradients in INP abundance and concentration across latitudes. The ASO had the lowest INP concentrations. The highest concentrations at cold temperatures were seen in a few spectra from the SSO, but concentrations were consistently higher across all temperatures in the ESO. The ESO and SSO samples were dominated by oceanic air masses and, thus, spectra exhibited organic and heat-labile signatures, as also found by McCluskey et al. (2018a) for CAPRICORN samples. On the other hand, the ASO was dominated by Antarctic air masses and the spectra displayed more inorganic signatures. As each of the sectors displayed distinct sources and prevailing meteorology, investigating INPs by sector helped to isolate sector-specific air masses and dominant INP types. The potential sources of these INPs will be discussed in the following section.

3.3 Antarctica as a source of INPs to the Southern Ocean

Although INP concentrations are generally low across the Southern Ocean, they exhibit clear sectoral variability, reflecting distinct regional dynamics. In the ESO, the presence of land masses modifies wind patterns and terrestrial sources can contribute to INP concentrations. Roughly centered around 50-55 °S, in between the SSO and ASO, the meandering polar jet stream helps to isolate the Antarctic continent. These circulation patterns can influence the transport of non-marine and sea spray INP sources, particularly south of 60 °S. Consequently, it is essential to evaluate the Antarctic continent's contributions to INPs within the ASO. This section therefore addresses the third research question: What are the main sources of INPs observed in the atmospheric boundary layer over the high-latitude Southern Ocean and coastal Antarctica?

Previous studies have demonstrated the outflow of continental Antarctic air and its impact on aerosol-cloud interactions in the high-latitude Southern Ocean (Uetake et al. 2020; Humphries et al. 2021; Tatzelt et al. 2022; Humphries et al. 2023; Mace et al. 2024). We focus on mineral dust here because that is the most likely source of INPs coming from the Antarctic continent, particularly from sediment-laden, ice-free regions such as coastal dry valleys that are prone to transport by the winds (Albani et al. 2012; Schüpbach et al. 2013; Gillies et al. 2013; Neff and Bertler 2015; Duprat et al. 2019; Corkill et al. 2025). While these locations are selected for their mineral dust potential, it is important to note that these exposed, ice-free areas can also provide microbial and other biogenic sources of INPs (Bottos et al. 2014; Panwar et al. 2022; Xu et al. 2023; Chelliah et al. 2024). Modeling transport from these ice-free regions of Antarctica is of interest to INP budgets, as both mineral dust and biogenic material can serve as INPs. Further, ice-free regions of Antarctica are expected to grow substantially in the next century due to the rapidly

changing climate (Lee et al. 2017), and hence their importance as potential INP sources may increase.

3.3.1 Limited Transport from Non-Antarctic Continental Sources

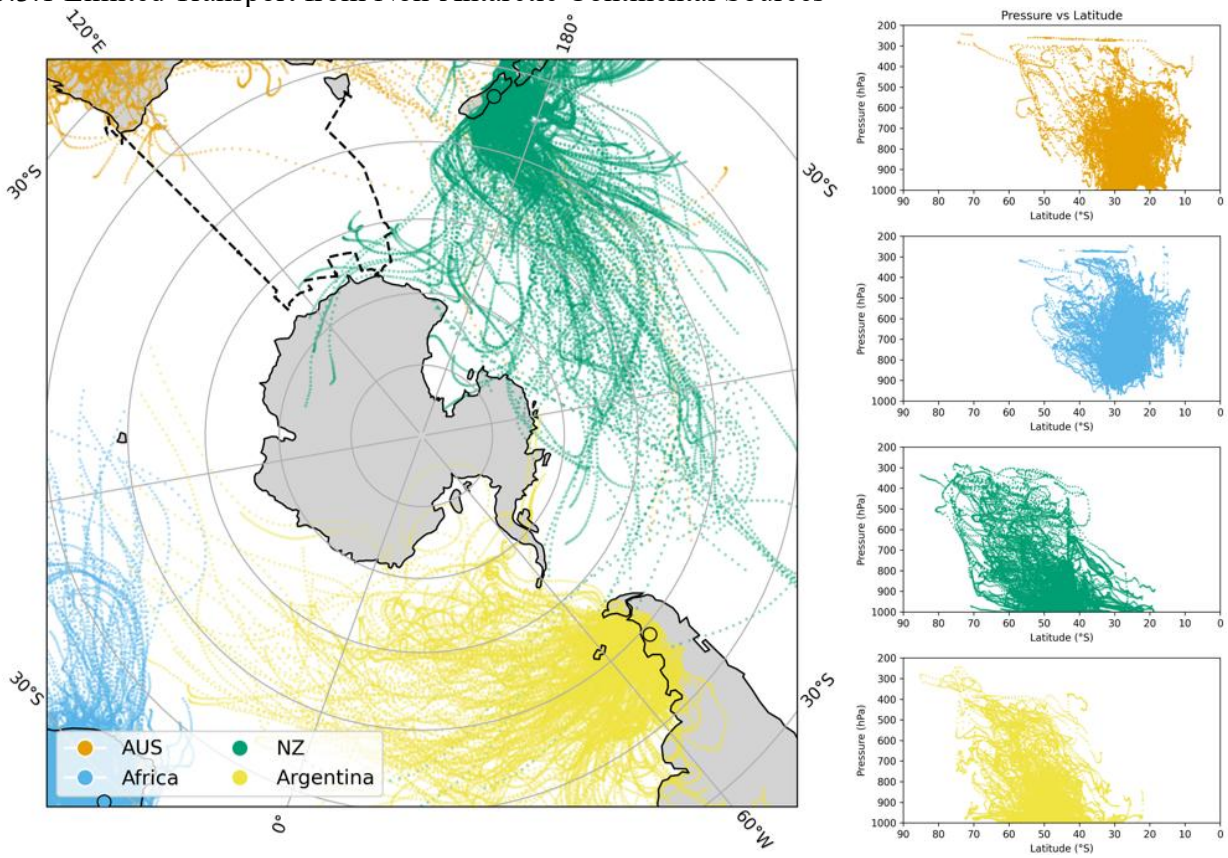

Figure 26. (Left panel) 5-day forward trajectories initiated at 100 m for MISO voyage days and originating from point sources representing four terrestrial dust sources: Argentina (yellow), South Africa (blue), Australia (AUS, orange), and New Zealand (NZ, green). MISO ship track shown as a dashed black line. (Right panel) Pressure-altitude (hPa) cross sections by latitude (°) for the same trajectories shown on the left.

Five-day forward trajectories were calculated for the entire voyage (5 January–3 March 2025) from the key continental dust sources defined by Neff and Bertler (2015) for the Southern Ocean and Antarctica (Figure 26). Although MISO took place during the austral summer, when the jet is historically weakest and more zonal (Figure 2), the westerlies were still strong enough to transport much of the lower-latitude continental air masses clockwise around the ASO rather than toward the continent, except for easterly trajectories originating from New Zealand (Figure

26). Additionally, Australian and African air masses remained lofted to upper levels of the troposphere, indicating that deposition to the surface was unlikely even if the transport made it to the sample region. Argentinian and New Zealand air masses did have some residence time in the lower boundary layer and/or intercepted the surface, but only a few trajectories from New Zealand arrived at our sampling region. While these source regions are not representative of all potential continental atmospheric transport, it is clear that the dominant lower-latitude dust sources discussed in Neff and Bertler (2015), were unlikely to represent a large contribution to the aerosol sampled during MISO.

3.3.2 Continental Antarctic Tracers and Transport Pathways

To identify days influenced by Antarctic air masses, we analyzed atmospheric Radon-222 (^{222}Rn) following Mallet et al. (2025) (Figure 27). Continental Australian influence was evident in the prominent Radon-222 peaks observed at the beginning and end of the voyage. Aside from these Australian signals, four notable peaks were observed within the ASO sector, ranging from approximately 230–350 mBq m^{-3}. Detailed information on dates, times, locations, Radon-222 values, and corresponding INP samples for these peaks is provided in Table 4.

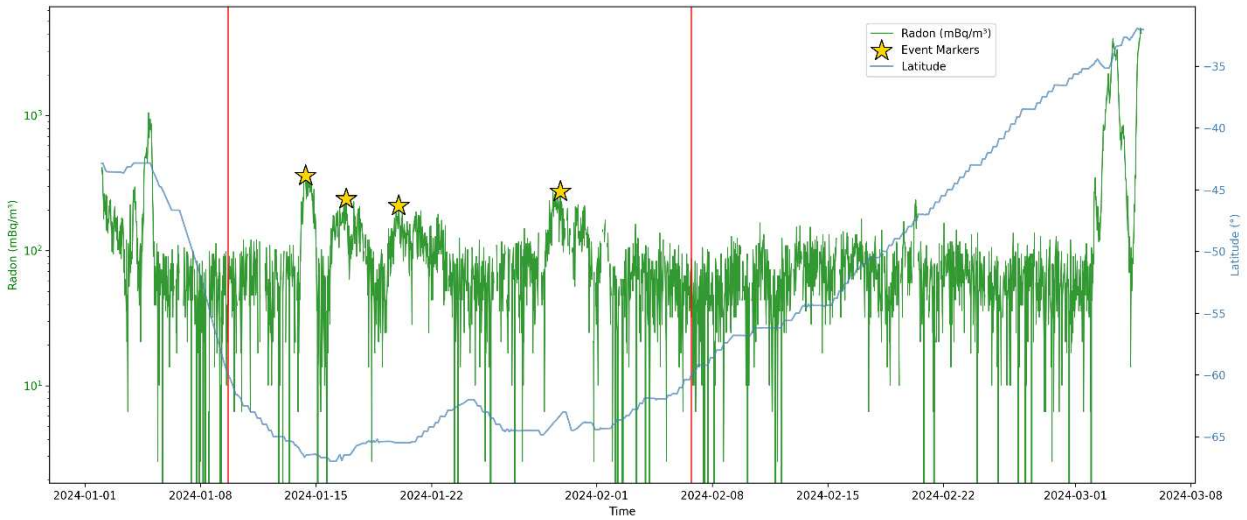

Figure 27. Atmospheric Radon-222 (^{222}Rn; mBq m^{-3}, green) and MISO ship latitude (°S, blue). Red horizontal lines mark the boundaries of the ASO (≥ 60 °S), and stars indicate ^{222}Rn peaks observed within this sector.

Table 4. Atmospheric Radon-222 peaks within the ASO (≥ 60 °S) during MISO leg 2 along the Antarctic coast.

Event Date & Time (UTC)	Corresponding INP Sample	Ship Latitude (°S)	Ship Longitude (°E)	Radon-222 (mBq/m^3)
20240114 1430	9	66.46538	144.93662	351.12
20240117 0700	11	66.04831	144.13424	230.10
20240120 0530	12	65.47416	140.31180	241.11
20240129 1900	19	63.27784	124.32173	274.11

Although our analysis indicated that long-range transport from continents other than Antarctica was infrequent during MISO (Figure 26), Rn-222, with a half-life of approximately 3.822 days, could still be detected following long-range advection (McCluskey et al. 2018a; Mallet et al. 2025). While the half-life is on the shorter end of long-range transport estimates which suggest 3-10+ days to reach East Antarctica (Li et al. 2010; Gassó et al. 2010; Neff and Bertler 2015), we cannot completely rule out lower-latitude sources based on these data alone. To better constrain the source of the Rn-222 spikes, we re-ran forward trajectories, adding local ice-free Antarctic regions known to contribute dust to East Antarctica (Figure 28). We identified four dominant source regions: Vestfold Hills, Victoria Land Highland (Talos Dome), Taylor Dome, and the McMurdo Dry Valleys (Albani et al. 2012; Schüpbach et al. 2013; Gillies et al. 2013; Duprat et al. 2019). These four source locations are expansive regions with exposed sediments and dry, windy conditions that can promote local transport. The locations were chosen based on their spatial extent, history of contribution to dust, and proximity to the MISO sample locations.

Forward trajectories during the MISO voyage indicated frequent transport from the selected Antarctic source regions to the ship track up to 50 °S. Trajectories from Talos Dome, Taylor Dome, and the McMurdo Dry Valleys were predominantly advected by polar easterlies, except above 60 °S, where they shifted back to westerly flow. Transport from Vestfold Hills was primarily westerly. All Antarctic point sources descended to 800–1000 hPa between 50–70 °S,

placing them well within the lower boundary layer and accessible for ship-based sampling. Thus, we conclude that the atmospheric Radon-222 peaks observed in the ASO sector were most likely Antarctic in origin.

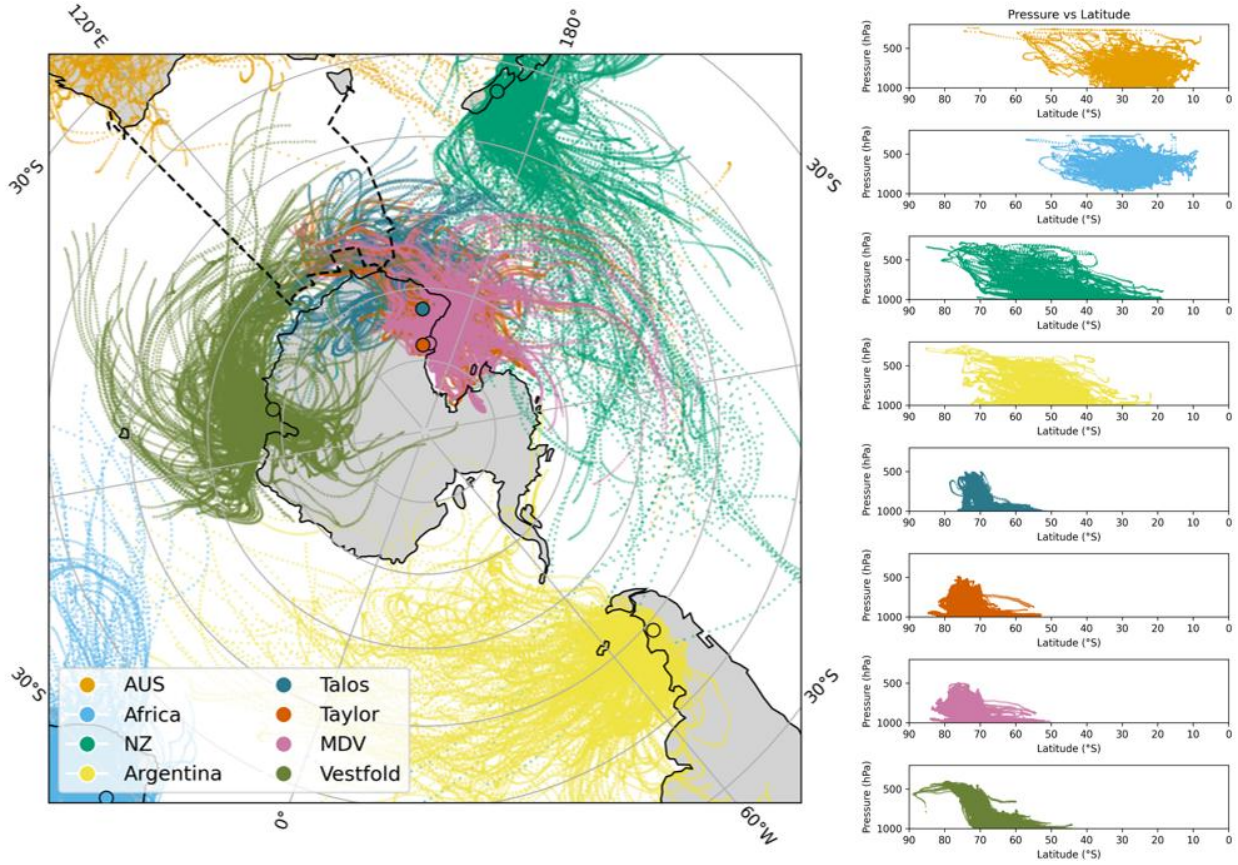

Figure 28. Same as Figure 26 but including back trajectories from Talos (Victoria Land highlands), Taylor, McMurdo Dry Valleys (MDV), and Vestfold Hills (Vestfold) during MISO.

3.3.3 Evaluation of Antarctic versus Open Ocean Case Days

Case day investigations were performed for select samples of interest, determined from the treatment spectra. A summary of our findings is shown in Table 5. For samples 40, 41 and 44, the dominance of organic INPs in oceanic air masses from the ESO and SSO aligned with previous studies (Bigg 1973, 1990; Wilson et al. 2015; DeMott et al. 2016; McCluskey et al. 2018a; Sanchez et al. 2021; Zhao et al. 2021; Tatzelt et al. 2022; Moore et al. 2024). Sample 19, collected within the ASO and associated with mostly organic INPs, was classified as a mixed

(Antarctic and Oceanic) air mass type. In this case, the sample was likely more influenced by the oceanic component. Samples 9, 10, 12, dominated by inorganic INPs and Antarctic or mixed air mass origins, are likely influenced by dust from Antarctic sources. Interestingly, inorganic INPs were also found to dominate sample 31, for which no atmospheric Radon-222 peak was observed, and air mass origins were classified as oceanic. Further information such as individual sample forward and back trajectories in the context of surface and vertical meteorological analyses were needed to assess origins and transport of the inorganic (dust) INPs, as these are unlikely to have their origins in sea spray. Below, we describe four of the cases in detail that represent a range of conditions from those in Table 5 (refer to the appendix for additional cases).

Table 5. Summary of case day findings. Blue, green, and purple shading indicates ASO, SSO, and ESO samples, respectively. Columns show INP concentration (INP L^{-1}) at – 27 °C, dominant air mass classification, dominant treatment classification, pressure tendency during the sampling period, total precipitation (mm) during the sample period, and presence of a katabatic signature. Sea level pressure information used to determine pressure tendency can be found in the Appendix (Figure A6).

Sample #	Concentration at –27 °C (INP L^{-1})	Dominant air mass	Dominant Treatment Classification	Sea level pressure tendency	Precipitation (mm)	Katabatic signature
9	1.2×10^{-2}	Antarctic	Inorganic	Slight decrease	0.60	Yes
10	1.2×10^{-2}	Antarctic	Inorganic	Decrease	0.07	Yes
12	5.2×10^{-2}	Mixed	Inorganic	Decrease	4.49	Yes
19	4.3×10^{-2}	Mixed	Organic	Slight increase	0.63	No
21	8.6×10^{-3}	Antarctic	Inorganic	Increase	0.12	Yes
31	6.1×10^{-1}	Oceanic	Inorganic	Increase	1.33	Yes
40	2.4×10^{-1}	Oceanic	Organic	Increase	12.6	No
41	1.8×10^{-1}	Oceanic	Organic	Slight increase	3.41	No
44	3.0×10^{-1}	Oceanic	Organic	Decrease	0.04	No

Sample 9 (1/14/2024 04:15 – 1/15/2024 02:26 UTC)

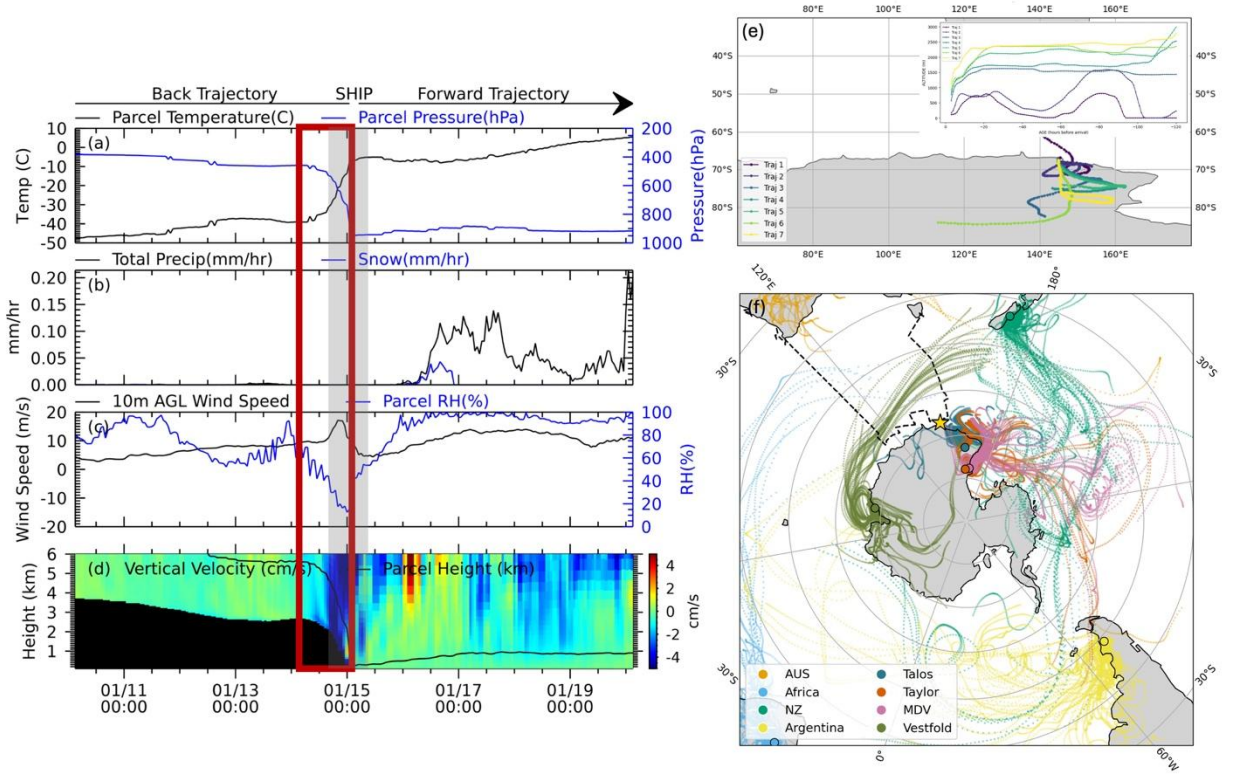

Figure 29. Meteorological quantities from MERRA-2 along backward and forward trajectories (adapted from Mace et al. 2024) including (a) Parcel temperature (°C) and pressure (hPa), (b) total (black) and snow (blue) precipitation rates (mm hr^{-1}), (c) parcel relative humidity (%) and 10 m wind speed (m s^{-1}), and (d) large-scale vertical motion (cm s^{-1}) and parcel height (black line). The red box highlights the INP filter sampling period and if present, katabatic conditions are shaded in grey. Panels (e) and (f) show HYSPLIT 5-day back trajectories from sampling location and 10-day forward trajectories from identified dust source regions, respectively. Inset in (e) shows altitude (m above mean sea level) along the back trajectory. In (f), the black dashed line = ship track, gold star = ship midpoint locations during the sample period, and the source regions are abbreviated as AUS = Australia, NZ = New Zealand, MDV = McMurdo Dry Valleys, Vestfold = Vestfold Hills, Talos = Victoria Land highlands, Taylor = Taylor Dome ice core site.

Figure 29 shows additional meteorological and air mass trajectory information for Sample 9. This sample exhibited relatively high INP concentrations for the ASO (1.2×10^{-2} INP L^{-1} at –27 °C). Additionally, sample 9 was characterized by Antarctic air influence and displayed an inorganic signature. Panels a-d show data from combined forward and backward trajectories ending or initiated at the sampling end time, with the sampling period outlined in the red box. The sampling period coincided with a strong katabatic event (Figure 29a-d, shaded grey region), evident from the abrupt increase in parcel temperature and an increase in parcel pressure via

adiabatic compression (Figure 29a), rapid increase in downward 10 m wind speed and steep decline in relative humidity (Figure 29c), and pronounced subsidence (negative vertical velocity, Figure 29d). During this period, winds observed from the ship were the strongest sampled during MISO, peaking near 46 knots. Back trajectories showed strong continental transport (Figure 29e), while forward trajectories indicated transport from the Victoria Land highlands and the McMurdo Dry Valleys with minimal influence from New Zealand sources (Figure 29f). These results indicate that transported dust from the Antarctic continent was likely a contributor to the inorganic INPs.

Sample 19 (1/28/2024 3:09 UTC – 1/30/2024 00:02 UTC)

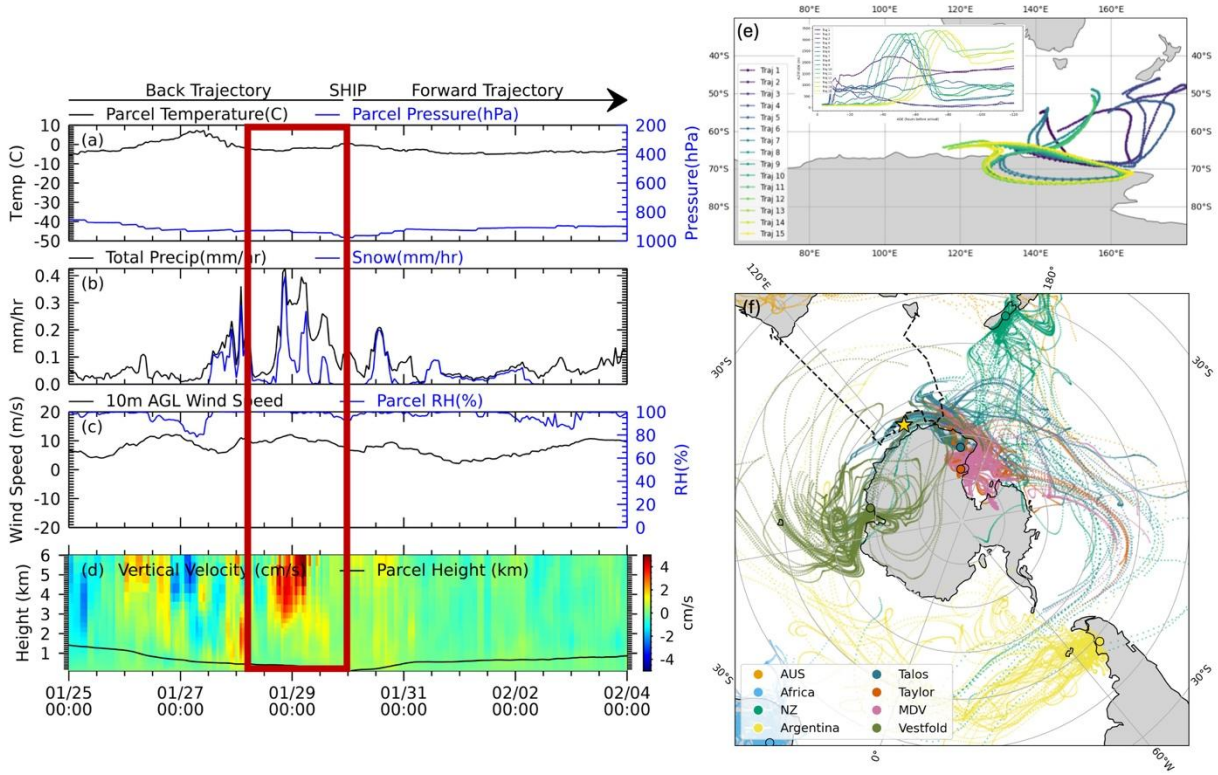

Figure 30. Same as Figure 29, but for sample 19.

Sample 19 exhibited a fairly high INP concentration in the ASO at –27 °C (4.3×10^{-2} INP L^{-1}) and was characterized as a mixed air mass (Antarctic and Oceanic), as indicated by the back

trajectories in Figure 30e. The sample 19 treatment spectrum was classified as organic. Even during the coastal sampling later in the period, no katabatic event was observed. The boundary layer was vertically quiescent (Figure 30d) as evidenced by the relatively minimal changes in parcel pressure at around 900 hPa and below (Figure 30a), stable wind speed and relative humidity (Figure 30c). Polar easterlies transported air primarily from the Victoria Land highlands, with some contribution from the New Zealand dust source (Figure 30f). The sample was collected during the passage of a low-pressure system (~978 hPa, Appendix Figure A6), with updrafts between 3–6 km (Figure 30d) producing a heavy snow event (Figure 30b). This evidence suggests that meteorological conditions during this event were less conducive to the transport of Antarctic INPs, despite the promising forward trajectories. With the organic signature and back trajectories, it is more likely that marine sea spray dominated the INP population. Notably, this sample was collected slightly farther from the coastline and more in the open ocean, as compared to ASO samples 9-12 which were closer to the marginal ice zone (Figure 25).

Sample 31 (2/10/2024 05:43 – 2/11/2024 07:07 UTC)

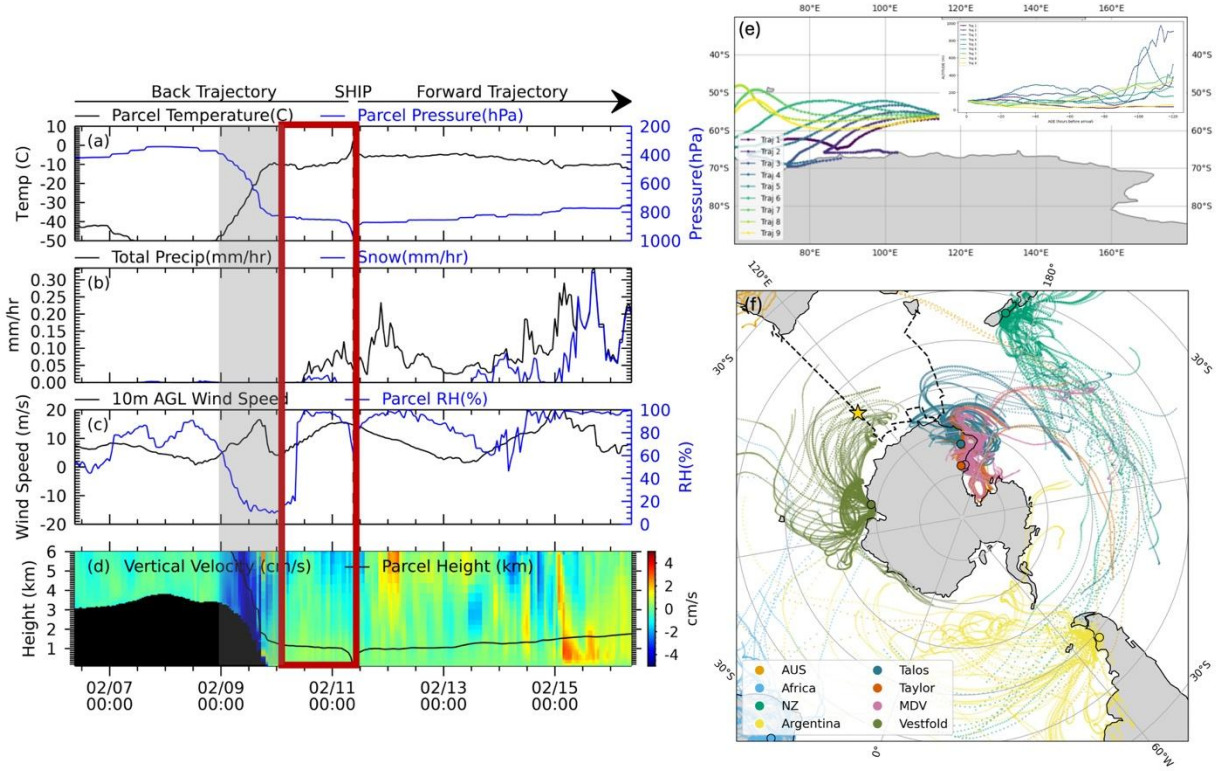

Figure 31. Same as Figure 29, but for sample 31.

Sample 31 was collected in the SSO region, just north of the ASO–SSO boundary at ~56 °S and exhibited the highest INP concentration of the voyage at –27 °C (6.1×10^{-1} INP L^{-1}). Although classified as an Oceanic air mass, treatment spectra indicated that the INPs were predominantly inorganic. This sample was taken during a low-pressure system (Appendix Figure A6) accompanied by some precipitation (Figure 31b). The beginning of the period coincided with the tail end of a strong katabatic event as evidenced by the strong subsidence and other katabatic features (Figure 31a-d). The first four back trajectories suggested that air during the initial half of the sampling period remained within the boundary layer (~300 m) until ~90 hours back (Figure 31e). Forward trajectories indicated that transport from the Vestfold Hills region likely contributed to the inorganic signature (Figure 31f). These findings suggest that although

this sample was collected in the SSO, its proximity to the ASO and continental outflow enabled the transport of Antarctic dust, which dominated the INP population in this case.

Sample 41 (2/21/2024 06:08 – 2/22/2024 07:00 UTC)

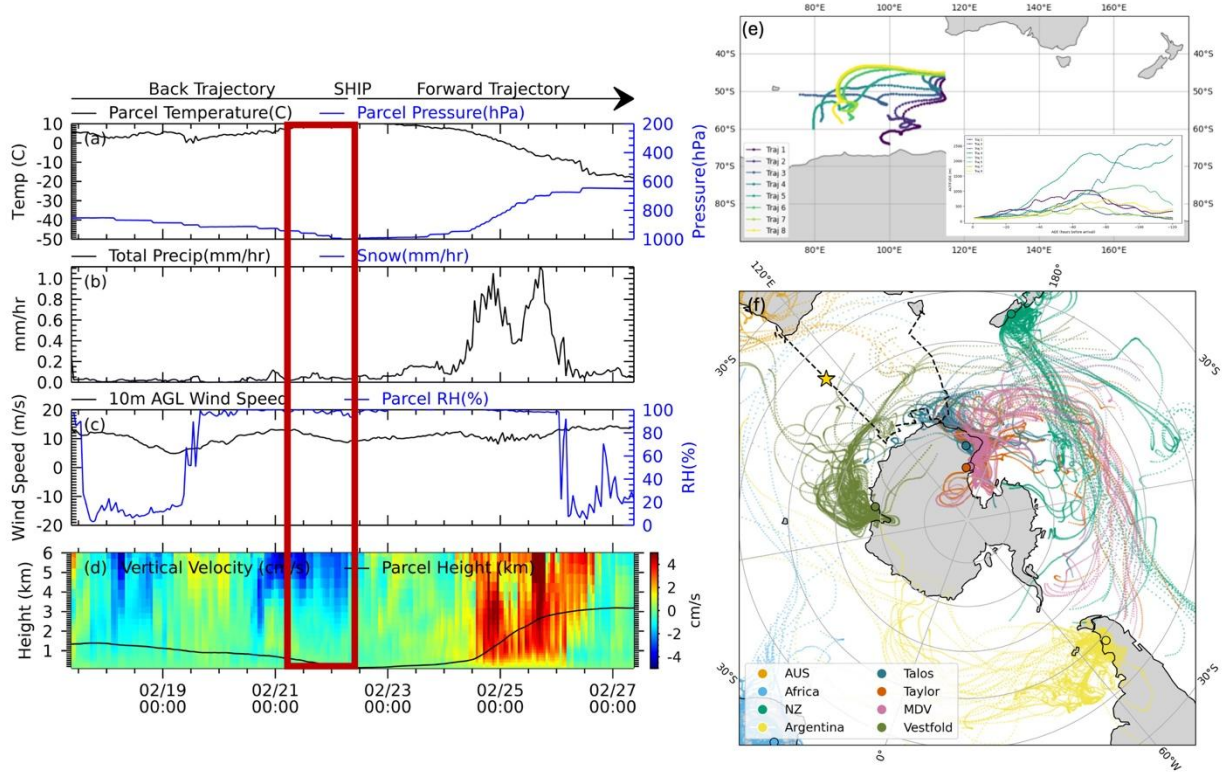

Figure 32. Same as Figure 29, but for sample 41.

Sample 41 was dominated by oceanic air masses (Figure 32e) and exhibited a primarily organic signature. This sample had 3.3×10^{-1} INP L^{-1} at –27 °C, within a factor of 2 of sample 31. Sample 41 also had the highest INP concentration of the entire voyage with 2.94 INP L^{-1} at –30 °C. The sample period was characterized by relatively stable conditions in terms of temperature and pressure (Figure 32a), moderate winds (Figure 32c), and a vertically quiescent layer extending up to 1–2 km (Figure 32d). While precipitation rates were generally low, more than 3 mm of precipitation were recorded during this period. This precipitation likely occurred as the low-pressure system preceding this sample period shifted eastward and high pressure took

over (Appendix Figure A6). Back trajectory altitudes also reflected this stability, remaining mostly below 1 km over the ocean (Figure 32e). Forward trajectories indicated that long-range dust transport was unlikely (Figure 32f). The likely source of the organic INP signature was local marine sea spray aerosols.

4. CONCLUSIONS

New data from the first three voyages of the CAISO project are presented as a robust dataset to build on previous INP observations in the Southern Ocean. To answer the first research question, INP concentrations were comparable to previous Southern Ocean measurements, aside from the ACE-SPACE and Bigg data. Both of the latter studies observed INP concentrations that were 1–2 orders of magnitude higher than observed during CAISO, likely due to methodological differences. This made the ACE-SPACE and Bigg not directly comparable to the voyages used in this study. INP concentrations active at colder temperatures in the higher-latitude Southern Ocean (ASO) samples were consistently lower by 1-2 orders of magnitude relative to the lower-latitude Southern Ocean (SSO and ESO) as well as other marine regions globally. When compared with existing ice nucleation parameterizations, V21 generally captured the observed spectral shape well, whereas D15 and M18 did not adequately represent the shape of our INP spectra. V21 was able to capture INP concentration values adequately for the Antarctic coastal sector, consistent with the data used to develop it, but was not representative across the entire Southern Ocean domain for all voyages.

To answer the second research question, distinct differences in INP concentrations, composition, and air mass influence were present across Southern Ocean latitudes during MISO. Prior studies have already demonstrated aerosol differences across latitude bands. Our work extends this methodology to INPs, demonstrating a gradient in INPs across latitudes. We present the variability in concentration and INP type based on changing wind patterns, meteorology, and local influences across latitudes. We have defined three distinct sectors based on our data: the extra-Antarctic sector (ESO) ≤ 45 °S, the sub-Antarctic sector (SSO) 45-60 °S, and the Antarctic

sector (ASO) ≥ 60 °S. MISO INP concentrations were nearly an order of magnitude lower within the ASO than in the other sectors, across all temperatures. While we saw the highest concentrations within the SSO, ESO samples were comparable. During MISO, Antarctic air masses were more common in the ASO, whereas oceanic air masses dominated in the SSO. MISO samples within the ESO were limited, so additional samples are needed before drawing conclusions on this sector. MISO samples influenced by Antarctic air masses tended to display more of an inorganic INP signature, whereas samples influenced by oceanic air masses displayed more heat-labile organic signatures consistent with marine SSA sources.

To answer the third research question, we investigated Antarctic and high-latitude Southern Ocean INP sources. As noted in the analysis for research question 2, within the Antarctic sector of the Southern Ocean, INP concentrations were the lowest. This region remained relatively isolated from continental influence other than from Antarctica throughout the duration of leg 2 of MISO (the coastal leg). Katabatic events and polar easterlies appeared to facilitate the transport of local INPs, including inorganics from snow and ice-free regions of the continent. Overall, our observations suggest that, while emissions fluxes are apparently small, local Antarctic sources can contribute INPs to the high latitude Southern Ocean boundary layer and thus may play a role in cloud formation in this region. Additionally, our analysis indicated that emissions from the New Zealand dust source also can be transported to the East Antarctic coast via polar easterlies. Further observations could help define whether New Zealand dust is also a significant contributor to inorganic INPs in this region.

Understanding the sector-specific INP concentrations and sources is a critical step in understanding cloud ice fraction and glaciation for Southern Ocean MPCs. Insights provided by the early CAISO voyages help confirm previous INPs concentrations over the open ocean and

give insights into varying sources by latitude. This is especially important in a changing Antarctic environment, in which more ice-free, exposed areas can contribute to dust and biogenic INPs. These findings can help improve future parameterizations and cloud microphysical models in order to resolve the shortwave radiative bias.

5. FUTURE WORK

While inter-seasonal and latitudinal trends are beginning to emerge from these observations, drawing firm conclusions remains challenging due to variability in cruise track, spatial coverage, years, seasons, sample handling, and processing standards. This work highlights the need for continued observations. We look forward to incorporating data from Denman, COAST-K, and the two years of data from Davis Station in our future work. These campaigns are especially promising given the consistency over all CAISO voyages in operating procedures and post-processing, which will help reduce methodological variability across voyages. While the Denman and COAST-K voyages were recently completed in May 2025, the Davis Station filter collections will remain active through April 2026. Incorporating results from these efforts into the CAISO database will help fill critical seasonal data gaps, particularly during the austral autumn, and expand the currently sparse coverage at high latitudes.

While most of the detailed analysis in this thesis focused on the MISO voyage, future work will extend the same approach to the SOTS, SWOT, Denman, and COAST-K voyages. Additional questions to be addressed include a more detailed examination of coastal transport events with the inclusion of Denman, as well as the role of phytoplankton and other marine biological INP sources in the different latitude sectors (ESO, SSO, and ASO). Seawater collected during the voyages can help provide insights into chlorophyll-a levels and possible phytoplankton activity that can lead to biogenic INP emissions. The COAST-K voyage will further provide a more complete dataset for the ESO sector, enabling a more robust analysis of INP sources to this region. DNA analysis will be conducted for the CAISO voyages following

Barry et al. (2025) to help elucidate the biological makeup and potential tracers of INPs across the latitude sectors.

While complete aerosol size distributions were not available for all of the CAISO cruises, future parameterization testing and development will include these data, as available, as inputs to determine INP concentrations from the D15 and M18 parameterizations. Some of the voyages, including MISO, only had access to a scanning mobility particle sizer (SMPS), which provides data for aerosol sizes in the lower range of particle diameters (15.1 to 800 nm). Measurements from Aerodynamic or Optical Particle Sizers are needed to obtain aerosol surface area concentrations and to determine the number concentration greater than 0.5μm. Suggestions for improved parameterizations will be tailored to the individual sectors of the greater Southern Ocean to better capture the distinct differences across latitudes, including the high-latitude Southern Ocean (ASO). These refined parameterizations will help improve the representation of cloud microphysical processes within global climate models.

We aim to further investigate Southern Ocean sectors by further classifying air masses by synoptic types, following (Truong et al. 2020; Mallet et al. 2025) to see if various post-frontal systems and other subsidence-based meteorological phenomena have an influence on INP concentrations. We also hope to further investigate the atmospheric dynamics at play within Southern Ocean, in order to improve our understanding of atmospheric boundaries affecting INP populations. Niu et al (2024) suggested another aerosol boundary at 50-60 °S, which might be of use pending more analysis. Additional seasonally-varying observations across this region are needed, particularly during austral autumn, spring, and especially winter. Although these are challenging for ship-based voyages, expanding ground-based campaigns at Antarctic and sub-Antarctic stations could help fill these gaps and provide a clearer seasonal gradient for the ASO

sector. Longitudinal-focused analysis may also be important to understanding INPs across the Southern Ocean, since continental influences vary strongly with longitude. We hope to investigate longitudinal and ocean basin (Indian, Pacific, Atlantic) variations in data across the CAISO and previous datasets. Until more Southern Ocean studies are performed, we plan to blank-correct ACE-SPACE data and potentially add in more studies such as TAN1502 (Welti et al. 2020) to incorporate more longitudinal coverage (162 to 175 °E).

REFERENCES

Aarons, S. M., S. M. Aciego, P. Gabrielli, B. Delmonte, J. M. Koornneef, A. Wegner, and M. A. Blakowski, 2016: The impact of glacier retreat from the Ross Sea on local climate: Characterization of mineral dust in the Taylor Dome ice core, East Antarctica. *Earth and Planetary Science Letters*, **444**, 34–44, https://doi.org/10.1016/j.epsl.2016.03.035.

Aarons, S. M., S. M. Aciego, J. R. McConnell, B. Delmonte, and G. Baccolo, 2019: Dust Transport to the Taylor Glacier, Antarctica, During the Last Interglacial. *Geophysical Research Letters*, **46**, 2261–2270, https://doi.org/10.1029/2018GL081887.

Agresti, A., and B. A. Coull, 1998: Approximate Is Better than 'Exact' for Interval Estimation of Binomial Proportions. *The American Statistician*, **52**, 119, https://doi.org/10.2307/2685469.

Albani, S., N. M. Mahowald, B. Delmonte, V. Maggi, and G. Winckler, 2012: Comparing modeled and observed changes in mineral dust transport and deposition to Antarctica between the Last Glacial Maximum and current climates. *Clim Dyn*, **38**, 1731–1755, https://doi.org/10.1007/s00382-011-1139-5.

Allison, L. C., H. L. Johnson, D. P. Marshall, and D. R. Munday, 2010: Where do winds drive the Antarctic Circumpolar Current? *Geophysical Research Letters*, **37**, 2010GL043355, https://doi.org/10.1029/2010GL043355.

Barry, K. R., T. C. J. Hill, C. Jentzsch, B. F. Moffett, F. Stratmann, and P. J. DeMott, 2021: Pragmatic protocols for working cleanly when measuring ice nucleating particles. *Atmospheric Research*, **250**, 105419, https://doi.org/10.1016/j.atmosres.2020.105419.

——, T. C. J. Hill, S. M. Kreidenweis, P. J. DeMott, Y. Tobo, and J. M. Creamean, 2025: Bioaerosols as indicators of central Arctic ice nucleating particle sources, https://doi.org/10.5194/egusphere-2025-128.

Bennetts, L. G., and Coauthors, 2024: Closing the Loops on Southern Ocean Dynamics: From the Circumpolar Current to Ice Shelves and From Bottom Mixing to Surface Waves. *Reviews of Geophysics*, **62**, e2022RG000781, https://doi.org/10.1029/2022RG000781.

Bigg, E. K., 1973: Ice Nucleus Concentrations in Remote Areas. *J. Atmos. Sci.*, **30**, 1153–1157, https://doi.org/10.1175/1520-0469(1973)030%253C1153:INCIRA%253E2.0.CO;2.

Bigg, E. K., 1990: Long-term trends in ice nucleus concentrations. *Atmospheric Research*, **25**, 409–415, https://doi.org/10.1016/0169-8095(90)90025-8.

Bjordal, J., T. Storelvmo, K. Alterskjær, and T. Carlsen, 2020: Equilibrium climate sensitivity above 5 °C plausible due to state-dependent cloud feedback. *Nat. Geosci.*, **13**, 718–721, https://doi.org/10.1038/s41561-020-00649-1.

Bodas-Salcedo, A., and Coauthors, 2014: Origins of the Solar Radiation Biases over the Southern Ocean in CFMIP2 Models*. *Journal of Climate*, **27**, 41–56, https://doi.org/10.1175/JCLI-D-13-00169.1.

Bottos, E. M., A. C. Woo, P. Zawar-Reza, S. B. Pointing, and S. C. Cary, 2014: Airborne Bacterial Populations Above Desert Soils of the McMurdo Dry Valleys, Antarctica. *Microb Ecol*, **67**, 120–128, https://doi.org/10.1007/s00248-013-0296-y.

Bracegirdle, T. J., P. Hyder, and C. R. Holmes, 2018: CMIP5 Diversity in Southern Westerly Jet Projections Related to Historical Sea Ice Area: Strong Link to Strengthening and Weak Link to Shift. *Journal of Climate*, **31**, 195–211, https://doi.org/10.1175/JCLI-D-17-0320.1.

Bullard, J. E., and Coauthors, 2016: High-latitude dust in the Earth system. *Rev. Geophys.*, **54**, 447–485, https://doi.org/10.1002/2016RG000518.

Burrows, S. M., and Coauthors, 2022: Ice-Nucleating Particles That Impact Clouds and Climate: Observational and Modeling Research Needs. *Reviews of Geophysics*, **60**, https://doi.org/10.1029/2021RG000745.

Caton Harrison, T., S. Biri, T. J. Bracegirdle, J. C. King, E. C. Kent, É. Vignon, and J. Turner, 2022: Reanalysis representation of low-level winds in the Antarctic near-coastal region. *Weather Clim. Dynam.*, **3**, 1415–1437, https://doi.org/10.5194/wcd-3-1415-2022.

Chambers, S. D., and Coauthors, 2018: Characterizing Atmospheric Transport Pathways to Antarctica and the Remote Southern Ocean Using Radon-222. *Front. Earth Sci.*, **6**, 190, https://doi.org/10.3389/feart.2018.00190.

Chelliah, D. S., A. E. Ray, E. Zhang, A. Terauds, and B. C. Ferrari, 2024: The Vestfold Hills are alive: characterising microbial and environmental dynamics in Old Wallow, eastern Antarctica. *Front. Microbiol.*, **15**, 1443491, https://doi.org/10.3389/fmicb.2024.1443491.

Corkill, M., and Coauthors, 2025: Dissolved iron release by sediment and dust particles in Antarctic seawater greater than glacial flour and sea-ice particles. *Marine Chemistry*, **270**, 104509, https://doi.org/10.1016/j.marchem.2025.104509.

Creamean, C. Hume, T. C. J. Hill, and Devadoss, Tim, 2024: Ice Nucleation Spectrometer (INS) Instrument Handbook.

Creamean, J. M., and Coauthors, 2013: Dust and Biological Aerosols from the Sahara and Asia Influence Precipitation in the Western U.S. *Science*, **339**, 1572–1578, https://doi.org/10.1126/science.1227279.

——, T. C. J. Hill, P. J. DeMott, J. Uetake, S. Kreidenweis, and T. A. Douglas, 2020: Thawing permafrost: an overlooked source of seeds for Arctic cloud formation. *Environ. Res. Lett.*, **15**, 084022, https://doi.org/10.1088/1748-9326/ab87d3.

——, and Coauthors, 2022: Annual cycle observations of aerosols capable of ice formation in central Arctic clouds. *Nat Commun*, **13**, 3537, https://doi.org/10.1038/s41467-022-31182-x.

DeMott, P. J., and Coauthors, 2010: Predicting global atmospheric ice nuclei distributions and their impacts on climate. *Proc. Natl. Acad. Sci. U.S.A.*, **107**, 11217–11222, https://doi.org/10.1073/pnas.0910818107.

——, and Coauthors, 2015: Integrating laboratory and field data to quantify the immersion freezing ice nucleation activity of mineral dust particles. *Atmos. Chem. Phys.*, **15**, 393–409, https://doi.org/10.5194/acp-15-393-2015.

DeMott, P. J., and Coauthors, 2016: Sea spray aerosol as a unique source of ice nucleating particles. *Proc. Natl. Acad. Sci. U.S.A.*, **113**, 5797–5803, https://doi.org/10.1073/pnas.1514034112.

——, and Coauthors, 2023: Atmospheric oxidation impact on sea spray produced ice nucleating particles. *Environ. Sci.: Atmos.*, **3**, 1513–1532, https://doi.org/10.1039/D3EA00060E.

Desai, N., M. Diao, Y. Shi, X. Liu, and I. Silber, 2023: Ship-Based Observations and Climate Model Simulations of Cloud Phase Over the Southern Ocean. *JGR Atmospheres*, **128**, e2023JD038581, https://doi.org/10.1029/2023JD038581.

Duprat, L., and Coauthors, 2019: Enhanced Iron Flux to Antarctic Sea Ice via Dust Deposition From Ice-Free Coastal Areas. *JGR Oceans*, **124**, 8538–8557, https://doi.org/10.1029/2019JC015221.

Fiddes, S. L., A. Protat, M. D. Mallet, S. P. Alexander, and M. T. Woodhouse, 2022: Southern Ocean cloud and shortwave radiation biases in a nudged climate model simulation: does the model ever get it right? *Atmos. Chem. Phys.*, **22**, 14603–14630, https://doi.org/10.5194/acp-22-14603-2022.

Gassó, S., A. Stein, F. Marino, E. Castellano, R. Udisti, and J. Ceratto, 2010: A combined observational and modeling approach to study modern dust transport from the Patagonia desert to East Antarctica. *Atmos. Chem. Phys.*, **10**, 8287–8303, https://doi.org/10.5194/acp-10-8287-2010.

GEBCO Bathymetric Compilation Group 2024, 2024: The GEBCO_2024 Grid - a continuous terrain model of the global oceans and land. NERC EDS British Oceanographic Data Centre NOC, accessed 24 July 2025, https://doi.org/10.5285/1C44CE99-0A0D-5F4F-E063-7086ABC0EA0F.

Geerts, B., and Coauthors, 2022: The COMBLE Campaign: A Study of Marine Boundary Layer Clouds in Arctic Cold-Air Outbreaks. *Bulletin of the American Meteorological Society*, **103**, E1371–E1389, https://doi.org/10.1175/BAMS-D-21-0044.1.

Gillies, J. A., W. G. Nickling, and M. Tilson, 2013: Frequency, magnitude, and characteristics of aeolian sediment transport: McMurdo Dry Valleys, Antarctica. *JGR Earth Surface*, **118**, 461–479, https://doi.org/10.1002/jgrf.20007.

Griffiths, A. D., S. D. Chambers, A. G. Williams, and S. Werczynski, 2016: Increasing the accuracy and temporal resolution of two-filter radon–222 measurements by correcting for the instrument response. *Atmos. Meas. Tech.*, **9**, 2689–2707, https://doi.org/10.5194/amt-9-2689-2016.

Hamilton, D. S., L. A. Lee, K. J. Pringle, C. L. Reddington, D. V. Spracklen, and K. S. Carslaw, 2014: Occurrence of pristine aerosol environments on a polluted planet. *Proc. Natl. Acad. Sci. U.S.A.*, **111**, 18466–18471, https://doi.org/10.1073/pnas.1415440111.

Hande, L. B., and C. Hoose, 2017: Partitioning the primary ice formation modes in large eddy simulations of mixed-phase clouds. *Atmos. Chem. Phys.*, **17**, 14105–14118, https://doi.org/10.5194/acp-17-14105-2017.

Hill, T. C. J., P. J. DeMott, Y. Tobo, J. Fröhlich-Nowoisky, B. F. Moffett, G. D. Franc, and S. M. Kreidenweis, 2016: Sources of organic ice nucleating particles in soils. *Atmos. Chem. Phys.*, **16**, 7195–7211, https://doi.org/10.5194/acp-16-7195-2016.

Hiranuma, N., and Coauthors, 2015: A comprehensive laboratory study on the immersion freezing behavior of illite NX particles: a comparison of 17 ice nucleation measurement techniques. *Atmos. Chem. Phys.*, **15**, 2489–2518, https://doi.org/10.5194/acp-15-2489-2015.

Hoose, C., and O. Möhler, 2012: Heterogeneous ice nucleation on atmospheric aerosols: a review of results from laboratory experiments. *Atmos. Chem. Phys.*, **12**, 9817–9854, https://doi.org/10.5194/acp-12-9817-2012.

Hoose, C., J. E. Kristjánsson, J.-P. Chen, and A. Hazra, 2010: A Classical-Theory-Based Parameterization of Heterogeneous Ice Nucleation by Mineral Dust, Soot, and Biological Particles in a Global Climate Model. *Journal of the Atmospheric Sciences*, **67**, 2483–2503, https://doi.org/10.1175/2010JAS3425.1.

Hoskins, B. J., and K. I. Hodges, 2005: A New Perspective on Southern Hemisphere Storm Tracks. *Journal of Climate*, **18**, 4108–4129, https://doi.org/10.1175/JCLI3570.1.

Huang, Y., A. Protat, S. T. Siems, and M. J. Manton, 2015: A-Train Observations of Maritime Midlatitude Storm-Track Cloud Systems: Comparing the Southern Ocean against the North Atlantic. *Journal of Climate*, **28**, 1920–1939, https://doi.org/10.1175/JCLI-D-14-00169.1.

Humphries, R. S., and Coauthors, 2021: Southern Ocean latitudinal gradients of cloud condensation nuclei. *Atmos. Chem. Phys.*, **21**, 12757–12782, https://doi.org/10.5194/acp-21-12757-2021.

——, and Coauthors, 2023: Measurement report: Understanding the seasonal cycle of Southern Ocean aerosols. *Atmos. Chem. Phys.*, **23**, 3749–3777, https://doi.org/10.5194/acp-23-3749-2023.

Hwang, Y.-T., and D. M. W. Frierson, 2013: Link between the double-Intertropical Convergence Zone problem and cloud biases over the Southern Ocean. *Proc. Natl. Acad. Sci. U.S.A.*, **110**, 4935–4940, https://doi.org/10.1073/pnas.1213302110.

Järvinen, E., and Coauthors, 2022: Evidence for Secondary Ice Production in Southern Ocean Maritime Boundary Layer Clouds. *JGR Atmospheres*, **127**, e2021JD036411, https://doi.org/10.1029/2021JD036411.

Kanji, Z. A., L. A. Ladino, H. Wex, Y. Boose, M. Burkert-Kohn, D. J. Cziczo, and M. Krämer, 2017: Overview of Ice Nucleating Particles. *Meteorological Monographs*, **58**, 1.1-1.33, https://doi.org/10.1175/amsmonographs-d-16-0006.1.

Kay, J. E., C. Wall, V. Yettella, B. Medeiros, C. Hannay, P. Caldwell, and C. Bitz, 2016: Global Climate Impacts of Fixing the Southern Ocean Shortwave Radiation Bias in the Community Earth System Model (CESM). *Journal of Climate*, **29**, 4617–4636, https://doi.org/10.1175/JCLI-D-15-0358.1.

Korolev, A., and T. Leisner, 2020: Review of experimental studies of secondary ice production. *Atmos. Chem. Phys.*, **20**, 11767–11797, https://doi.org/10.5194/acp-20-11767-2020.

——, and Coauthors, 2020: A new look at the environmental conditions favorable to secondary ice production. *Atmos. Chem. Phys.*, **20**, 1391–1429, https://doi.org/10.5194/acp-20-1391-2020.

Kremser, S., and Coauthors, 2021: Southern Ocean cloud and aerosol data: a compilation of measurements from the 2018 Southern Ocean Ross Sea Marine Ecosystems and Environment voyage. *Earth Syst. Sci. Data*, **13**, 3115–3153, https://doi.org/10.5194/essd-13-3115-2021.

Lamy, F., and Coauthors, 2024: Five million years of Antarctic Circumpolar Current strength variability. *Nature*, **627**, 789–796, https://doi.org/10.1038/s41586-024-07143-3.

Lee, J. R., B. Raymond, T. J. Bracegirdle, I. Chadès, R. A. Fuller, J. D. Shaw, and A. Terauds, 2017: Climate change drives expansion of Antarctic ice-free habitat. *Nature*, **547**, 49–54, https://doi.org/10.1038/nature22996.

Li, F., P. Ginoux, and V. Ramaswamy, 2008: Distribution, transport, and deposition of mineral dust in the Southern Ocean and Antarctica: Contribution of major sources. *J. Geophys. Res.*, **113**, 2007JD009190, https://doi.org/10.1029/2007JD009190.

——, ——, and ——, 2010: Transport of Patagonian dust to Antarctica. *J. Geophys. Res.*, **115**, 2009JD012356, https://doi.org/10.1029/2009JD012356.

Lukas, M., R. Schwidetzky, R. J. Eufemio, M. Bonn, and K. Meister, 2022: Toward Understanding Bacterial Ice Nucleation. *J. Phys. Chem. B*, **126**, 1861–1867, https://doi.org/10.1021/acs.jpcb.1c09342.

Mace, G. G., and A. Protat, 2018a: Clouds over the Southern Ocean as Observed from the R/V Investigator during CAPRICORN. Part I: Cloud Occurrence and Phase Partitioning. *Journal of Applied Meteorology and Climatology*, **57**, 1783–1803, https://doi.org/10.1175/JAMC-D-17-0194.1.

——, and ——, 2018b: Clouds over the Southern Ocean as Observed from the R/V Investigator during CAPRICORN. Part II: The Properties of Nonprecipitating Stratocumulus. *Journal of Applied Meteorology and Climatology*, **57**, 1805–1823, https://doi.org/10.1175/jamc-d-17-0195.1.

——, Q. Zhang, M. Vaughan, R. Marchand, G. Stephens, C. Trepte, and D. Winker, 2009: A description of hydrometeor layer occurrence statistics derived from the first year of merged Cloudsat and CALIPSO data. *J. Geophys. Res.*, **114**, 2007JD009755, https://doi.org/10.1029/2007JD009755.

——, and Coauthors, 2021: Southern Ocean Cloud Properties Derived From CAPRICORN and MARCUS Data. *JGR Atmospheres*, **126**, https://doi.org/10.1029/2020jd033368.

——, S. Benson, R. Humphries, P. M. Gombert, and E. Sterner, 2023: Natural marine cloud brightening in the Southern Ocean. *Atmos. Chem. Phys.*, **23**, 1677–1685, https://doi.org/10.5194/acp-23-1677-2023.

——, ——, E. Sterner, A. Protat, R. Humphries, and A. G. Hallar, 2024: The Association Between Cloud Droplet Number over the Summer Southern Ocean and Air Mass History. *JGR Atmospheres*, **129**, e2023JD040673, https://doi.org/10.1029/2023JD040673.

Mallet, M. D., and Coauthors, 2025: Biological enhancement of cloud droplet concentrations observed off East Antarctica. *npj Clim Atmos Sci*, **8**, 113, https://doi.org/10.1038/s41612-025-00990-5.

Martin, J. E., 2007: *Mid-latitude atmospheric dynamics: a first course*. Wiley 324pp.

McCluskey, C. S., and Coauthors, 2018a: Observations of Ice Nucleating Particles Over Southern Ocean Waters. *Geophysical Research Letters*, **45**, 11,989-11,997, https://doi.org/10.1029/2018GL079981.

McCluskey, C. S., and Coauthors, 2018b: Marine and Terrestrial Organic Ice-Nucleating Particles in Pristine Marine to Continentally Influenced Northeast Atlantic Air Masses. *JGR Atmospheres*, **123**, 6196–6212, https://doi.org/10.1029/2017JD028033.

——, and Coauthors, 2018c: A Mesocosm Double Feature: Insights into the Chemical Makeup of Marine Ice Nucleating Particles. *Journal of the Atmospheric Sciences*, **75**, 2405–2423, https://doi.org/10.1175/jas-d-17-0155.1.

——, and Coauthors, 2023: Simulating Southern Ocean Aerosol and Ice Nucleating Particles in the Community Earth System Model Version 2. *JGR Atmospheres*, **128**, e2022JD036955, https://doi.org/10.1029/2022JD036955.

McFarquhar, G. M., and Coauthors, 2021: Observations of Clouds, Aerosols, Precipitation, and Surface Radiation over the Southern Ocean: An Overview of CAPRICORN, MARCUS, MICRE, and SOCRATES. *Bulletin of the American Meteorological Society*, **102**, E894–E928, https://doi.org/10.1175/bams-d-20-0132.1.

Moore, K. A., and Coauthors, 2022: Estimation of Sea Spray Aerosol Surface Area Over the Southern Ocean Using Scattering Measurements. *JGR Atmospheres*, **127**, e2022JD037009, https://doi.org/10.1029/2022JD037009.

——, and Coauthors, 2024: Characterizing Ice Nucleating Particles Over the Southern Ocean Using Simultaneous Aircraft and Ship Observations. *JGR Atmospheres*, **129**, e2023JD039543, https://doi.org/10.1029/2023JD039543.

Moran, J. M., 2022: *Weather studies: introduction to atmospheric science*. Seventh edition. E.W. Mills, Ed. American Meteorological Society.

Neff, P. D., and N. A. N. Bertler, 2015: Trajectory modeling of modern dust transport to the Southern Ocean and Antarctica. *JGR Atmospheres*, **120**, 9303–9322, https://doi.org/10.1002/2015JD023304.

Niemand, M., and Coauthors, 2012: A Particle-Surface-Area-Based Parameterization of Immersion Freezing on Desert Dust Particles. *Journal of the Atmospheric Sciences*, **69**, 3077–3092, https://doi.org/10.1175/jas-d-11-0249.1.

Niu, Q., and Coauthors, 2024: 62°S Witnesses the Transition of Boundary Layer Marine Aerosol Pattern Over the Southern Ocean (50°S–68°S, 63°E–150°E) During the Spring and Summer: Results From MARCUS (I). *JGR Atmospheres*, **129**, https://doi.org/10.1029/2023jd040396.

Panwar, P., T. J. Williams, M. A. Allen, and R. Cavicchioli, 2022: Population structure of an Antarctic aquatic cyanobacterium. *Microbiome*, **10**, 207, https://doi.org/10.1186/s40168-022-01404-x.

Parish, T. R., and D. H. Bromwich, 2007: Reexamination of the Near-Surface Airflow over the Antarctic Continent and Implications on Atmospheric Circulations at High Southern Latitudes*. *Monthly Weather Review*, **135**, 1961–1973, https://doi.org/10.1175/MWR3374.1.

Pei, Z., and Coauthors, 2025: Refining the Simulation of Mixed-phase Clouds Over Coastal Antarctica with a Tailored Ice Nucleating Particle Parameterization, https://doi.org/10.22541/essoar.175339123.30294645/v1.

Pruppacher, H. R., and J. D. Klett, 2010: *Microphysics of Clouds and Precipitation*. Springer Netherlands, https://doi.org/10.1007/978-0-306-48100-0.

Raman, A., and Coauthors, 2023: Long-term variability in immersion-mode marine ice-nucleating particles from climate model simulations and observations. *Atmos. Chem. Phys.*, **23**, 5735–5762, https://doi.org/10.5194/acp-23-5735-2023.

Rintoul, S. R., 2007: Rapid freshening of Antarctic Bottom Water formed in the Indian and Pacific oceans. *Geophysical Research Letters*, **34**, 2006GL028550, https://doi.org/10.1029/2006GL028550.

Rolph, G., A. Stein, and B. Stunder, 2017: Real-time Environmental Applications and Display sYstem: READY. *Environmental Modelling & Software*, **95**, 210–228, https://doi.org/10.1016/j.envsoft.2017.06.025.

Sanchez, K. J., and Coauthors, 2021: Measurement report: Cloud processes and the transport of biological emissions affect southern ocean particle and cloud condensation nuclei concentrations. *Atmos. Chem. Phys.*, **21**, 3427–3446, https://doi.org/10.5194/acp-21-3427-2021.

Sauerland, F., N. Souverijns, A. Possner, H. Wex, P. Van Overmeiren, A. Mangold, K. Van Weverberg, and N. Van Lipzig, 2024: Ice-nucleating particle concentration impacts cloud properties over Dronning Maud Land, East Antarctica, in COSMO-CLM^2. *Atmos. Chem. Phys.*, **24**, 13751–13768, https://doi.org/10.5194/acp-24-13751-2024.

Schmale, J., and Coauthors, 2019: Overview of the Antarctic Circumnavigation Expedition: Study of Preindustrial-like Aerosols and Their Climate Effects (ACE-SPACE). *Bulletin of the American Meteorological Society*, **100**, 2260–2283, https://doi.org/10.1175/BAMS-D-18-0187.1.

Schnell, R. C., and G. Vali, 1976: Biogenic Ice Nuclei: Part I. Terrestrial and Marine Sources. *J. Atmos. Sci.*, **33**, 1554–1564, https://doi.org/10.1175/1520-0469(1976)033%253C1554:binpit%253E2.0.co;2.

Schüpbach, S., U. Federer, S. Albani, C. Barbante, T. F. Stocker, and H. Fischer, 2013: Sources and transport of dust to East Antarctica: new insights from high-resolution terrestrial and marine aerosol records from the Talos Dome ice core, https://doi.org/10.5194/cpd-9-3321-2013.

Scientific Committee on Antarctic Research (SCAR),: Jet Latitude Index. *SCAR Jet Latitude Index (JLI)*. Accessed 15 August 2025, https://scar.org/science/research-programmes/antclimnow/climate-indicators/jet-latitude-index.

Stein, A. F., R. R. Draxler, G. D. Rolph, B. J. B. Stunder, M. D. Cohen, and F. Ngan, 2015: NOAA's HYSPLIT Atmospheric Transport and Dispersion Modeling System. *Bulletin of the American Meteorological Society*, **96**, 2059–2077, https://doi.org/10.1175/BAMS-D-14-00110.1.

Suski, K. J., T. C. J. Hill, E. J. T. Levin, A. Miller, P. J. DeMott, and S. M. Kreidenweis, 2018: Agricultural harvesting emissions of ice-nucleating particles. *Atmos. Chem. Phys.*, **18**, 13755–13771, https://doi.org/10.5194/acp-18-13755-2018.

Tan, I., T. Storelvmo, and M. D. Zelinka, 2016: Observational constraints on mixed-phase clouds imply higher climate sensitivity. *Science*, **352**, 224–227, https://doi.org/10.1126/science.aad5300.

Tatzelt, C., and Coauthors, 2022: Circum-Antarctic abundance and properties of CCN and INPs. *Atmos. Chem. Phys.*, **22**, 9721–9745, https://doi.org/10.5194/acp-22-9721-2022.

Testa, B., and Coauthors, 2021: Ice Nucleating Particle Connections to Regional Argentinian Land Surface Emissions and Weather During the Cloud, Aerosol, and Complex Terrain Interactions Experiment. *JGR Atmospheres*, **126**, https://doi.org/10.1029/2021jd035186.

Truong, S. C. H., Y. Huang, F. Lang, M. Messmer, I. Simmonds, S. T. Siems, and M. J. Manton, 2020: A Climatology of the Marine Atmospheric Boundary Layer Over the Southern Ocean From Four Field Campaigns During 2016–2018. *JGR Atmospheres*, **125**, e2020JD033214, https://doi.org/10.1029/2020JD033214.

Turner, J., H. Dierssen, O. Schofield, H. Kim, S. Stammerjohn, D. Munro, and M. Kavanaugh, 2024: Changing phytoplankton phenology in the marginal ice zone west of the Antarctic Peninsula. *Mar. Ecol. Prog. Ser.*, **734**, 1–21, https://doi.org/10.3354/meps14567.

Twohy, C. H., and Coauthors, 2021: Cloud-Nucleating Particles Over the Southern Ocean in a Changing Climate. *Earth's Future*, **9**, e2020EF001673, https://doi.org/10.1029/2020EF001673.

Uetake, J., T. C. J. Hill, K. A. Moore, P. J. DeMott, A. Protat, and S. M. Kreidenweis, 2020: Airborne bacteria confirm the pristine nature of the Southern Ocean boundary layer. *Proc. Natl. Acad. Sci. U.S.A.*, **117**, 13275–13282, https://doi.org/10.1073/pnas.2000134117.

Vali, G., 1966: Sizes of Atmospheric Ice Nuclei. *Nature*, **212**, 384–385, https://doi.org/10.1038/212384a0.

——, 1971: Quantitative Evaluation of Experimental Results an the Heterogeneous Freezing Nucleation of Supercooled Liquids. *Journal of the Atmospheric Sciences*, **28**, 402–409, https://doi.org/10.1175/1520-0469(1971)028%253C0402:QEOERA%253E2.0.CO;2.

——, 1994: Freezing Rate Due to Heterogeneous Nucleation. *Journal of the Atmospheric Sciences*, **51**, 1843–1856, https://doi.org/10.1175/1520-0469(1994)051%253C1843:FRDTHN%253E2.0.CO;2.

Vali, G., M. Christensen, R. W. Fresh, E. L. Galyan, L. R. Maki, and R. C. Schnell, 1976: Biogenic Ice Nuclei. Part II: Bacterial Sources. *J. Atmos. Sci.*, **33**, 1565–1570, https://doi.org/10.1175/1520-0469(1976)033%253C1565:binpib%253E2.0.co;2.

Vignon, É., and Coauthors, 2021: Challenging and Improving the Simulation of Mid-Level Mixed-Phase Clouds Over the High-Latitude Southern Ocean. *Journal of Geophysical Research: Atmospheres*, **126**, e2020JD033490, https://doi.org/10.1029/2020JD033490.

Welti, A., and Coauthors, 2020: Ship-based measurements of ice nuclei concentrations over the Arctic, Atlantic, Pacific and Southern oceans. *Atmos. Chem. Phys.*, **20**, 15191–15206, https://doi.org/10.5194/acp-20-15191-2020.

Willis, M. D., and Coauthors, 2023: Polar oceans and sea ice in a changing climate. *Elem Sci Anth*, **11**, 00056, https://doi.org/10.1525/elementa.2023.00056.

Wilson, T. W., and Coauthors, 2015: A marine biogenic source of atmospheric ice-nucleating particles. *Nature*, **525**, 234–238, https://doi.org/10.1038/nature14986.

Xi, B., X. Dong, X. Zheng, and P. Wu, 2022: Cloud phase and macrophysical properties over the Southern Ocean during the MARCUS field campaign. *Atmos. Meas. Tech.*, **15**, 3761–3777, https://doi.org/10.5194/amt-15-3761-2022.

Xu, J. Z., J. Yang, Z. H. Du, J. Chen, Z. J. Wu, and C. D. Xiao, 2023: Characteristics of atmospheric ice nucleating particles over East Antarctica retrieved from the surface snow. *Science of The Total Environment*, **888**, 164181, https://doi.org/10.1016/j.scitotenv.2023.164181.

Yu, L., X. Jin, E. W. Schulz, and S. A. Josey, 2017: Air-sea interaction regimes in the sub-Antarctic Southern Ocean and Antarctic marginal ice zone revealed by icebreaker measurements. *JGR Oceans*, **122**, 6547–6564, https://doi.org/10.1002/2016JC012281.

Zhao, X., X. Liu, S. M. Burrows, and Y. Shi, 2021: Effects of marine organic aerosols as sources of immersion-mode ice-nucleating particles on high-latitude mixed-phase clouds. *Atmos. Chem. Phys.*, **21**, 2305–2327, https://doi.org/10.5194/acp-21-2305-2021.

Zhong, R., K. Hodges, Q. Yang, and D. Chen, 2025: Revisiting the Interaction Between Antarctic Sea Ice and Southern Ocean Cyclones. *JGR Atmospheres*, **130**, e2024JD042914, https://doi.org/10.1029/2024JD042914.

APPENDIX

Analysis of Additional MISO Case Days from Table 5

Sample 10 (1/15/2024 02:33 – 1/16/2024 02:23 UTC)

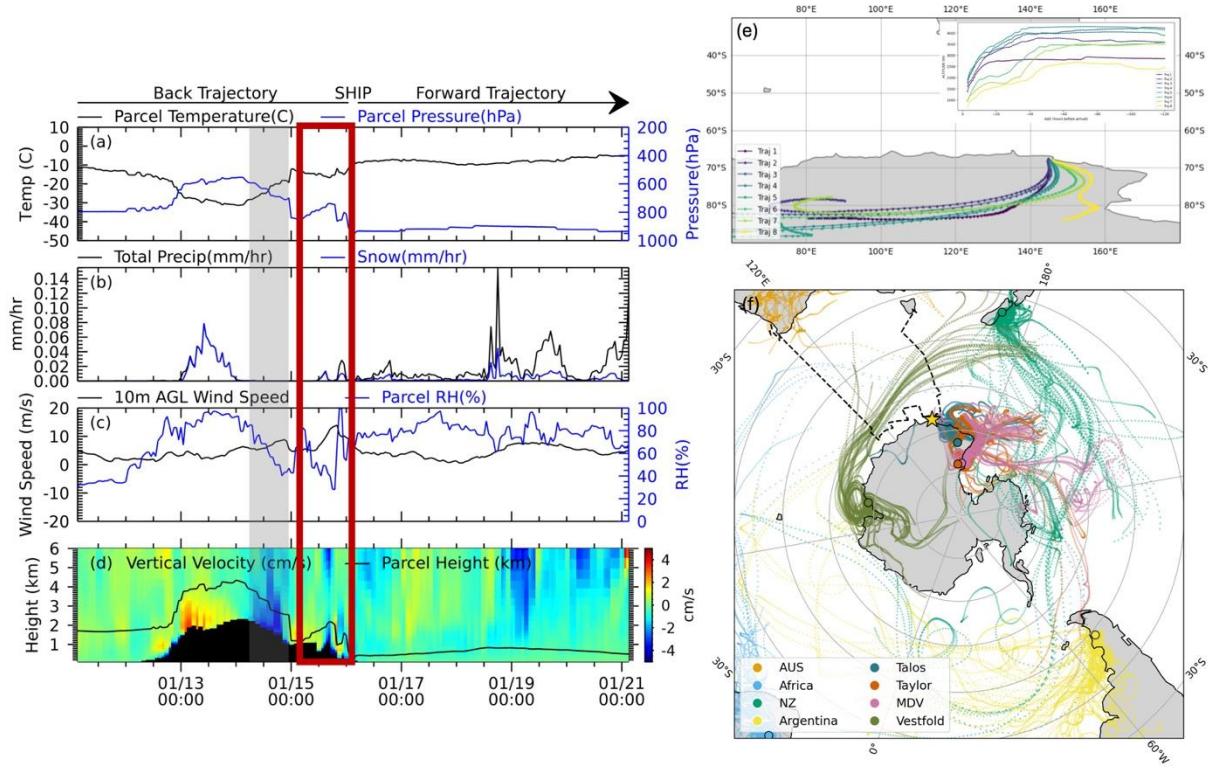

Figure A1. Same as Figure 29, but for sample 10.

The treatment spectra for sample 10 exhibited an inorganic signature under Antarctic air mass influence like sample 9. This sample was collected during the waning phase of the katabatic event associated with sample 9, though with reduced subsidence (Figure A1d). Winds reaching up to 39 knots, slight adiabatic warming, and parcel drying, are further evidence of katabatic influence during this period (Figure A1a, c). Back trajectories indicate air masses originated from deep within the Antarctic continent (Figure A1e), while forward trajectories suggest possible influence from the Victoria Land highlands and McMurdo Dry Valleys (Figure

A1f). Overall, these results parallel those of sample 9, supporting the interpretation that INPs during this case day were most likely transported dust from the Antarctic continent.

Sample 12 (1/18/2024 03:03 – 1/21/2024 01:17 UTC)

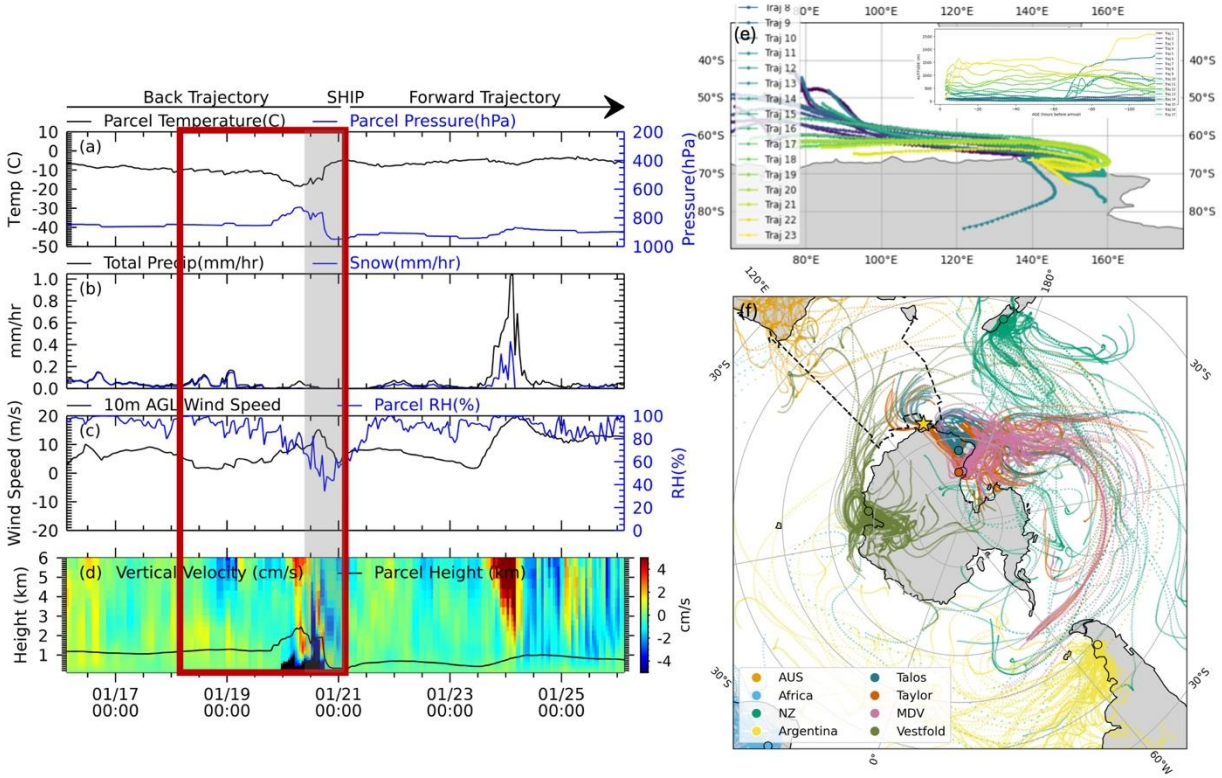

Figure A2. Same as Figure 29, but for sample 12.

This sample exhibited one of the higher ASO concentrations (5.2×10^{-2} INP L^{-1} at –27 °C) and showed a predominantly inorganic signature, with a slight heat-labile signature at colder temperatures. This sample was influenced by a Mixed (Oceanic–Antarctic) air mass, with the Oceanic component dominating but shifting to Antarctic twice—once near the midpoint of the sample period and again toward the end. The final 24 hours were also affected by a brief katabatic event, characterized by adiabatic warming (Figure A2a), a wind speed maximum of 45 knots and decreasing relative humidity (Figure A2c), and subsidence (Figure A2d). During this period, several strong cold frontal passages occurred, and atmospheric pressure reached a minimum of 976 hPa. Earlier back trajectories remained low within the marine boundary layer (~

< 250 m), whereas later back trajectories were more elevated, likely reflecting continental influence (Figure A2e). Forward trajectories suggest possible transport from the Victoria Land highlands, McMurdo Dry Valleys, and Taylor Dome regions (Figure A2f). Overall, this sample reflects the combined influence of an minimal katabatic event and marine boundary layer air, resulting in mixed INP types but ultimately dominated by an inorganic signature.

Sample 21 (1/31/2024 09:05 – 2/01/2024 06:36 UTC)

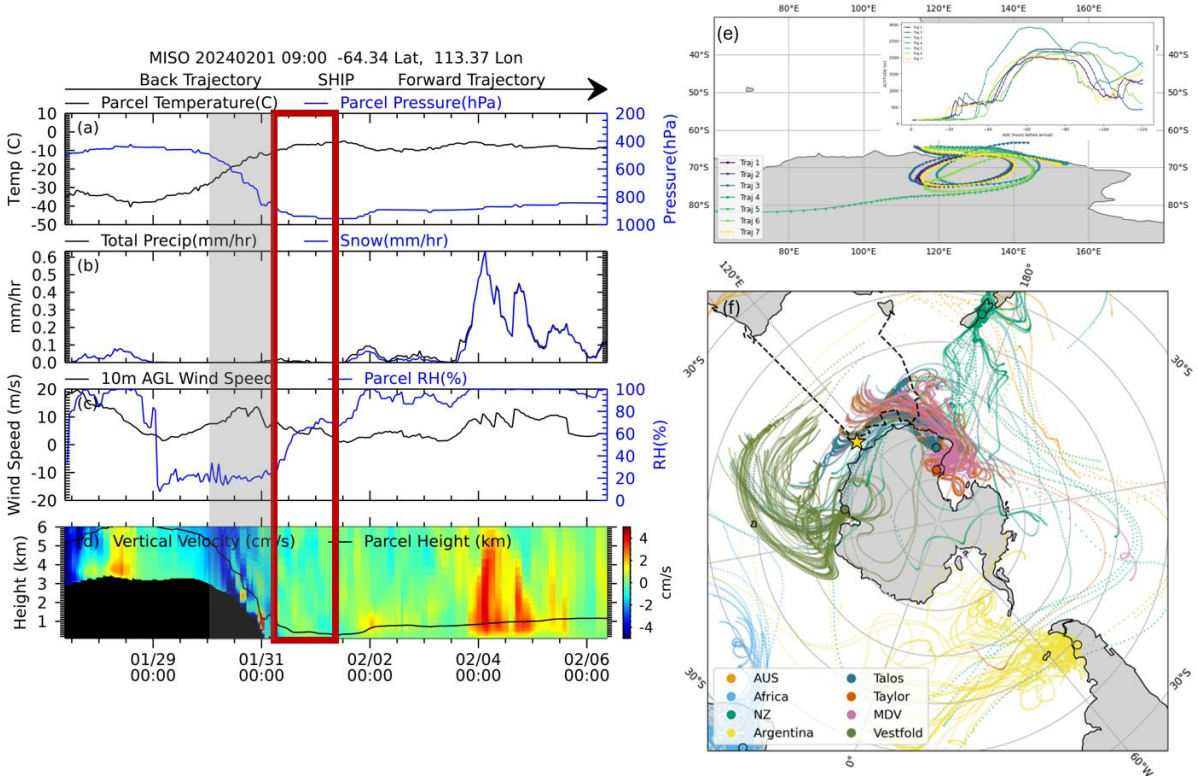

Figure A3. Same as Figure 29, but for sample 21.

Sample 21 exhibited an inorganic signature (see Figure A7) and had a low concentration of 8.6×10^{-3} INP L^{-1} at –27 °C in the ASO. This sample was classified as an Antarctic air mass, which is confirmed by the back trajectories (Figure A3e). There was a strong katabatic signature just prior to sampling as evident by the increasing temperature and decreasing pressure (Figure A3a), low relative humidity (Figure A3c), and negative vertical velocity (Figure A3d). Forward

trajectories indicated there was transport from the Victoria Land highlands, Taylor dome, and the McMurdo Dry Valleys (Figure A3f). Overall, this sample had a clear signal of being impacted by residual katabatic influence from Antarctica, transporting what was likely dust INPs although in very low concentration.

Sample 40 (2/19/2024 06:26 – 2/21/2024 06:04 UTC)

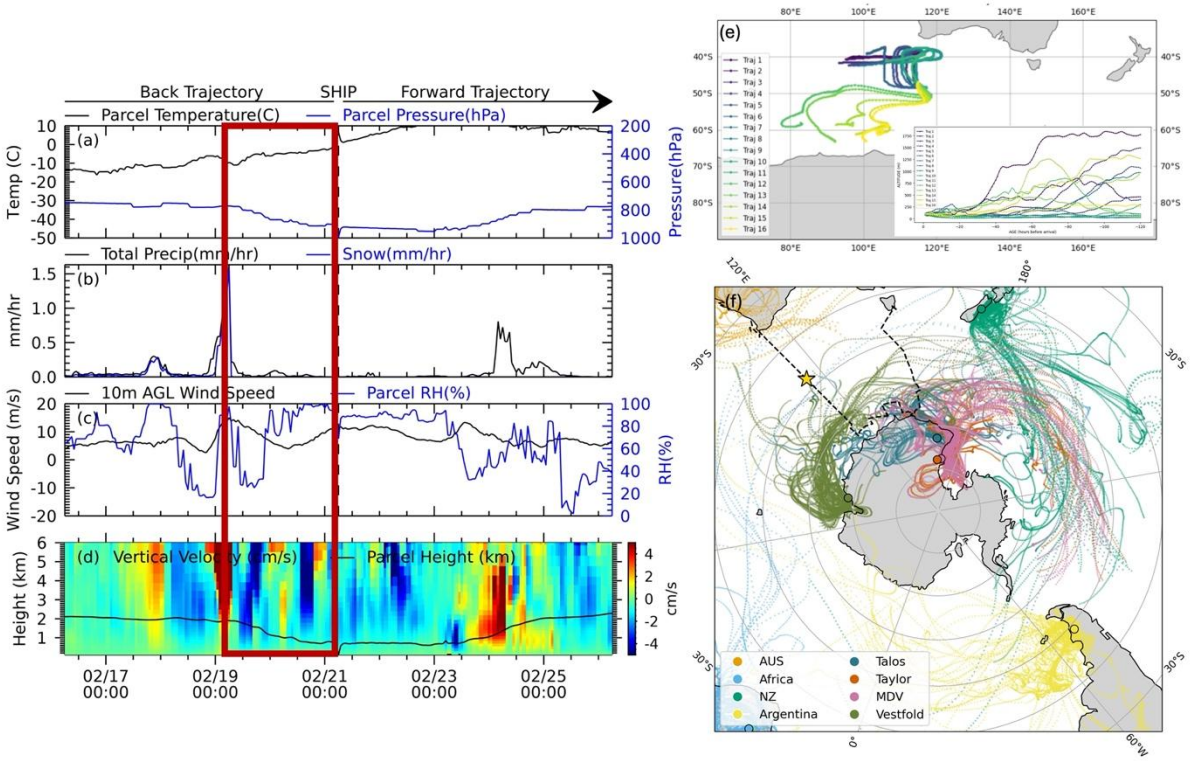

Figure A4. Same as Figure 29, but for sample 40.

The treatment spectra for sample 40 indicate an organic signature consistent with the Oceanic air mass classification. This sample exhibited a relatively high concentration at –27 °C (2.4×10^{-1} INP L^{-1}). This sample was collected at the tail end of a low-pressure system, with a minimum pressure of 987 hPa early in the period before transitioning to higher pressure (Figure A4a). Back trajectories consistently show influence from open ocean, though with latitudinal differences: earlier trajectories traversed 42–52° S, while later ones extended farther south to 52–65° S (Figure A4e). The trajectories from the middle of the sample period remained near the

surface, largely below 250 m. Long-range transport was limited, with only a few forward trajectories originating from the Vestfold Hills and McMurdo Dry Valleys reaching the sampling location (Figure A4f). Overall, this sample resembled sample 41 in that it displayed a clear separation from Antarctic sources, with clean marine air supplying the organic INPs.

Sample 44 (2/24/2024 05:16 – 2/25/2024 06:10 UTC)

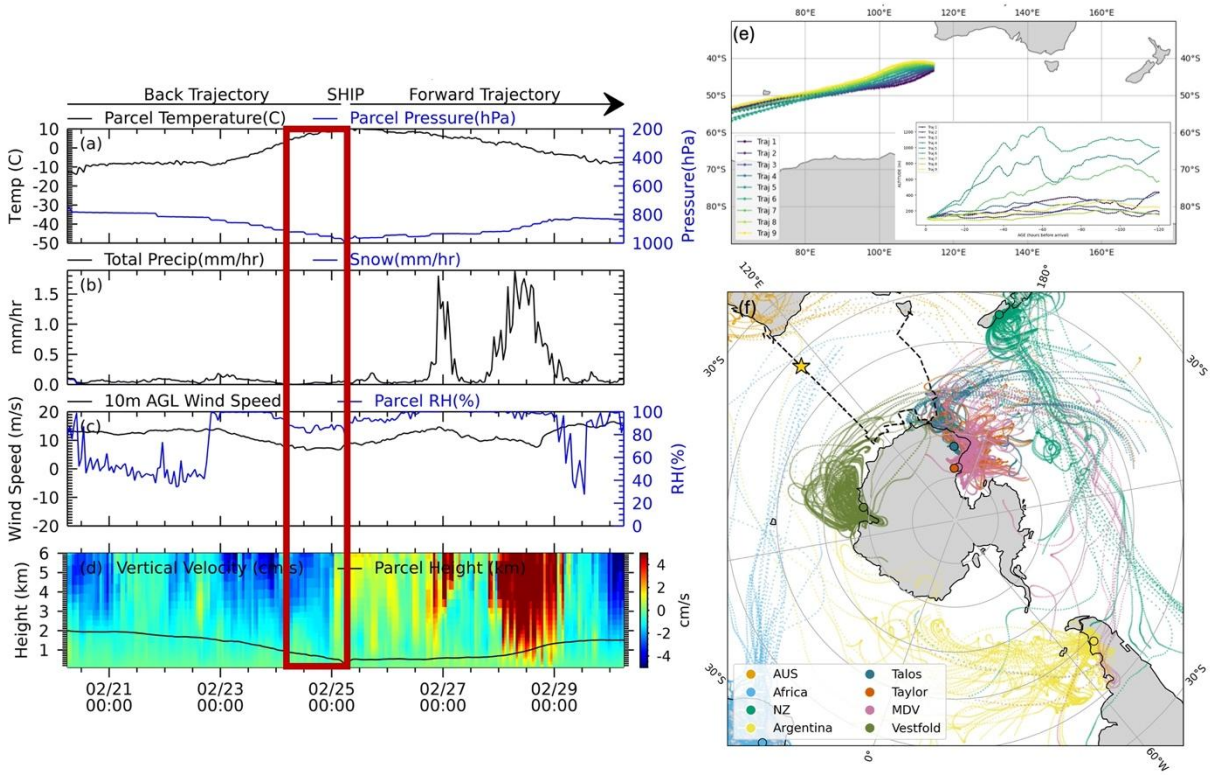

Figure A5. Same as Figure 29, but for sample 44.

The last case day was in the ESO region and classified as an Oceanic air mass with a predominantly organic signature. Sample 44 exhibited a relatively low concentration for this region, with 3.0×10^{-1} INP L^{-1} at –27 °C. This period was characterized by higher pressure (Figure A6), averaging 1017 hPa, along with a distinct subsidence signature as evident by the negative vertical velocity above 1 km (Figure A5d). A vertically quiescent layer extended up to ~1 km, consistent with the fact that most back trajectory altitudes remained below 1 km throughout the duration of this large-scale westerly transport (Figure A5e). Long-range transport

was limited, though a few forward trajectories from the African source region intersected the sampling period (Figure A5f). Like samples 40 and 41, this case reflected a marine organic INP influence.

MISO Sea Level Pressure (hPa) data from the Investigator

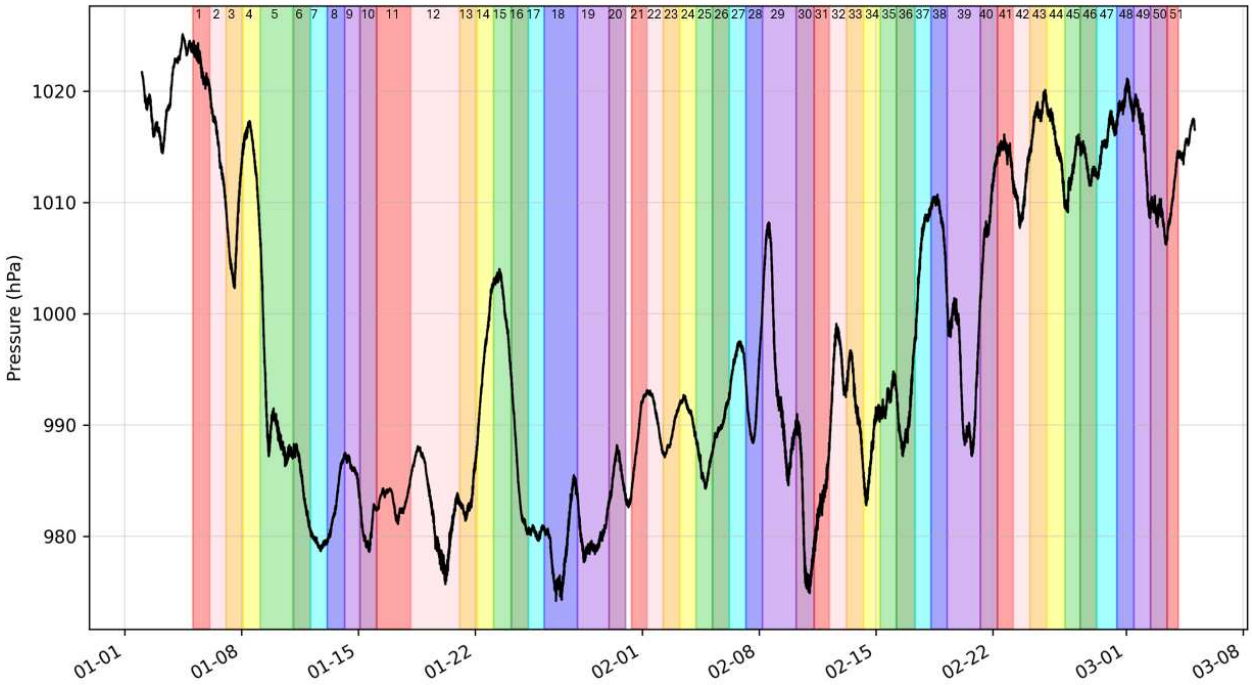

Figure A6. MISO sea level pressure as recorded on the Investigator, with overlay of sample periods as indicated by the varying colors. Sample period numbers are indicated at the top.

MISO additional treatment spectra

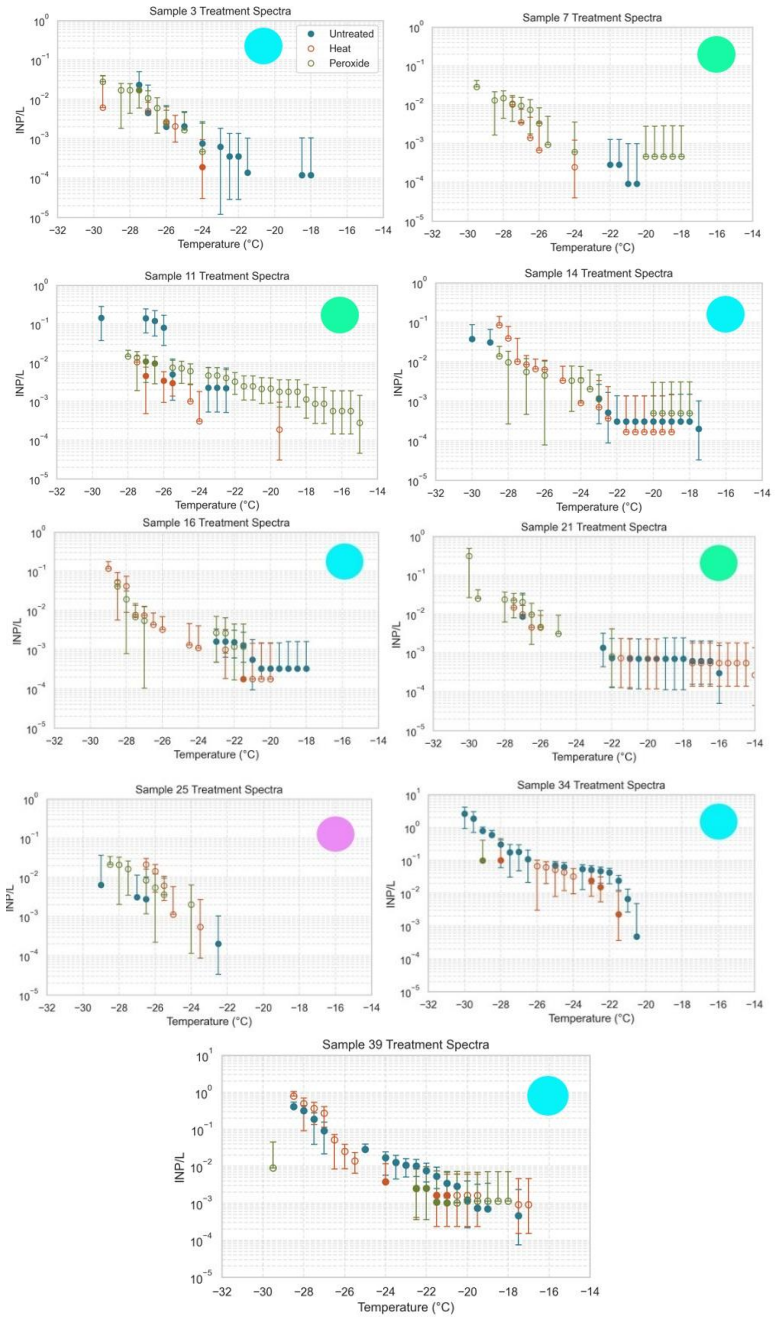

Figure A7. Additional MISO treatment INP spectra showing total (blue), heat-treated (red), and heat + peroxide-treated (green) values. Heat and heat + peroxide values are filled only if the treatment differed significantly from the unamended value (Z >1.64, corresponding to a 95% confidence under a one-tailed test). Vertical bars represent 95% confidence intervals. Inlaid circles indicate air mass classifications corresponding to Figure 21. MISO total INP concentrations at a freezing temperature of –28.5 °C along the ship track (white), categorized by air mass type. Solid green and teal lines indicate the 45 °S and 60 °S latitude boundaries, respectively. Circle sizes correspond to the same concentrations as in the –28 °C panel of Figure 20 with colors matching the Figure 20 concentration color bar. Numbers inside circles indicate sample IDs. Bathymetry and topography are shown in Figure 5.: light green = Antarctic, purple = Mixed (Antarctic–Oceanic), blue = Oceanic.

ABBREVIATIONS

ESO – Extra-Antarctic sector of the Southern Ocean (≤ 45 °S)

SSO – Sub-Antarctic sector of the Southern Ocean (45-60 °S)

ASO – Antarctic sector of the Southern Ocean (≥ 60 °S)

SOTS – Southern Ocean Time Series

SWOT – Surface Water Open Topography

MISO – Multidisciplinary Investigations of the Southern Ocean

COAST-K – Clean Ocean Air Sampling upwind of Tasmania - Kennaook

MARCUS – Measurements of Aerosols, Radiation, and Clouds Over the Southern Ocean

CAPRICORN – Clouds, Aerosols, Precipitation, Radiation, and Atmospheric Composition Over the Southern Ocean

SOCRATES – Southern Ocean Clouds, Radiation, and Aerosol Transport Experimental Study

ACE (or ACE-SPACE) – Antarctic Circumnavigation Expedition – Study of Pre-industrial Aerosols and their Climate Effects

INP – Ice nucleating particle

CCN – Cloud condensation nuclei

IS – Ice spectrometer

MPC – mixed-phase cloud

RV – research vessel

RSV – research and supply vessel

NOAA - National Oceanic and Atmospheric Administration

NCAR – National Center for Atmospheric Research

ECMWF – European Centre for Medium-range Weather Forecasting

ERA5 – ECMWF Reanalysis version 5

HYSPLIT – Hybrid Single-Particle Lagrangian Integrated Trajectory Model